INFORMATION TO USERS

This manuscript has been reproduced from the microfilm master. UMI films the text directly from the original or copy submitted. Thus, some thesis and dissertation copies are in typewriter face, while others may be from any type of computer printer.

The quality of this reproduction is dependent upon the quality of the copy submitted. Broken or indistinct print, colored or poor quality illustrations and photographs, print bleedthrough, substandard margins, and improper alignment can adversely affect reproduction.

In the unlikely event that the author did not send UMI a complete manuscript and there are missing pages, these will be noted. Also, if unauthorized copyright material had to be removed, a note will indicate the deletion.

Oversize materials (e.g., maps, drawings, charts) are reproduced by sectioning the original, beginning at the upper left-hand corner and continuing from left to right in equal sections with small overlaps. Each original is also photographed in one exposure and is included in reduced form at the back of the book.

Photographs included in the original manuscript have been reproduced xerographically in this copy. Higher quality 6" x 9" black and white photographic prints are available for any photographs or illustrations appearing in this copy for an additional charge. Contact UMI directly to order.

UMI

A Bell & Howell Information Company
300 North Zeeb Road, Ann Arbor MI 48106-1346 USA
313/761-4700 800/521-0600

DISTRIBUTION OF LARGE CALANOID COPEPODS IN RELATION TO PHYSICAL OCEANOGRAPHIC CONDITIONS AND FORAGING AUKLETS IN THE WESTERN ALEUTIAN ISLANDS

A

THESIS

Presented to the Faculty

of the University of Alaska Fairbanks

in Partial Fulfillment of the Requirements

for the Degree of

DOCTOR OF PHILOSOPHY

By

Kenneth O. Coyle, B.S., M.S.

Fairbanks, Alaska

May 1997

DISTRIBUTION OF LARGE CALANOID COPEPODS IN RELATION TO PHYSICAL OCEANOGRAPHIC CONDITIONS AND FORAGING AUKLETS IN THE WESTERN ALEUTIAN ISLANDS

By

Kenneth O. Coyle

RECOMMENDED:

Advisory committee chair

Department Head

APPROVED:

Dean, School of Fisheries
and Ocean Science

Dean of the Graduate School

4-2-97

Date

Abstract

Acoustic measurements and net sampling were used to estimate zooplankton abundance and biomass relative to water mass types and flow fields in the western Aleutian Islands during June and July, 1992 and 1993. Observations are interpreted relative to the distribution and abundance of least auklets (*Aethia pusilla*), which forage on zooplankton. Highest zooplankton biomass (up to 7 g m^{-3}) occurred during June 1992, in the pycnocline separating the upper mixed layer from the cold intermediate layer north of a front separating Bering Sea and Alaska Stream water. The large calanoid *Neocalanus flemingeri* had highest abundance but the larger *Neocalanus cristatus* accounted for most of the biomass. *N. cristatus* and *N. flemingeri* were absent south of the Bering Sea front, where the community was dominated by *Neocalanus plumchrus* and *Eucalanus bungii*. Auklets were foraging almost exclusively north of the Bering Sea front.

Neocalanus spp. abundance in the upper mixed layer was much lower in July 1993, than in June 1992. *Neocalanus* occurred primarily in scattered aggregates near the pycnocline over Bering Sea Intermediate water and at the surface in Pacific water. Auklets shifted their foraging activities to passes and shelf areas among the

islands, where tidally generated divergences and convergences upwelled and concentrated prey into patches in the mixed layer. Elevated densities of *Neocalanus* were observed in convergence zones in Delarov Pass and over a ridge south of Kiska Island. Convergence zones were identified by intense sound scattering from entrained bubbles and by deceleration of the horizontal velocity components in acoustic doppler current data, a record of current speed and direction beneath the vessel.

Densities of auklet prey in the study area during June were apparently influenced by the position of the front between Bering Sea and Pacific water masses. The position of the front was influenced by Alaska Stream flow anomalies lasting for several years. Prey densities on the shelves and in the passes during July were influenced by tidal currents at spatial scales of tens of meters to ten kilometers and lasting one tidal cycle.

Table of Contents

List of Figures

List of Tables

Preface

The research, of which this dissertation is a part, was designed to address the influence of physical mechanisms on energy transfer to apex predators. Since physical features such as convergences, divergences, fronts and pycnoclines can markedly affect prey concentrations, such features ultimately influence energy flow through pelagic food webs. This is especially true of those species of fish, baleen whales and seabirds that depend on small prey such as zooplankton. This dissertation covers that part of the research project dealing with zooplankton distribution relative to physical features.

The hypotheses driving the research as a whole were the following:

1) Large planktivorous predators require elevated prey densities. Birds forage where food concentrations near the surface are predictable in space and time. By elevated prey densities, we mean densities which are substantially higher than average. We were therefore not concerned with average concentrations but with regions where prey densities exceeded mean concentrations.

2) Currents interacting with the bathymetry form upwellings and fronts which concentrate prey at specific locations.

3) The life history strategies of the major prey taxa impact the timing and location of prey aggregates.

Least auklets were chosen as a model predator to test the above hypotheses for the following reasons:

1) They are very abundant and therefore provide a strong signal when foraging flocks are encountered. Densities increase by one to two orders of magnitude where active foraging is occurring.

2) Auklets nest in June and July. During the nesting season, breeding auklets are limited in the range over which they can forage due to requirements to provision the chicks and incubate the eggs. This behavioral limitation decreased the search area necessary to find foraging flocks and substantially increased the probability of successfully encountering foraging auklets.

3) Auklets can be seen from the bridge of a ship, thus facilitating the search for foraging flocks.

4) Auklets are planktivorous. I was therefore able to catch the prey organisms with the plankton nets available on our research vessel.

5) The auklets can be collected to verify their diets.

Given the above hypotheses and our choice of predator, the objectives of the research were as follows:

1) Locate flocks of foraging auklets. The distribution

of foraging auklets to a large extent drove the sampling design.

2) Determine the horizontal and vertical distribution of prey aggregates.

3) Determine the physical and biological factors influencing distribution of the prey and predators. Such factors included the species composition of the prey, water column structure, currents and phytoplankton densities.

This dissertation emphasizes primarily application of high-frequency acoustics to determine the biomass and distribution of zooplankton forage relative to water masses and fronts. The results are presented and discussed in relation to the physical oceanography of the region and the distribution of foraging auklets. The techniques and limitations of acoustic measurements are summarized in Appendix I. A separate section addressing application of net tows to scaling of the acoustic data is presented in Appendix II. Data collection was done during two field seasons: June 1992 and July 1993. The methods for both field seasons were identical and are presented in a single section. The results from the 1992 and 1993 field seasons differed and are presented in separate chapters along with discussion.

While some examples of seabird distribution are

presented in both sections to illustrate relationships between zooplankton densities and auklet foraging, detailed examination of the seabird data is being undertaken by George Hunt, University of California Irvine, and will not be addressed here. When the actual auklet distributional data were not available to me, the general observations on auklet distribution presented in the discussion sections were provided by Dr. Hunt (personal communication). The physical data for this dissertation were collected by Tom Weingartner and Shelton Gay. Technical assistance with the MOCNESS and acoustics were provided by Michelle Miller, Steve Hartz and Mark Valarino. Technical assistance in processing zooplankton samples was provided by Elizabeth Stockmar. Statistical assistance was provided by Ronald Barry. I express my gratitude to my committee (Dr. R. T. Cooney, Dr. J. J. Goering, Dr. R. C. Highsmith, Dr. E. C. Murphy and Dr. T. C. Royer) for their advice in conducting this research and preparing the dissertation. This research was funded by the National Science Foundation Office of Polar Programs.

1. Introduction

Traditionally, estimation of the distribution and density of fish and zooplankton has been done with nets. Due to the large amounts of labor and time required to complete net surveys, information on distribution of zooplankton has often been limited to broad descriptions of zoogeographic range and preferred depth intervals (e.g. Brodskiy, 1948; 1955; 1957; Motoda and Minoda 1972; Heinrich, 1959). Examining processes influencing energy transfer to apex predators, however, requires more detailed spatial data because the physical processes influencing zooplankton distribution occur over a broad range of spatial scales (Haury *et al.*, 1978; Haury and Pieper, 1987; Haury and Wiebe, 1982). Physical and biological samples from discrete locations at wide spatial intervals are often insufficient to resolve the detail which may be key to understanding processes influencing energy transfer in the sea.

The development and application of remote sensing technologies for examination of biological and physical variables at a variety of scales may aid in the identification and quantification of specific biological oceanographic processes involved in energy transfer to apex

predators. Quantitative acoustics is one such technology. Although applied historically to fisheries management and stock assessment, the ability of acoustics to estimate biomass of planktonic and nektonic organisms at fine scales makes it an important research tool in biological oceanography (Pieper, 1979; Holliday and Pieper, 1980; Pieper 1983; Green *et al.*, 1988; Simmard and Mackas, 1989; Cockrane *et al.*, 1991; Green et al., 1991; Coyle *et al.*, 1992; Coyle and Cooney, 1993; Napp *et al.*, 1993; Macaulay *et al.*, 1995).

Acoustic techniques were applied in this study to document the distribution of zooplankton biomass relative to physical conditions affecting its distribution and abundance in the western Aleutians. In particular, I sought to examine the spatial distribution of water masses and fronts relative to the distribution of forage species for apex predators in an effort to identify the physical conditions responsible for concentrating prey sufficiently to permit efficient energy transfer through the food web. Least auklets (*Aethia pusilla*) were the predator of choice because they are easily observed and identified from surface ships and they forage on large calanoid copepods (Hunt *et al.*, 1993), which can be detected acoustically and collected with standard plankton nets. In addition, roughly a million

least auklets nest in the Aleutian Island archipelago; they therefore produce a strong abundance signal in regions favorable for foraging. Least auklets incubate eggs and rear chicks during June and July (Sowls *et al.*, 1978), a period when plankton biomass is likely to be maximum in the Aleutians (Coyle *et al.*, 1996). This research was therefore done in the western Aleutians near Gareloi, Kiska and Buldir Islands, where over 350,000 least auklets nest annually (Sowls *et al.*, 1978).

2. METHODS

The study area included regions around Buldir, Kiska, Gareloi and the Delarov Islands in the western Aleutian Islands (Fig. 2-1). The Aleutians are a string of volcanic peaks rising from the sea floor to several thousand meters above sea level and separating the Gulf of Alaska from the Bering Sea. The shelf is narrow, the continental slope is steep, and the plankton community is oceanic (Coyle *et al.*, 1996; Motoda and Minoda,1974). Sampling during 1992 and 1993 was done aboard the R/V Alpha Helix. Sampling dates for the individual regions are outlined in Table 2-1. Methods for collection and processing of acoustic, CTD and zooplankton data are outlined below.

Acoustics

Acoustically determined biomass (ADB) was measured at frequencies of 200 and 420 kHz along transects at integration intervals of 30 seconds (horizontal distance covered = 120 m) using a Biosonics[1] model 120 echosounding system and integration board. The transducers were deployed in a v-fin depressor at 5 m depth and towed at 4 m sec^{-1} beside the vessel about 3 m from the hull. The 420 kHz system resolved volume scattering intensity (S_v) in 1-m depth intervals from 5 to 55 m depth. Volume scattering was

[1]Biosonics Corp., Seattle Washington, USA

measured by the 200 kHz data in 2-m depth intervals from 5 to 165 m depth. The calibration information is presented in Table 2-2. Latitude and longitude were simultaneously recorded with a GPS interfaced to the computer.

Volume scattering was converted to biomass using a scaling factor (g/dB) estimated by regression of S_v against zooplankton wet weight biomass determined from net tows taken simultaneously with S_v measurements at selected stations. I wrote a program to match the location and depth of each S_v estimate to the net track, thus insuring that S_v and net data could be matched as closely as possible in space and time. Nevertheless, at any given time, the net was 50-100 m behind the towed transducers. The S_v estimates were scaled by the volume of water fished by the net at each specific depth and summed over the net track to estimate ADB taken by each net. Net biomass estimates could then be compared directly with S_v to estimate the effective target strength of the zooplankton. Nets which fished above or below the range of the 420 kHz sounder (5 and 55 m) were excluded from the analysis. Nets were not fished below the range of the 200 kHz system (165 m). The regression method was also evaluated using a two frequency inversion solution to the Stanton fluid sphere model (Stanton, 1989). The

results from the Stanton model were similar to biomass scaled by net tows and regression. A detailed discussion of scaling of the acoustic data is presented in Appendix II.

The ADB or S_v were contoured using minimum curvature gridding. Aggregates of sound scattering organisms in the contour plots appear horizontally compressed due to scaling; the horizontal axis is scaled in latitude while the vertical axis is scaled in meters (1 minute of latitude = 1850 m). The aggregates actually occurred as layers.

Zooplankton

Zooplankton were collected with a MOCNESS (multiple opening closing net and environmental sampling system). The locations of net tows for each region and sampling period are shown in their respective chapters. Each tow consisted of up to 9 nets which were opened and closed at specific depths above, below and in the sound-scattering layers observed at each site. The mesh size of the MOCNESS nets was 0.505 mm, the effective mouth opening was 1 m^2, and the system simultaneously recorded conductivity, temperature, depth, fluorescence, volume fished and net angle. Samples were preserved in 10% formalin for later processing.

In the laboratory the samples were sequentially split with a Folsom splitter to produce a hierarchical series of subsamples containing 100-200 organisms. Systematic

examination of each subsample permitted identification and enumeration of the dominant organisms of each major size category in the samples. The specimens were sorted, identified to the lowest taxonomic level possible, copepodid stages were determined and wet weights were measured.

Two of the most common copepod species in the mixed layer were *Neocalanus plumchrus* and *Neocalanus flemingeri*. These species are practically identical to one another morphologically and were recognized as distinct only recently (Miller, 1988). The fifth copepodid stage of preserved specimens can usually be identified by the cephalosome-prosome length ratio, the size of the second maxilla and by dissection and mounting of mandibles. The *Neocalanus* in our region were a mixture of both species and are pooled in the plots as *Neocalanus* with a Roman numeral indicating the stage. Therefore, *Neocalanus* or *Neocalanus* spp. in figures and text refers to *Neocalanus plumchrus/flemingeri*, not to *Neocalanus cristatus*.

Analysis of variance (ANOVA) was used to test for differences in the mean abundance of the dominant taxa relative to water masses. Abundance estimates from individual nets taken at the same station were averaged to produce single values for each station and the station mean was log transformed before analysis. Canonical correlation

analysis was used to examine the correlations between major species groups and physical oceanographic variables. Analyses were done with an INGRES data base and FORTRAN software with calls to IMSL statistics routines for the ANOVA and canonical correlation analyses.

Hydrography and currents

Conductivity-temperature-depth measurements were collected with a Neil Brown CTD. *In situ* fluorescence was measured with a model Q fluorometer mounted on the CTD. The *in situ* fluorometer was calibrated using water samples collected at discrete depths. The samples were extracted in 90% acetone and fluorescence was measured on a Turner Design bench fluorometer as outlined in Parsons *et al.* (1984). The bench fluorometer was calibrated using a Hitachi spectrophotometer and chlorophyll extract as outlined in Parsons *et al.* (1984). Measurements of surface salinity and temperature were taken every 0.5-2 minutes along transects using Seabird sensors mounted in a sea chest on the ship. Current measurements were made along transects using a hull-mounted RD Instruments[2] 307 kHz Acoustic Doppler Current Profiler (ADCP) on the RV Alpha Helix. Horizontal velocity estimates were collected in 2 minute ensembles averaged in 4 m depth bins. At typical vessel speeds of 10 km h^{-1} each

[2]RD Instruments, San Diego California

ensemble integrated over a distance of about 500 m. Velocities at depths above 14 m were not used due to hull induced contamination and velocities within 15% of the bottom depth were omitted due to bottom contamination. The velocities were written to a computer interfaced with the ship's satellite navigation system to provide date, time and position for each ensemble.

All contour plots were computer generated using a minimum curvature gridding algorithm. The west and south ends of all transect plots are always on the left side of the page. Geographic plots were generated with GMT (Generic Mapping Tool[3]) software.

[3]Geodynamic Branch, Geosciences Laboratory, NOAA

Table 2-1. Sampling locations (Fig. 2-1) and dates for various regions in the western Aleutian Islands, surveyed during the June 1992 and July-August 1993.

Northern Kiska Island:	6 June to 11 June 1992
	24 June to 28 June 1992
	22 July to 25 July 1993
	28 July to 29 July 1993
Southern Kiska Island:	12 June 1992
	26 July to 28 July 1993
Buldir Island:	13 June to 23 June 1992
Northern Gareloi Island:	9 July to 12 July 1993
Delarov Pass:	13 July to 20 July-1993
	5 August to 6 August 1993

Table 2-2. Calibration data for the 200 khz and 420 kHz echo integration systems.

	Year			
	1992		1993	
	200 kHz	420 kHz	200 kHz	420 kHz
Receiver Sensitivity (dB):	-151.800	-147.867	-152.209	-147.538
Source Level (dB):	221.186	219.265	220.814	219.435
Beam Pattern Factor:	0.001194	0.001060	0.001091	0.001048

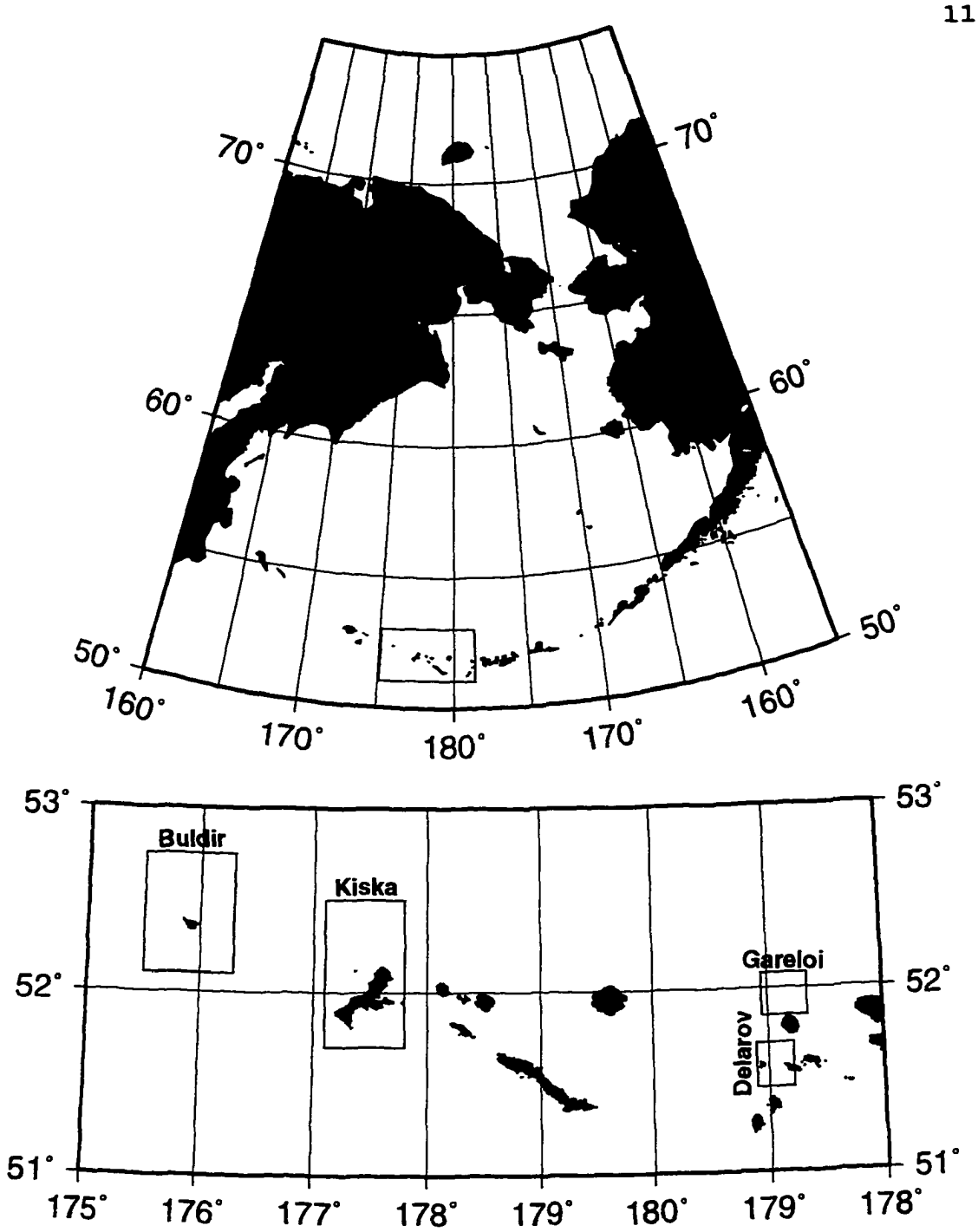

Fig. 2-1. Sampling locations in the western Aleutian Islands during June 1992 and July-August 1993. Boxes enclose sampling regions.

3. The composition and distribution of zooplankton relative to water masses and foraging auklets in the western Aleutians during June, 1992

INTRODUCTION

Two of the large scale factors influencing zooplankton distribution are the temporal and geographic distribution of water masses and the frontal systems dividing them. One of the most important factors influencing the distribution of frontal zones in the Bering Sea is bathymetry (Coachman, 1986). Frontal zones separating coastal and oceanic zooplankton communities substantially influence energy flow to benthic and water column communities in the southeastern and northern Bering Sea (Cooney and Coyle, 1982; Smith and Vidal, 1986; Springer *et al.*, 1989) and the resulting differences in energy partitioning between benthic and planktonic ecosystems in turn influence energy flow to apex predators such as whales (Highsmith and Coyle, 1992; Coyle and Highsmith, 1994) and marine birds (Hunt and Harrison, 1990; Hunt *et al.*, 1990).

In contrast to the southeastern and northern Bering Sea, the Aleutian archipelago lacks a broad shelf zone and

zooplankton communities to the north and south of the Aleutians have similar species composition (Coyle *et al.*, 1996). We therefore did not anticipate finding marked differences in the zooplankton community to the north and south of Buldir and Kiska Islands. Nevertheless, least auklets consistently fed on the northern side of the archipelago during June, 1992 (See data below). Subsequent analyses revealed substantial north-south differences in zooplankton abundance and distribution, apparently driving the preference of auklets to feed to the north of the Aleutians. This chapter examines the differences in zooplankton communities to the north and south of the islands and the physical factors affecting those differences. The locations of net tows taken in the Buldir-Kiska region are shown in Fig. 3-1.

RESULTS

Water masses and ADB (Acoustically determined biomass)

CTD transects were taken within 24 hours of acoustic transects around Kiska and Buldir Islands to determine water mass distributions relative to acoustic biomass (Fig. 3-2). The water column north and south of the Aleutian Islands showed greater thermo- and halo-stratification than the water column in the passes (Fig.

3-3a). Elevated surface salinity and lowered surface temperature in the passes relative to regions north and south of the islands indicated mixing (Fig. 3-3a). The southern boundary of Bering Sea Surface Water occurred at a fairly sharp front between 52.1° and 52.2° N. The downward slope of isohaline lines between 52.2° and 52.4° N. (Fig. 3-3a) suggests the presence of a convergence zone. Elevated chlorophyll concentrations were measured on the northern stratified side of the Bering Sea front. A distinct surface front also occurred between 51.9° and 52.0° N. near the southern end of Kiska Island (Fig. 3-3a). Pacific Ocean surface water was characterized by elevated temperatures and low salinities. In contrast to the Bering Sea front, elevated chlorophyll concentrations were not observed on the southern stratified side of the Pacific Ocean front. ADB was elevated in the upper mixed layer along the transects north of the Bering Sea front (Fig. 3-3a) but was absent south of the front. Sound-scattering organisms were apparently concentrated and pushed downward in the convergence zone at about 52.0° N. The major difference between water masses north and south of the Aleutian Islands was the presence of the cold winter remnant layer north of the Bering Sea front. The winter layer appears as a temperature depression between

50 and 200-250 m depth on TS diagrams comparing stations at the opposite ends of transects through Murray Canyon (Fig. 3-3b). Water masses below the winter layer were similar on both sides of the Aleutian archipelago.

Transects north of Kiska on 8 June showed elevated chlorophyll concentrations and ADB north of the Bering Sea front as a fairly continuous layer extending to the end of the transect (Fig. 3-4). Consecutive runs of the transect revealed consistent layers of maximum ADB near the 26.12 isopycnal line. The scattering layer ascended northward with the shallowing pycnocline and surfaced between 52.3° and 52.4° N., just south of the minimum pycnocline depth. A fairly strong convergence zone was apparent around 52.2° N., where the isopycnals formed a trough (Fig. 3-4; see also Fig. 3-3). By late June the region of maximum chlorophyll was north of 52.5° N., where dense aggregates of sound scattering organisms were observed above the pycnocline in the chlorophyll maximum layer (Fig. 3-5). Aggregates also occurred in the thermocline south to the salinity front at 52.25° N.

CTD transects near Buldir Island also revealed distinct frontal regions, probably the same front as that occurring at about 52.5° and 52.3° N. on the northern and eastern transects, respectively (Fig. 3-6; Fig. 3-7).

Elevated chlorophyll concentrations and acoustic biomass occurred in Bering Sea surface water on the stratified side of the front. Fronts on both sides of the Aleutian ridge separated mixing zones in the passes, however, elevated chlorophyll and acoustic biomass were usually confined to the stratified side of the Bering Sea front, where surface water occurred over a cold winter layer with temperatures under 4°C to depths of 200 m (Fig. 3-6; Fig. 3-7).

A shaded contour plot of ADB in the upper mixed layer near Buldir Island revealed regions of elevated zooplankton biomass to the north and east of the surface expression of the front separating Bering Sea water from the mixed regions in the shallows and passes (Fig. 3-8). Flocks of least auklets were observed along or near the stratified side of the frontal region to a distance of about 30 km from Buldir Island (Fig. 3-8). Auklet densities and ADB were averaged in 0.2 km radius bins and plotted as circles north of Kiska, due to the lesser coverage by transect data relative to the Buldir region. The transect lines are indicated by the locations of the circles on the plots of auklet density and ADB (Fig. 3-9). Biomass measured 24 - 28 June in the upper mixed layer along replicate transects north and west of Kiska Island

revealed patches to the north of the Bering Sea front (Fig. 3-9). Auklet numbers were highest within 30 km of the island and north of the front. Maximum ADB occurred about 20 to 40 km to the west and north of Kiska Island.

Species composition of zooplankton in the scattering layers

Analysis of variance was done on stations north and south of the Bering Sea front to detect any significant differences in abundance of the major zooplankton taxa with respect to water mass. The Bering Sea group included Tows 1, 2, 3, 6, 7, 14, 15, 16, 18, 19 and 20. The Pacific group included Tows 8, 9, 10, 11, 12, 14 and 17. *Neocalanus flemingeri* stage V, *Neoalanus cristatus* stage V and *Limacina helicina* were significantly more abundant north of the Bering Sea front (Table 3-1). *Calanus marshallae* stage V, *Eucalanus bungii* stages III and IV, *Metridia pacifica* adult females and euphausiid eggs were more abundant south of the front. *Neocalanus plumchrus* stage V tended to be more abundant in Pacific water (e.g. P = 0.058).

Canonical correlation analysis revealed significant correlations between twelve of the most abundant taxonomic groups and acoustic biomass, sigma-t, depth and

fluorescence in Bering Sea water (Table 3-2). The first canonical variable was dominated by acoustic biomass which was highly correlated with abundance of *Neocalanus cristatus* stages IV and V. The first canonical variable was also correlated to sigma-t, but negligibly correlated with depth and fluorescence. The second canonical variable was negatively correlated with sigma-t and depth but positively correlated with fluorescence; the second canonical group was positively correlated with abundance of *Neocalanus plumchrus/flemingeri*, *Parathemisto pacifica*, *Sagitta elegans* and *Limacina helicina* (Table 3-2). The correlations therefore indicate that *Neocalanus cristatus* was the primary sound scattering organism and its distribution was moderately correlated with regions of elevated water density. In contrast, *Neocalanus plumchrus/flemingeri*, *Parathemisto pacifica*, *Sagitta elegans* and *Limacina helicina* were more abundant in shallower water of lower density and with elevated fluorescence.

Neocalanus plumchrus/flemingeri stages III-V were most abundant and often comprised more than 60% of the total population in samples from the scattering layers north of the Bering Sea front (Figs. 3-10-12). However, *N. cristatus* is about six times more massive than *N.*

plumchrus/flemingeri and was apparently the dominant sound scattering organism north of the Bering Sea front. About 80% of the biomass in the scattering layers consisted of *N. cristatus* copepodid stage V. The main scattering layer usually occurred at 15 to 30 m depth near the pycnocline separating the upper mixed layer from the cold subsurface winter layer (Fig. 3-10, 3-12, 3-13). A region of minimal scattering occurred above the main scattering layer and a secondary scattering layer was occasionally observed within several meters of the transducer. ADB and *N. cristatus* densities in the surface scattering layer were generally lower than in the deeper layer. However, maximum abundance of *N. plumchrus/flemingeri* generally occurred in the upper layer about 5-10 m above the main scattering layer. *N. cristatus* densities were high in surface waters when a distinct mixed layer above the pycnocline was absent (Fig. 3-11), usually well north of the Bering Sea front. The highest biomass recorded during the study occurred in a dense plankton layer near the bottom of the mixed layer on an intense pycnocline at about 25-35 m depth on 26 June (Fig. 3-13).

Although *N. plumchrus* were occasionally dominant in samples taken from south of the Bering Sea front, *Neocalanus cristatus* were either totally absent or present

at low densities (Fig. 3-14-15). In the absence of *N. cristatus*, ADB was usually under 1 g m^{-3}. *Eucalanus bungii* stage III were often dominant; all stages combined occasionally made up more than 70% of total abundance, especially in samples taken below the pycnocline both north and south of the Bering Sea front. *Metridia pacifica* was also occasionally abundant in the frontal regions.

Preliminary results from seven MOCNESS tows taken north of Kiska Island in June, 1995, indicated average biomass of 17 g m^{-2} in the upper 50 m, compared with 16 and 44 g m^{-2} in the upper 50 m for Pacific and Bering Sea water respectively, in 1992. No obvious convergences or frontal zones were present along the 1995 transects, but Bering Sea intermediate water was present beneath the surface layer and an intense bloom was occurring north of 52.5° N. Maximum volume scattering occurred north of 52.6° N and *Neocalanus cristatus* were absent from the samples. Therefore, the species composition and biomass in 1995 was closer to that of Pacific water in 1992 than Bering Sea water.

Discussion

Due to its large size, *Neocalanus cristatus* was probably the dominant sound scatterer north of the Bering Sea front. This species occurred predominantly in the

pycnocline and was present at the surface only when the pycnocline was pushed to the surface, displacing the mixed layer. In contrast to the subarctic Pacific gyre (Mackas *et al.*, 1993), we found no evidence of vertical separation between *N. cristatus* and the other *Neocalanus* species. Although *N. cristatus* was generally absent from the mixed layer, all *Neocalanus* taxa co-occurred in the pycnocline layer. The preference of *N. cristatus* for the pycnocline and subpycnocline layers is apparently typical of its vertical distribution in the subarctic Pacific (Mackas *et al.*, 1993). Its absence from the upper mixed layer may be related to feeding strategy or a general aversion to turbulence (Mackas *et al.*, 1993). *N. cristatus* is a passive filter feeder, and unlike many omnivorous copepods, it does not actively pursue prey (Dagg, 1993a; Landry and Faggerness, 1988; Green and Landry, 1988). Rather, it seeks out regions of maximum particle concentration or flux and remains stationary for extended periods while filtering food organisms from the water column (Green and Landry, 1988). The active feeding stages of *N. cristatus* in the North Pacific gyre are most abundant between the seasonal thermocline and the permanent halocline, 45-150 m depth (Mackas *et al.*, 1993). In contrast to the Pacific, the halocline and thermocline

in the Bering Sea overlapped, *N. cristatus* were concentrated in the pycnocline, a depth interval of 10-20 m in the upper 30 m, and copepod densities were minimal in the underlying cold intermediate layer.

Although *Neocalanus cristatus* was absent from surface waters south of the Aleutian Islands, it is a common subarctic copepod and has been reported in the euphotic zone of the western North Pacific in May and June (Tsuda *et al.*, 1993; Tsuda, 1995). The absence of *N. cristatus* in Pacific waters near the Aleutians may be related to differences in origin of the water masses on either side of the archipelago. Water to the north of the Bering Sea front was apparently resident Bering Sea water, as indicated by the cold intermediate layer between 50 and 300 m depth. The intermediate layer is produced by cooling and convective mixing of the surface layer during winter (Dobrovol'skiy and Arseneyev, 1961) and is conspicuously absent south of the Aleutian archipelago (Reed and Stabeno, 1993). Alaska Stream water occurs south of the Pacific Ocean front and is characterized by temperatures above 4°C to depths of about 200 m (Fig. 3-2) (Reed, 1984; Stabeno and Reed, 1992).

The Alaska Stream is an intense, westward flowing current with a maximum speed of about 100 cm/sec and an

average transport of 12 X 10^6 m^3 s^{-1} (Reed, 1984). It flows along the shelf break from the eastern Gulf of Alaska to the western Aleutian Islands and forms the northern boundary of the Pacific subarctic gyre. Water south of the Aleutians therefore originates in the Pacific hundreds of kilometers to the east of the study site. Thus, local Bering Sea hydrographic and climatic conditions influence the species composition, abundance, timing and duration of successional events in the zooplankton north of the Bering Sea front, whereas hydrographic and climatic conditions along the central and eastern Gulf of Alaska shelf break influence zooplankton in Alaska Stream water. Average wet weight biomass of 15 years of zooplankton samples from the upper 80 m of the water column to the south and north of the western Aleutians was 14.3-18 and 24.1-28.4 g m^{-2} respectively (Motoda and Minoda, 1974). The above long-term Japanese biomass estimates for Pacific water are similar to the biomass I measured in Pacific Water in 1992 and north of Kiska in 1995. However, average biomass from north of Kiska in 1992 was identical to Japanese estimates from the Kamchatka Basin north of the Commander Islands (44 g m^{-2}).

Under normal conditions, Alaska Stream water flows through Near Strait and divides; a portion flows eastward

and a portion westward along the northern edge of the Aleutian archipelago (Reed and Stabeno, 1993; Stabeno and Reed, 1992; Arsenev, 1967)(Fig. 3-16). Flow out of the Kamchatka Basin is through Kamchatka Pass. During 1990 and 1991 flow through Near Strait was virtually suspended but had been reestablished by fall of 1992 (Stabeno and Reed, 1992; Reed and Stabeno, 1993). During fall of 1991 a buoy released in the Kamchatka Basin drifted eastward and passed just north of Kiska Island (Stabeno and Reed, 1992). If the 1990-1991 flow anomaly persisted through the winter of 1991-1992, then the zooplankton north of Kiska in spring 1992 would have been from the Kamchatka Basin, whereas under normal conditions zooplankton north of Kiska are probably a mixture of resident Bering Sea populations and Pacific populations carried through Near Strait and eastward toward Kiska Island. The abnormally low average zooplankton biomass from north of Kiska in June 1995 may have resulted from elevated flow through Near Pass and Buldir Pass. By fall of 1992 Pacific water was moving through Near and Buldir Passes and trajectories of satellite-tracked drift buoys indicated that it had penetrated into the Bering Sea at least as far north as 54° N. Lat. (Reed and Stabeno, 1993).

The absence of *N. flemingeri* south of the Aleutians

may indicate that seasonal successional events in the plankton community in the Alaska Stream are accelerated relative to Bering Sea Water. The population modes of the copepodid stages of *N. flemingeri* are ahead of those of *N. plumchrus* by about one month (Mackas *et al.*, 1993; Miller and Clemons, 1988). Thus, the *N. flemingeri* south of the Aleutians may have completed their foraging and descended to overwintering depth prior to our sampling season. Suspension of flow through the passes causes lower surface water temperatures, higher surface salinities, deeper winter convective mixing and lower temperatures in the intermediate layer on the Bering Sea side of the Aleutians (Stabeno and Reed, 1992). Lower temperatures would probably further retard successional stages in the plankton community in resident Bering Sea water relative to that in Alaska Stream water.

Model simulations using wind data from 1985-1992 indicate that the transport anomalies observed by Stabeno and Reed (1992) may be driven by long-term variations in wind stress curl over the Pacific (Overland et al., 1994). Integration of biological parameters into such flow models might produce quantitative links between climatic anomalies and large-scale variations in the spatial patterns of zooplankton communities in the Bering Sea.

The distribution of foraging least auklets in Bering Sea water to the North of the Aleutian Islands suggested that zooplankton in the resident Bering Sea water were an important food source in June during the early reproductive period. Any physical conditions affecting the abundance and distribution of *Neocalanus* will therefore influence foraging conditions for least auklets. Because breeding auklets must return to their colonies two to three times daily, their foraging range during the nesting period will reflect a compromise between prey density and distance from the colony (Obst et al., 1995). Distributional data suggest that nesting least auklets did not forage much north of 52° 30' N., a distance of about 40 km from Kiska Island. Climatic conditions restricting flow through the western passes in the Aleutian Islands will probably result in optimal foraging conditions for nesting auklets, whereas strong flow through the passes may displace the Bering Sea zooplankton populations northward, and result in less favorable foraging conditions for least auklets during June.

Table 3-1. Mean abundance (No./m^3) of the five most abundant species in any tow from Pacific and Bering Sea water masses near Kiska and Buldir Islands during June, 1992. P is t-test probability of equal means.

Taxa	Bering	Pacific	P
NEOCALANUS FLEMINGERI V	9.2	2.1	0.001
NEOCALANUS PLUMCHRUS V	2.9	6.0	0.058
NEOCALANUS IV	19.7	14.2	0.197
NEOCALANUS III	7.3	6.3	0.661
NEOCALANUS II	1.6	1.2	0.365
NEOCALANUS CRISTATUS V	16.4	1.8	0.000
NEOCALANUS CRISTATUS IV	2.5	1.3	0.031
NEOCALANUS CRISTATUS III	1.7	1.3	0.141
NEOCALANUS CRISTATUS II	1.1	1.1	0.916
CALANUS MARSHALLAE V	1.0	1.1	0.021
CALANUS MARSHALLAE IV	1.0	1.3	0.118
CALANUS MARSHALLAE III	0.0	1.1	0.083
EUCALANUS BUNGII AF	1.9	3.1	0.239
EUCALANUS BUNGII AM	2.3	4.7	0.078
EUCALANUS BUNGII V	2.6	5.9	0.094
EUCALANUS BUNGII IV	3.4	10.5	0.043
EUCALANUS BUNGII III	6.0	22.2	0.023
EUCALANUS BUNGII II	2.9	4.3	0.314
METRIDIA PACIFICA AF	1.0	1.7	0.008
METRIDIA PACIFICA V	3.6	2.8	0.604
METRIDIA PACIFICA IV	1.4	1.2	0.617
PSEUDOCALANUS 2 MM AF	1.4	1.2	0.732
SCOLECITHRICELLA MINOR V	1.1	1.8	0.271
EUPHAUSIID FURCILIA	4.9	4.3	0.543
EUPHAUSIID EGGS	1.1	1.6	0.047
PARATHEMISTO PACIFICA	4.3	3.3	0.389
SAGITTA ELEGANS	4.1	3.0	0.211
EUKROHNIA HAMATA	1.2	1.8	0.165
LIMACINA HELICINA	2.7	2.0	0.135
AGLANTHA DIGITALE	1.2	1.4	0.190
CLIONE LIMACINA	2.2	1.5	0.021

Table 3-2. Canonical correlation analysis on MOCNESS tows from the Bering Sea water mass near Kiska and Buldir Islands in June 1992.

Physical variables used:

1. Acoustically determined biomass (420 kHz).
2. Sigma-t.
3. Depth of net (m) normalized for volume filtered.
4. Fluorescence normalized for volume filtered.

Biological variables = abundances (No. m^{-3}) of following groups:

1. *Neocalanus* IV & V
2. *Neocalanus* III
3. *Neocalanus cristatus* IV & V
4. *Eucalanus bungii* adult
5. *Eucalanus bungii* V
6. *Eucalanus bungii* IV & III
7. *Metridia pacifica* adult
8. Euphausiid furcilia
9. *Parathemisto pacifica*
10. *Oikopleura* spp.
11. *Sagitta elegans*
12. *Limacina helicina*

*** Canonical Correlations Statistics ***

	Canonical Correlations	Wilks Lambda	Raos F	Num. df	Denom. df	Prob. of Larger F
1	0.8836	0.0184	5.776	48	152.3	0.0000
2	0.8403	0.0840	4.736	33	118.6	0.0000
3	0.7768	0.2858	3.569	20	82.0	0.0000
4	0.5287	0.7205	1.810	9	42.0	0.0948

Table 3-2. Continued.

Correlations Between the Group One Variables and the Group One Canonical Scores

	1	2	3	4
1	-0.9686	0.1009	0.2205	0.0547
2	0.4252	-0.6040	0.6674	-0.0942
3	0.2823	-0.8767	-0.0519	0.3860
4	-0.2599	0.7991	-0.0709	0.5374

Correlations Between the Group Two Variables and the Group Two Canonical Scores

	1	2	3	4
1	-0.1318	0.6639	-0.0186	0.3297
2	0.0318	0.5983	0.3105	-0.1480
3	-0.8943	0.0044	0.2615	-0.0531
4	-0.0323	-0.2081	-0.0997	-0.1953
5	-0.0863	-0.1617	-0.1459	-0.1573
6	-0.1949	-0.0371	-0.3345	-0.1824
7	0.2516	-0.0646	0.3944	0.0464
8	0.2316	0.2542	-0.0619	-0.7500
9	-0.2482	0.6186	-0.3798	0.2887
10	0.2115	0.0698	0.4322	0.1136
11	-0.3558	0.7329	-0.0593	0.1866
12	0.1902	0.7801	0.2460	-0.2070

Fig. 3-1. Location of MOCNESS tows taken near Kiska Island (upper) and Buldir Island (lower) during June 1992. Bathymetry in meters.

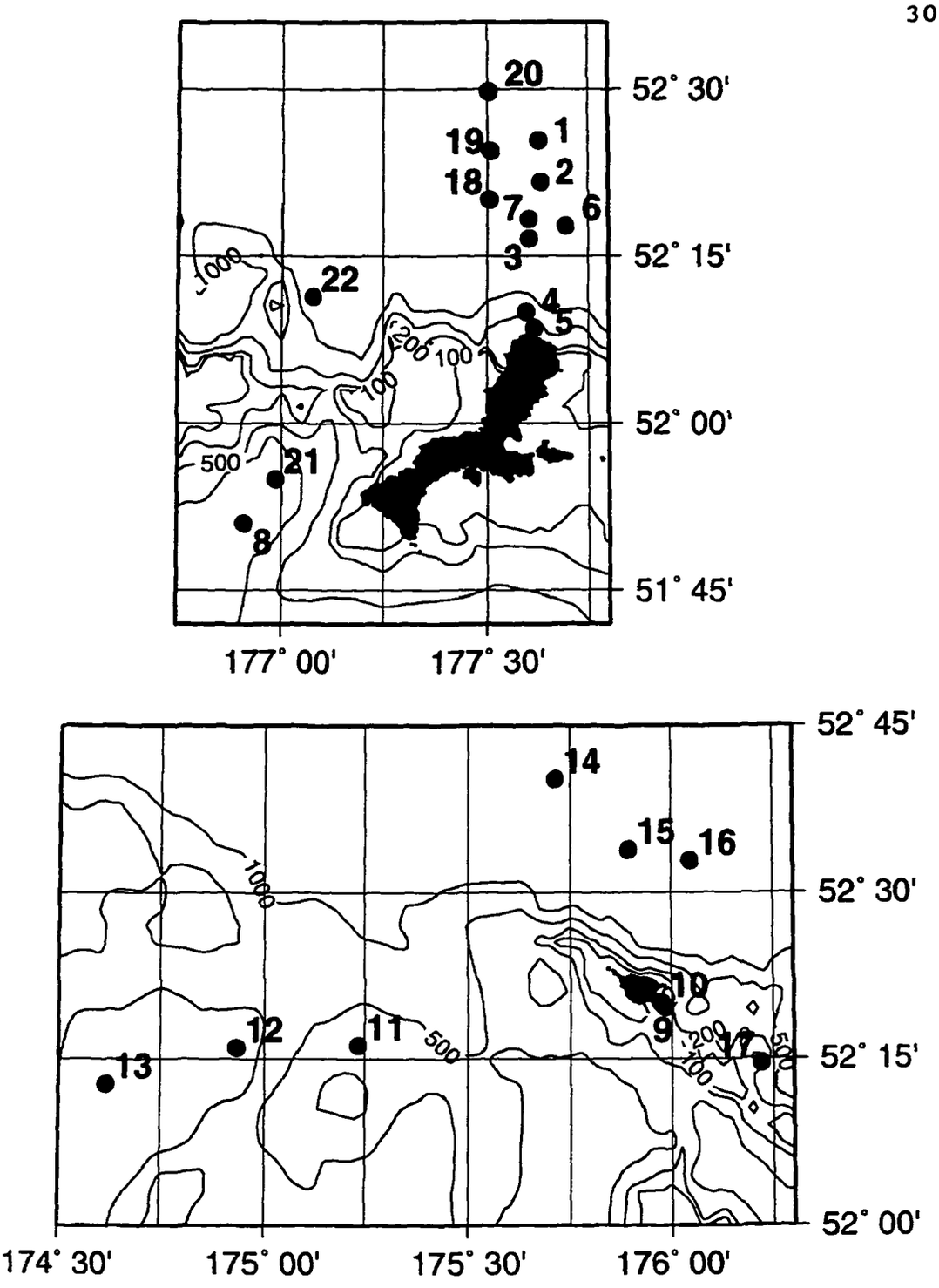

Fig. 3-2. CTD transects (station numbers) and acoustic transects (solid lines) taken during June 1992 through Murray Canyon (upper left), north of Kiska Island (upper right) and around Buldir Island (lower).

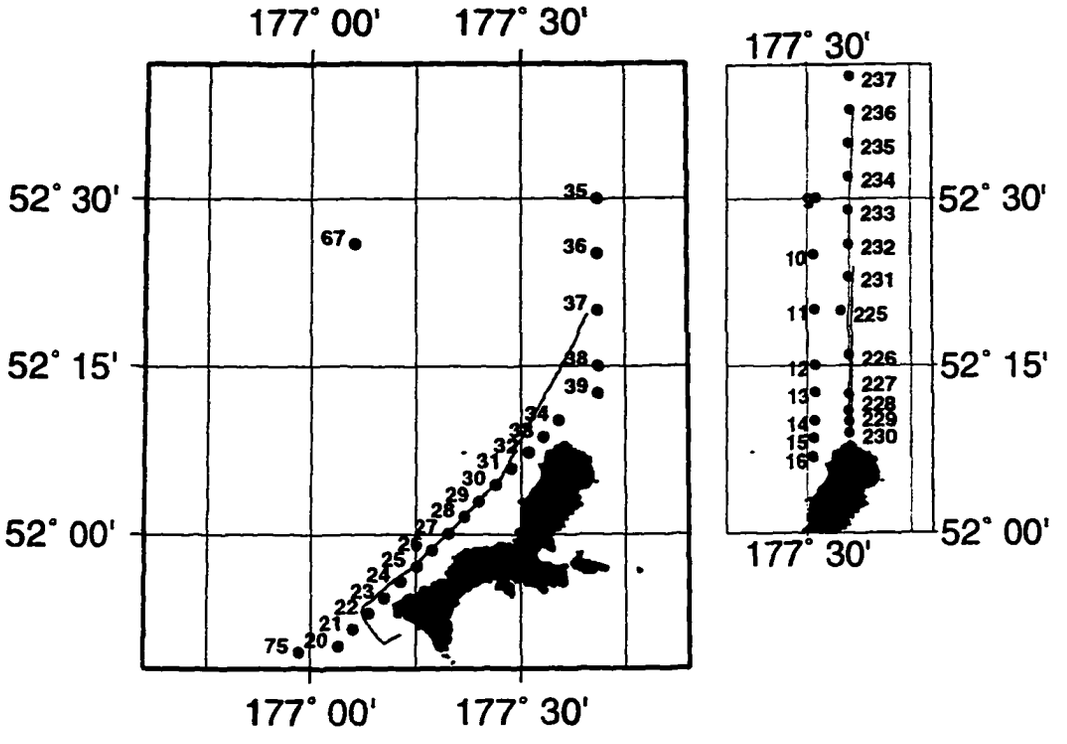

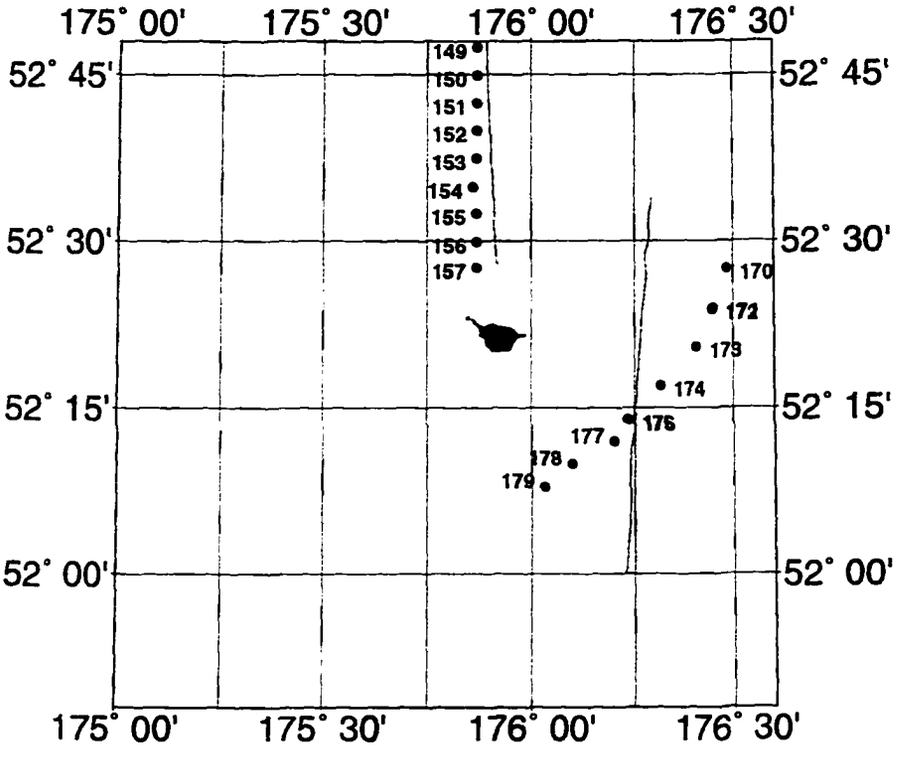

Fig. 3-3a. Temperature, salinity, chlorophyll and acoustic biomass profiles (g m^{-3}) along Transect 1 through Murray Canyon (Fig. 3-2; Stations 20-39); triangles along top axis mark locations of stations. Horizontal axes on upper and lower figures aligned.

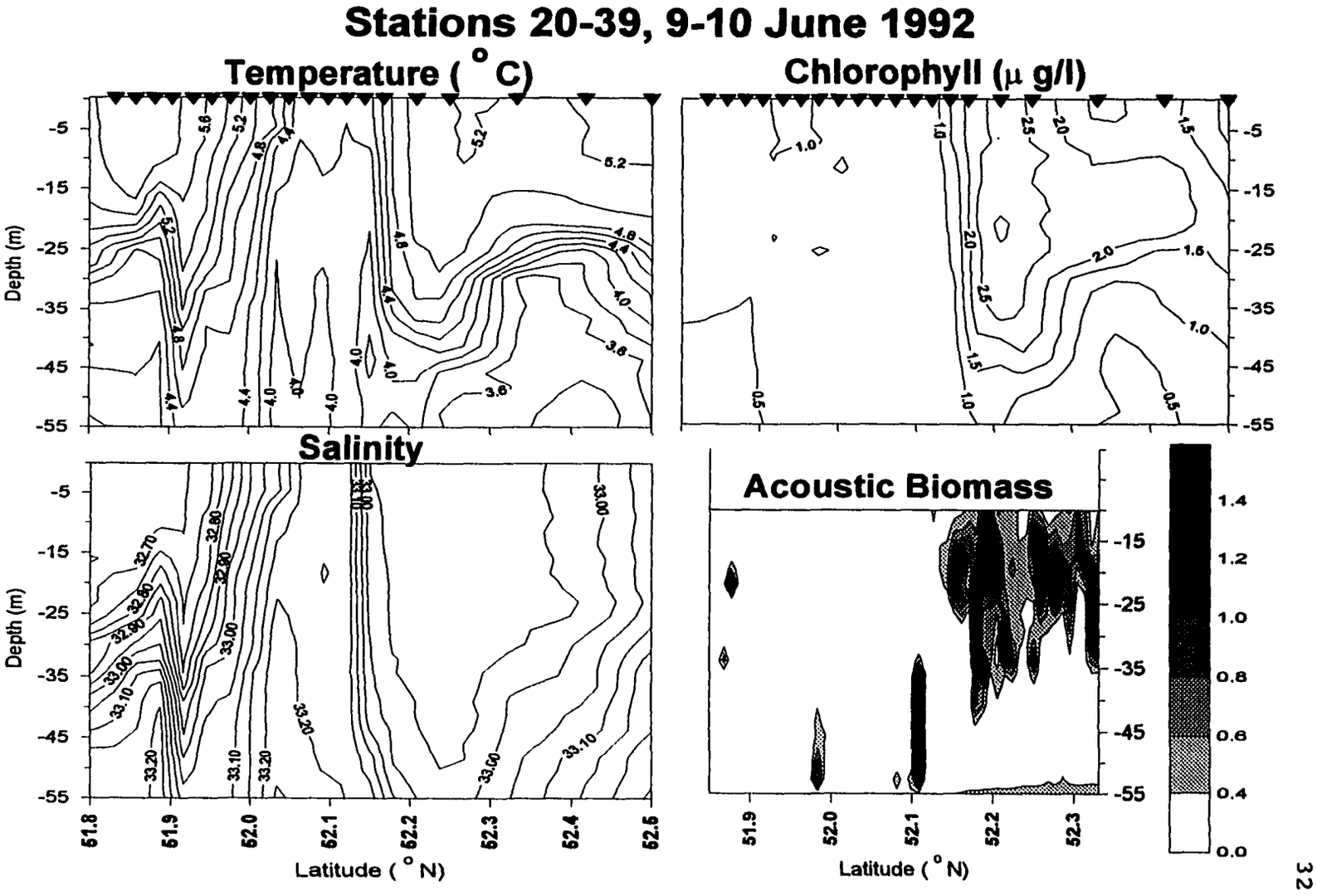

Fig. 3-3b. Temperature (°C) - salinity plots for northern stations (35 and 67; solid line), and southern stations (20 and 75, dotted line)(Station locations in Fig. 3-2) taken June 1992 near Kiska Island. Numbers 1 through 4 on TS plots are depth markers between 100 and 400 m depth.

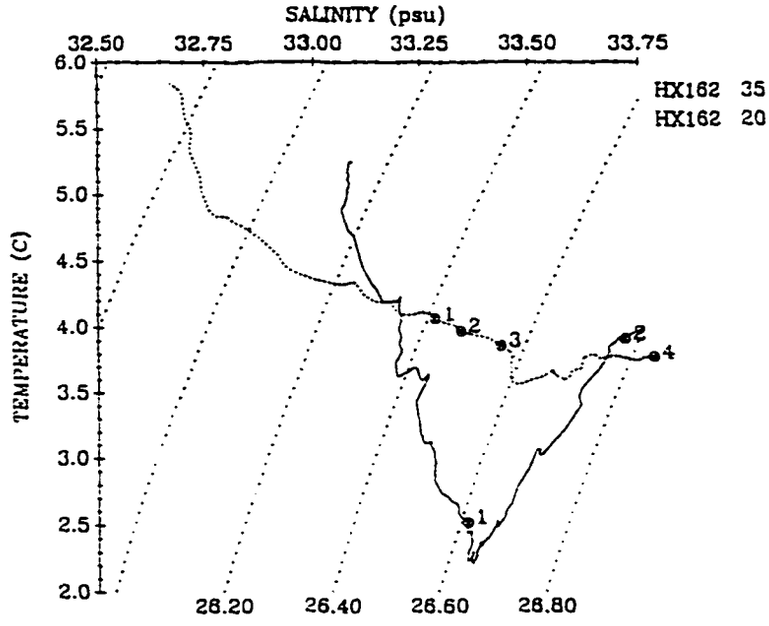

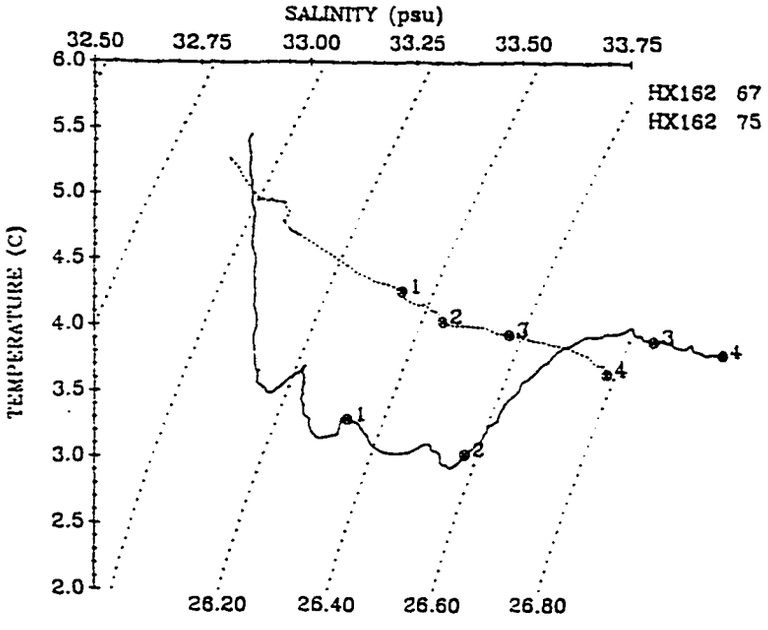

Fig. 3-4. Density, chlorophyll and acoustic biomass profiles (g m^{-3}) taken sequentially along a transect north of Kiska Island (Stations 9-16 and the short acoustic transect, Fig. 3-2). Triangles along upper axes mark CTD station locations. Horizontal axes on upper and lower figures aligned.

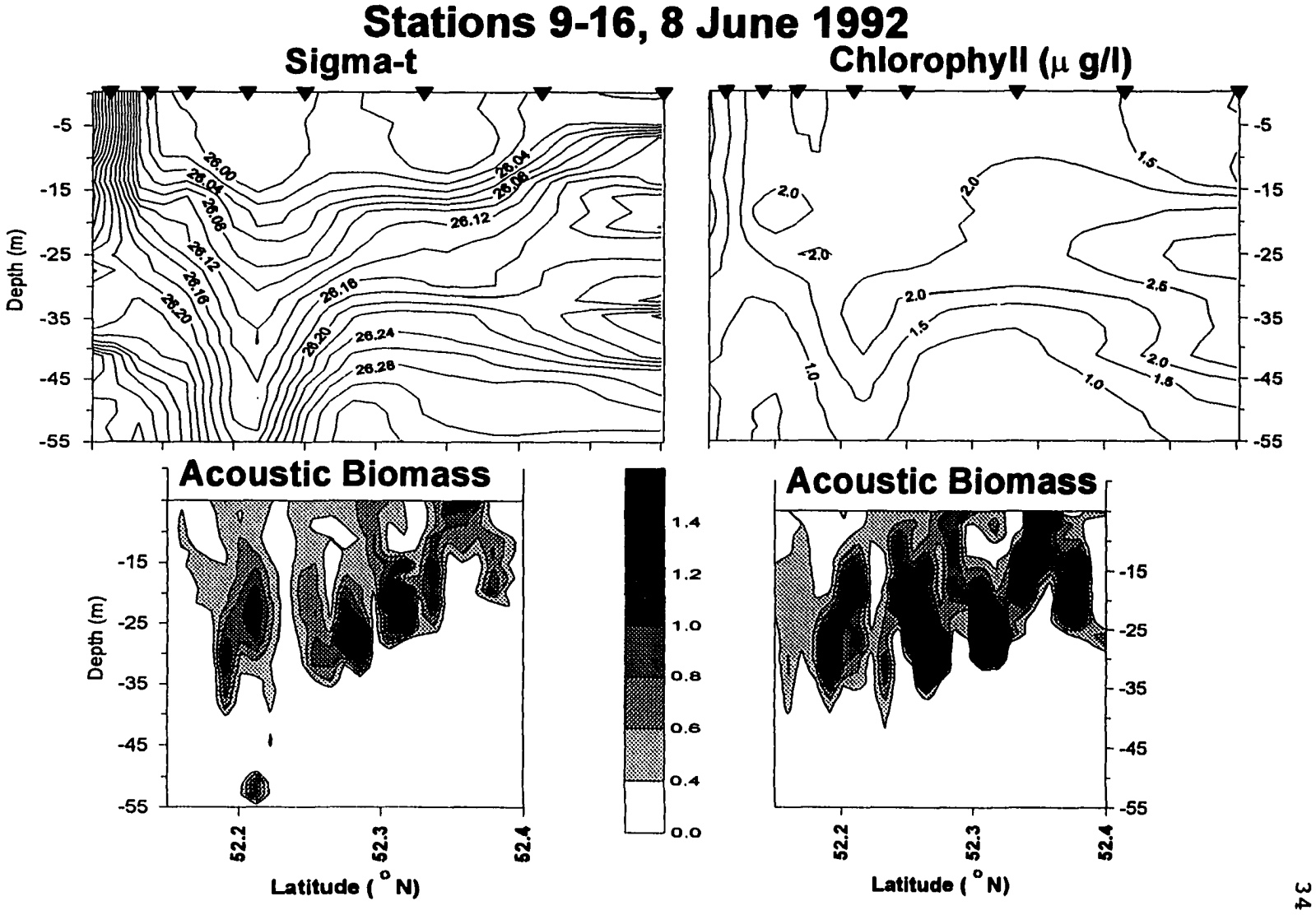

Fig. 3-5. Temperature, salinity, chlorophyll and acoustic biomass profiles along a transect north of Kiska Island (Stations 225-237 and the long acoustic transect, Fig. 3-2). Triangles along upper axes mark CTD station locations. Horizontal axes on upper and lower figures aligned.

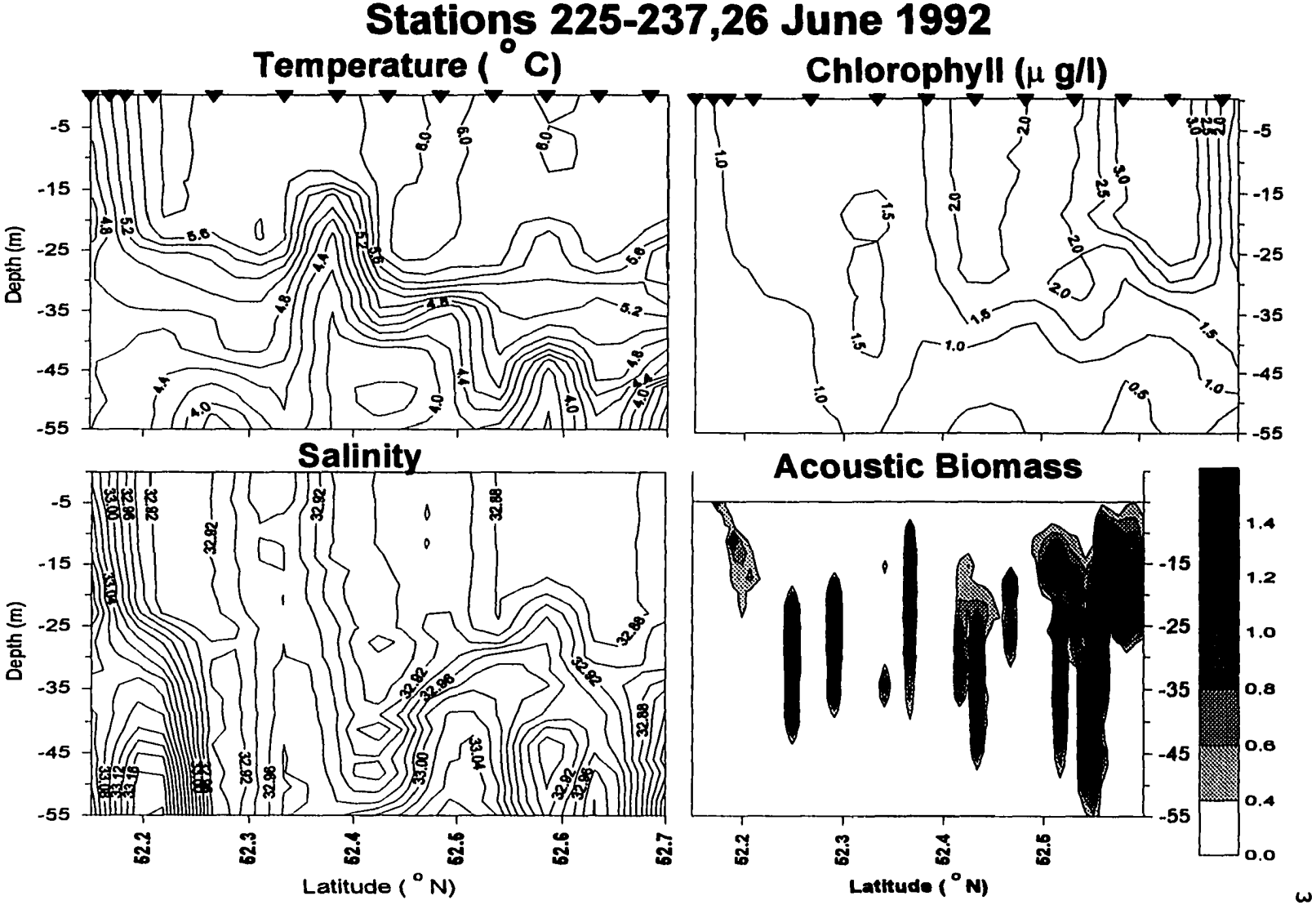

Fig. 3-6. Temperature, salinity, chlorophyll and acoustic biomass (g m^{-3}) profiles along the transect north of Buldir Island (Fig. 2, Stations 149-157). Triangles along upper axes mark CTD station locations. Horizontal axes on upper and lower figures aligned.

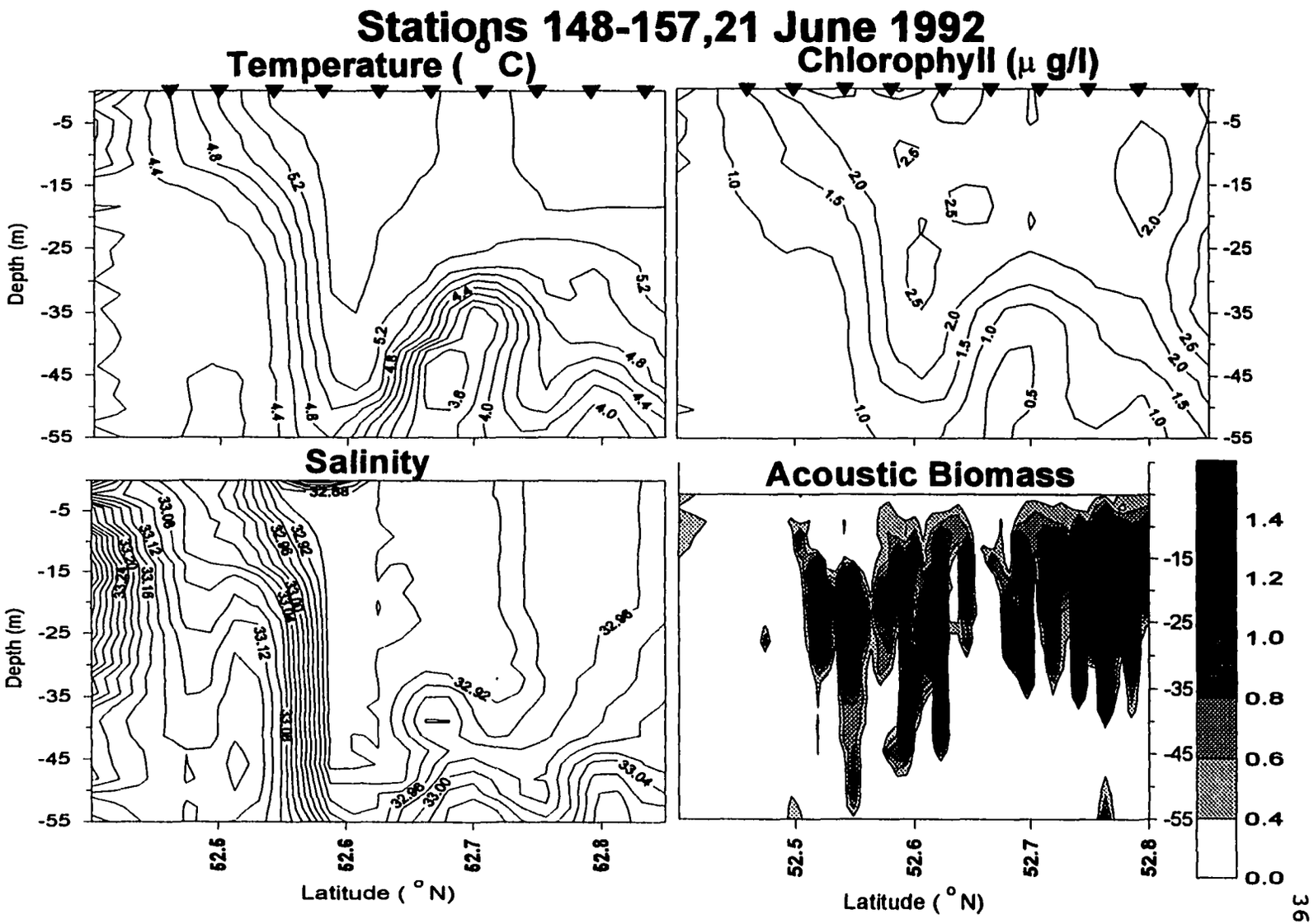

Fig. 3-7. Temperature, salinity, chlorophyll and acoustic biomass (g m^{-3}) profiles along the transect east of Buldir Island (Fig. 2). Triangles along upper axes mark CTD station locations. Horizontal axes on upper and lower figures aligned.

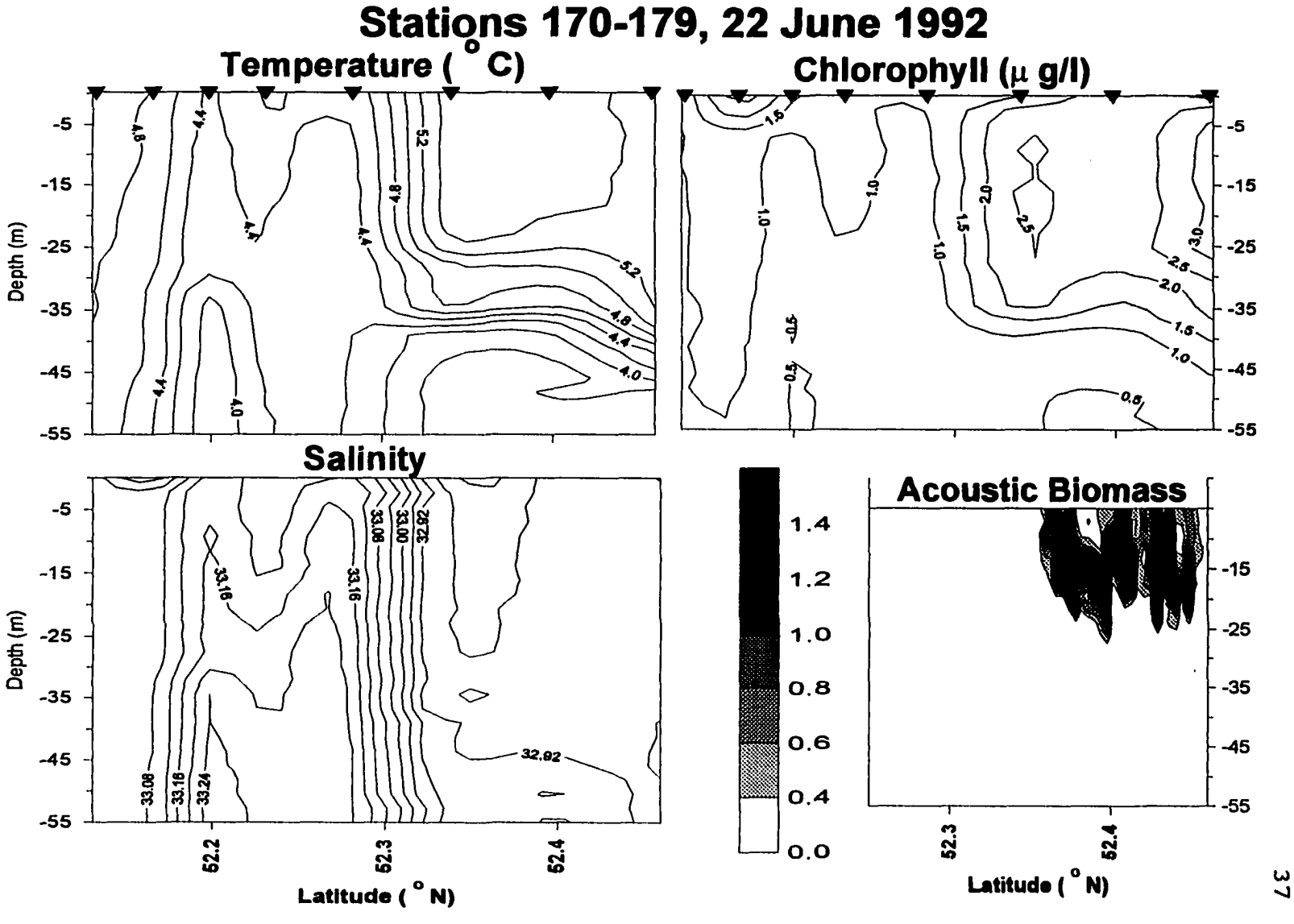

Fig. 3-8. Least auklet densities and transect lines (left); acoustic biomass in the upper mixed layer and contours of sea- surface temperature (°C) (right) around Buldir Island, 13-24 June 1992.

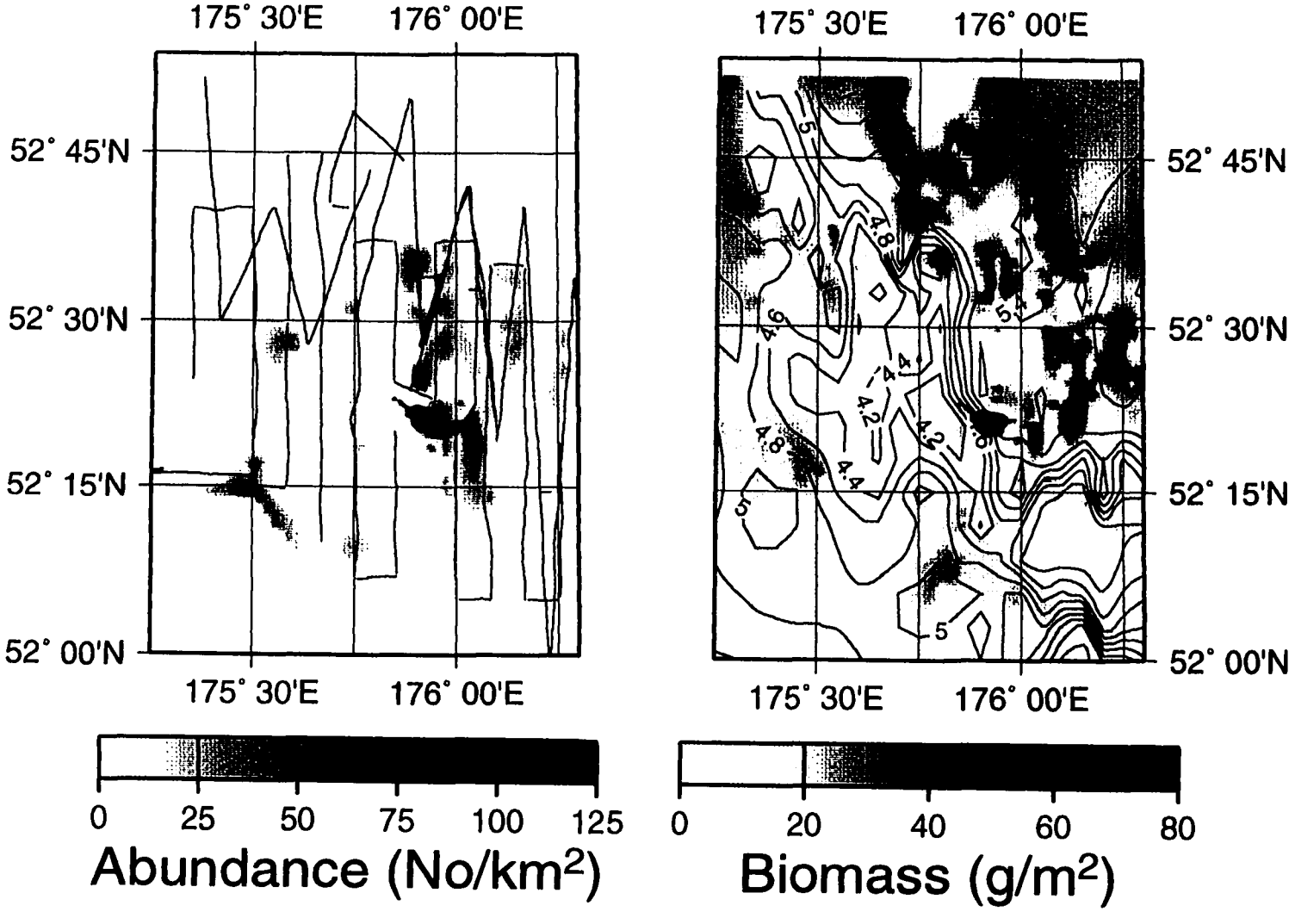

Fig. 3-9. Acoustic biomass in the upper mixed layer and contours of sea surface temperature (°C)(left); least auklet densities in 4 km segments (right) on replicate transects taken north of Kiska Island, 24-28 June 1992.

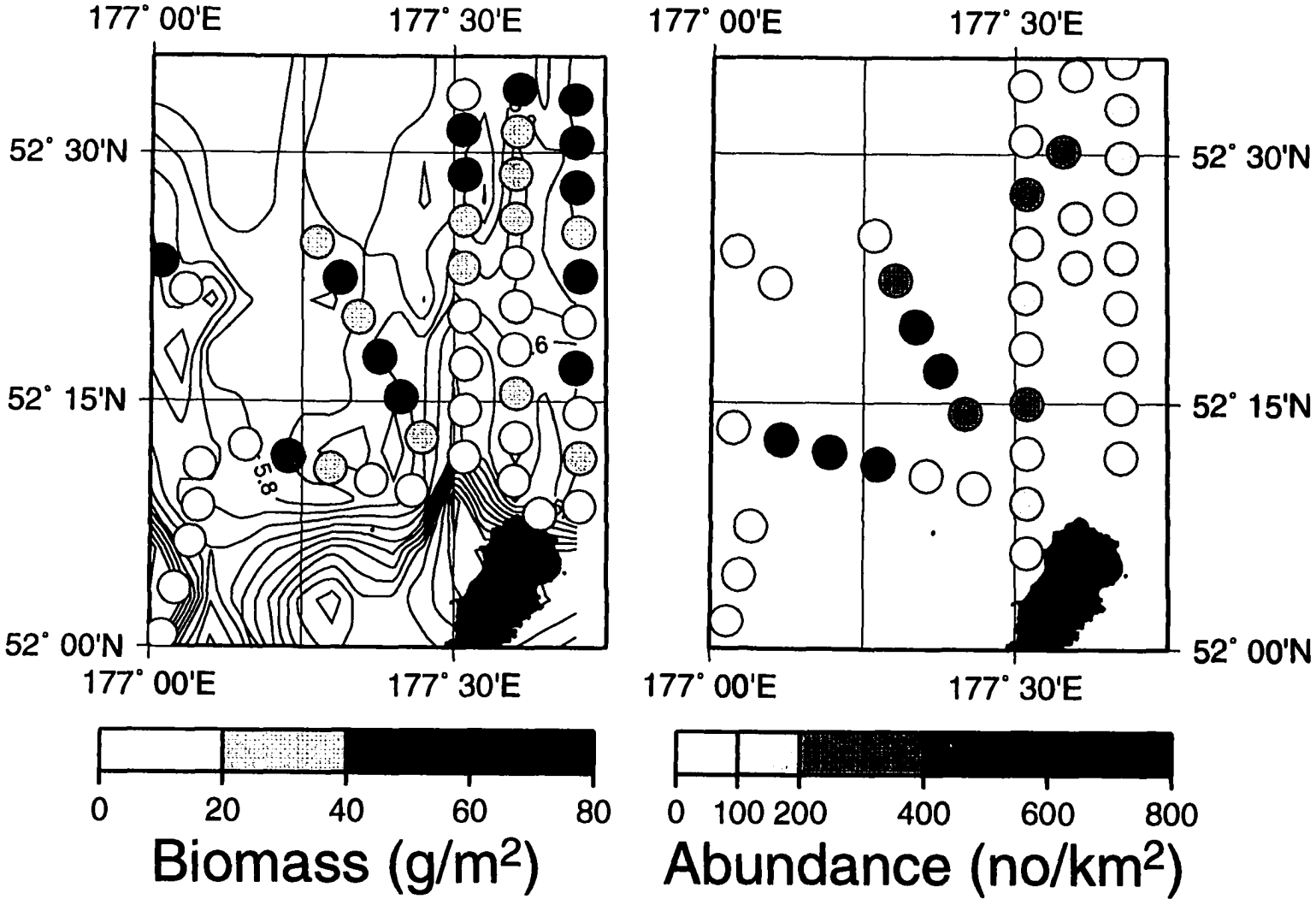

Fig. 3-10. Acoustic biomass (g m^{-3}) measured during Tow 1 north of Kiska Island, 6 June 1992; the solid line depicts the net track (upper left). Salinity (ppt, dashed line), temperature (°C, solid line) and fluorometry (dotted line) profiles from Tow 1 (lower left). Abundance (upper right) and biomass (lower right) of the seven dominant taxa in each discrete sample from Tow 1 (net number printed above the bars).

Abundance, no m-3
200
175
150
125
100
75
50
25
0
2
3
4
5
6
7
8
9
24-40
8-23
9-28
28-42
31-42
11-32
8-32
32-62
Tow Depth, m
NEOCALANUS V
NEOCALANUS IV
NEOCALANUS CRISTATUS V
NEOCALANUS CRISTATUS IV
EUCALANUS BUNGII III
EUCALANUS BUNGII IV
EUCALANUS BUNGII V
EUCALANUS BUNGII AM
NEOCALANUS II
METRIDIA PACIFICA V
EUPHAUSIID EGGS
EUPHAUSIID FURCILIA
METRIDIA PACIFICA IV
NEOCALANUS CRISTATUS II
SAGITTA ELEGANS
NEOCALANUS CRISTATUS III
NEOCALANUS I
CLIONE LIMACINA
PARATHEMISTO PACIFICA
OTHERS

Biomass, g m-3
1.0
0.9
0.8
0.7
0.6
0.5
0.4
0.3
0.2
0.1
0.0
2
3
4
5
6
7
8
24-40
8-23
9-28
28-42
31-42
11-32
8-32
32-62
Tow Depth, m
NEOCALANUS V
NEOCALANUS IV
NEOCALANUS CRISTATUS V
NEOCALANUS CRISTATUS IV
EUCALANUS BUNGII III
EUCALANUS BUNGII IV
EUCALANUS BUNGII V
EUCALANUS BUNGII AM
NEOCALANUS II
AGLANTHA DIGITALE
SAGITTA ELEGANS
METRIDIA PACIFICA V
CLIONE LIMACINA
NEOCALANUS CRISTATUS III
PARATHEMISTO PACIFICA
OTHERS

Fig. 3-11. Acoustic biomass (g m^{-3}) measured during Tow 2 north of Kiska Island, 6 June 1992; the solid line depicts the net track (upper left). Salinity (ppt, dashed line), temperature (°C, solid line) and fluorometry (dotted line) profiles from Tow 2 (lower left). Abundance (upper right) and biomass (lower right) of the seven dominant taxa in each discrete sample from Tow 2 (net number printed above the bars).

Abundance, no m-3
300
250
200
150
100
50
0
2
4
5
6
7
8
9
2-22
39-52
19-40
0-19
0-22
23-52
20-52
Tow Depth, m
NEOCALANUS V
NEOCALANUS IV
NEOCALANUS CRISTATUS V
NEOCALANUS CRISTATUS IV
EUCALANUS BUNGII III
EUCALANUS BUNGII IV
EUCALANUS BUNGII V
EUCALANUS BUNGII AM
EUCALANUS BUNGII AF
EUPHAUSIID FURCILIA
EUCALANUS BUNGII II
NEOCALANUS II
EUKROHNIA HAMATA
METRIDIA PACIFICA V
EUPHAUSIID EGGS
LIMACINA HELICINA
SAGITTA ELEGANS
OTHERS

Biomass, g m-3
1.6
1.4
1.2
1.0
0.8
0.6
0.4
0.2
0.0
2
4
5
6
7
8
9
2-22
39-52
19-40
0-19
0-22
23-52
20-52
Tow Depth, m
NEOCALANUS V
NEOCALANUS IV
NEOCALANUS CRISTATUS V
NEOCALANUS CRISTATUS IV
EUCALANUS BUNGII III
EUCALANUS BUNGII IV
EUCALANUS BUNGII V
EUCALANUS BUNGII AM
AGLANTHA DIGITALE
EUCALANUS BUNGII AF
SAGITTA ELEGANS
EUKROHNIA HAMATA
CLIONE LIMACINA
LIMACINA HELICINA
OTHERS

Fig. 3-12. Acoustic biomass (g m^{-3}) measured during Tow 6 north of Kiska Island, 10 June 1992; the solid line depicts the net track (upper left). Salinity (ppt, dashed line), temperature (°C, solid line) and fluorometry (dotted line) profiles from Tow 6 (lower left). Abundance (upper right) and biomass (lower right) of the seven dominant taxa in each discrete sample from Tow 6 (net number printed above the bars).

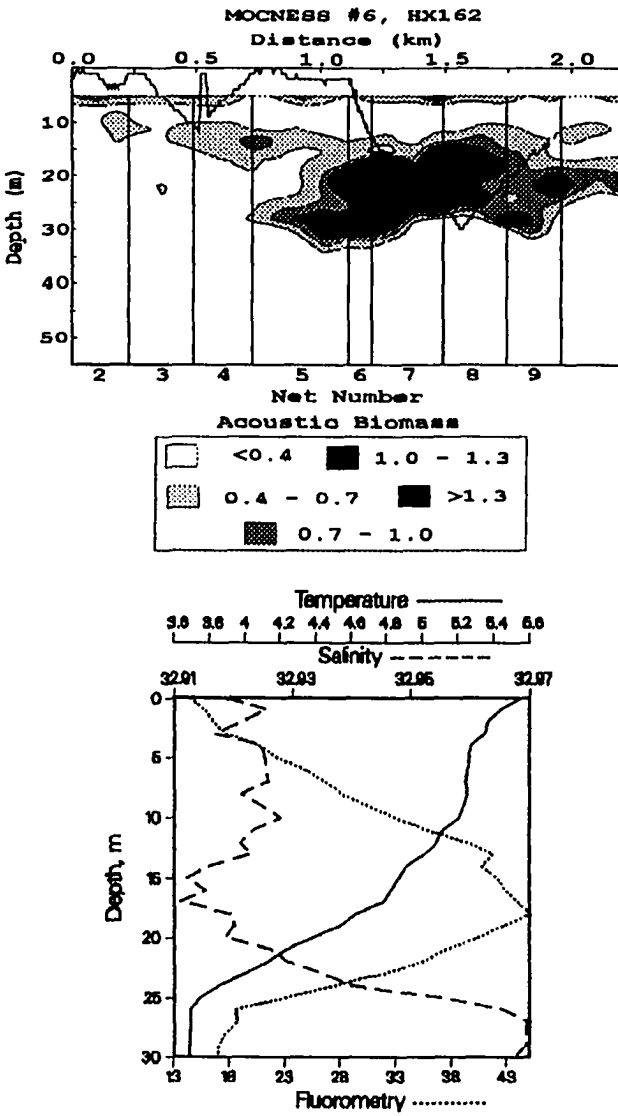

Abundance, no m-3
450
400
350
300
250
200
150
100
50
0
2
3
4
5
6
7
8
9
0-4
1-10
1-12
0-3
2-13
13-25
21-30
12-20
Tow Depth, m
NEOCALANUS V
NEOCALANUS IV
NEOCALANUS CRISTATUS V
NEOCALANUS CRISTATUS IV
EUCALANUS BUNGII III
EUCALANUS BUNGII IV
EUCALANUS BUNGII V
EUCALANUS BUNGII AM
NEOCALANUS III
METRIDIA PACIFICA V
NEOCALANUS CRISTATUS III
EUCALANUS BUNGII II
EUPHAUSIID FURCILIA
METRIDIA PACIFICA IV
SAGITTA ELEGANS
PARATHEMISTO PACIFICA
CLIONE LIMACINA
LIMACINA HELICINA
OIKOPLEURA SP.
OTHERS

Biomass, g m-3
3.5
3.0
2.5
2.0
1.5
1.0
0.5
0.0
2
3
4
5
6
7
8
9
0-4
1-10
1-12
0-3
2-13
13-25
21-30
12-20
Tow Depth, m
NEOCALANUS V
NEOCALANUS IV
NEOCALANUS CRISTATUS V
NEOCALANUS CRISTATUS IV
EUCALANUS BUNGII III
EUCALANUS BUNGII IV
EUCALANUS BUNGII V
EUCALANUS BUNGII AM
SAGITTA ELEGANS
CLIONE LIMACINA
PARATHEMISTO PACIFICA
NEOCALANUS III
METRIDIA PACIFICA V
EUKROHNIA HAMATA
LIMACINA HELICINA
TYPHLOSCOLEX MULLERI
UNKNOWN EGG
OTHERS

Fig. 3-13. Acoustic biomass (g m^{-3}) measured during Tow 19 north of Kiska Island, 26 June 1992; the solid line depicts the net track (upper left). Salinity (ppt, dashed line), temperature (°C, solid line) and fluorometry (dotted line) profiles from Tow 19 (lower left). Abundance (upper right) and biomass (lower right) of the seven dominant taxa in each discrete sample from Tow 19 (net number printed above the bars).

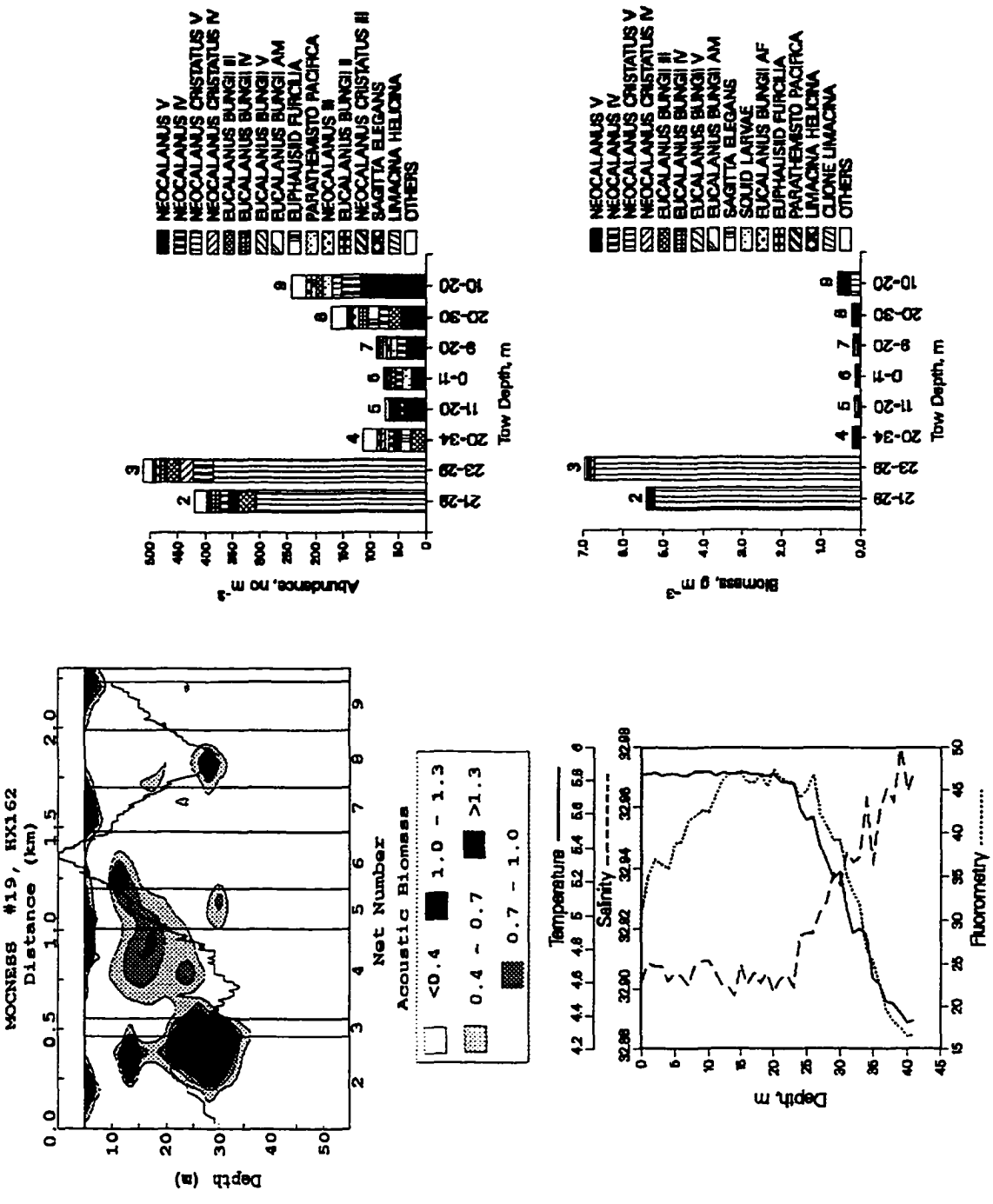

Fig. 3-14. Acoustic biomass (g m^{-3}) measured during Tow 22 west of Kiska Island 27 June 1992; the solid line depicts the net track (upper left). Salinity (ppt, dashed line), temperature (°C, solid line) and fluorometry (dotted line) profiles from Tow 22 (lower left). Abundance (upper right) and biomass (lower right) of the seven dominant taxa in each discrete sample from Tow 22 (net number printed above the bars).

NEOCALANUS V
NEOCALANUS IV
NEOCALANUS CRISTATUS V
NEOCALANUS CRISTATUS IV
EUCALANUS BUNGII III
EUCALANUS BUNGII IV
EUCALANUS BUNGII V
EUCALANUS BUNGII AM
METRIDIA PACIFICA V
PARATHEMISTO PACIFICA
METRIDIA PACIFICA IV
EUPHAUSIID FURCILIA
SAGITTA ELEGANS
NEOCALANUS III
NEOCALANUS CRISTATUS III
EUKROHNIA HAMATA
NEOCALANUS CRISTATUS II
EUCALANUS BUNGII AF
LIMACINA HELICINA
OTHERS
1
2
3
4
5
6
7
8
2-9
10-24
25-51
30-51
10-30
1-71
12-31
26-51
10-26
Tow Depth, m

NEOCALANUS V
NEOCALANUS IV
NEOCALANUS CRISTATUS V
NEOCALANUS CRISTATUS IV
EUCALANUS BUNGII III
EUCALANUS BUNGII IV
EUCALANUS BUNGII V
EUCALANUS BUNGII AM
EUCALANUS BUNGII AF
SAGITTA ELEGANS
METRIDIA PACIFICA V
CLIONE LIMACINA
EUPHAUSIID FURCILIA
EUKROHNIA HAMATA
PARATHEMISTO PACIFICA
LIMACINA HELICINA
NEOCALANUS III
OTHERS
1
2
3
4
5
6
7
8
2-9
10-24
25-51
30-51
10-30
1-71
12-31
26-51
10-26
Tow Depth, m

Fig. 3-15. Acoustic biomass (g m^{-3}) measured during Tow 11 west of Buldir Island, 19 June 1992; the solid line depicts the net track (upper left). Salinity (ppt, dashed line), temperature (°C, solid line) and fluorometry (dotted line) profiles from Tow 11 (lower left). Abundance (upper right) and biomass (lower right) of the seven dominant taxa in each discrete sample from Tow 11 (net number printed above the bars).

NEOCALANUS V
NEOCALANUS IV
NEOCALANUS CRISTATUS V
NEOCALANUS CRISTATUS IV
EUCALANUS BUNGII III
EUCALANUS BUNGII IV
EUCALANUS BUNGII V
EUCALANUS BUNGII AM
EUCALANUS BUNGII II
EUKROHNIA HAMATA
EUPHAUSIID FURCILIA
EUCALANUS BUNGII AF
NEOCALANUS III
METRIDIA PACIFICA V
METRIDIA PACIFICA AF
CALANUS MARSHALLAE II
OTHERS
2
3
4
5
6
7
8
9
0-3
0-19
20-49
49-82
52-85
21-51
20-84
49-84
Tow Depth, m

NEOCALANUS V
NEOCALANUS IV
NEOCALANUS CRISTATUS V
NEOCALANUS CRISTATUS IV
EUCALANUS BUNGII III
EUCALANUS BUNGII IV
EUCALANUS BUNGII V
EUCALANUS BUNGII AM
EUCALANUS BUNGII AF
EUKROHNIA HAMATA
AGLANTHA DIGITALE
SAGITTA ELEGANS
DIMOPHYES ARCTICA
OTHERS
2
3
4
5
6
7
8
9
0-3
0-19
20-49
49-82
52-85
21-51
20-84
49-84
Tow Depth, m

Fig. 3-16. Major current patterns in the western Aleutians and approximate location of front dividing Bering Sea from Pacific water. Upper: normal condition with flow northward through Near Strait. Lower: flow anomaly, with suspended flow through Near Strait and eastward flow from the Kamchatka Basin on the north side of the archipelago (see Stabeno and Reed, 1992; Reed and Stabeno, 1993).

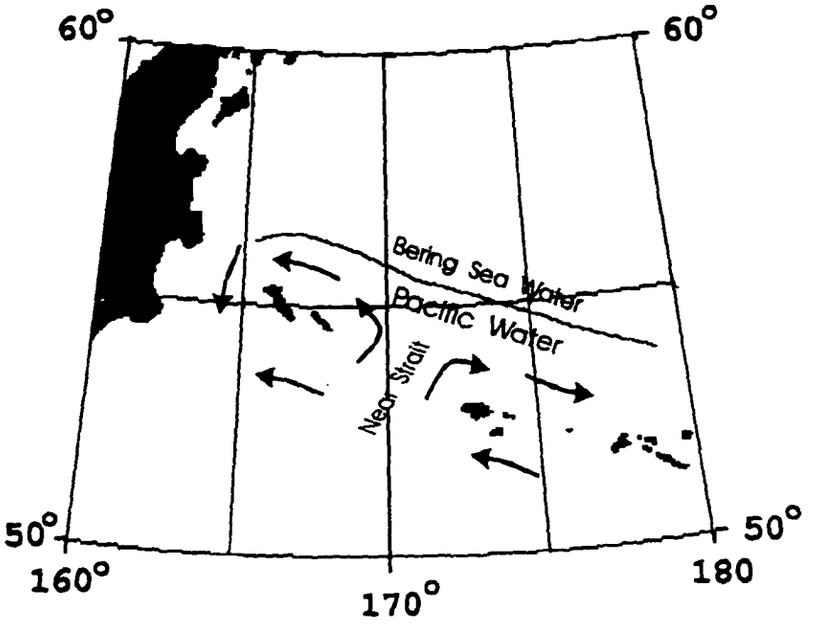

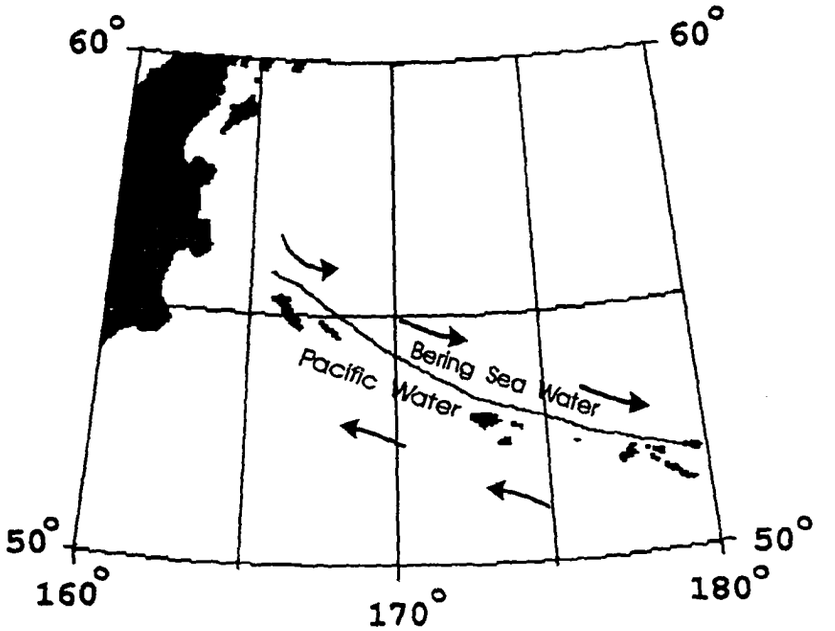

4. Life history influences on zooplankton abundance, biomass, species composition and distribution in the western Aleutian Islands, July 1993.

During the first cruise of the Aleutian Bird project, from 6 June to 1 July, 1992, acoustic data and net samples documented dense layers of *Neocalanus cristatus, N. plumchrus* and *N. flemingeri* in the surface mixed layer over resident Bering Sea water to the north of the Aleutian Islands. Based on the distribution of foraging least auklets, these layers apparently provided an important food source for the auklets during the first half of their nesting season. The second cruise, from 7 July to 6 August 1993, took place approximately one month later in the seasonal cycle of interzonal copepods. Most of the *N. cristatus* and *N. flemingeri* were absent from the upper 100 m of the water column (see below). Although some *Neocalanus* were still present in the surface layers, their concentrations had substantially declined and the species composition had shifted from *N. cristatus* and *N. flemingeri* to *N. plumchrus*, which tends to complete its foraging period somewhat later than the former taxa (Miller and Clemons, 1988). In this section, data are presented to illustrate the changes in species composition

and biomass in July-August 1993 relative to samples collected in June of 1992. Tow locations are illustrated in Figs. 4-1, a-b. Tows within the Delarov are covered in the next chapter.

Statistics:

Statistical analysis of acoustic data is complicated because individual acoustic records are highly autocorrelated, and the sample distribution is contagious and non-normal. Standard parametric statistical techniques are therefore not valid when analyzing acoustic data. Statistical analysis was limited to the following procedure. ADB for a given region (as defined below) was integrated to 40 m depth, the approximate depth of the pycnocline, linked into a single long transect and treated as a time series. Autocorrelation analysis was run on the linked data set to estimate the lag between data points required to minimize the autocorrelation. A random number technique was used to select a starting point along the data set and a transect was extracted equal in length to the minimum autocorrelation lag. A mean was computed for the transect and served as an individual data point in subsequent analysis. The transect was replaced and the procedure repeated 1000 times. The means were ranked and

the 25th and 975th values were taken as the upper and lower 95% confidence intervals for the mean estimate. Bootstrapping was suggested by Lyman McDonald, WEST Inc., 2003 Central Ave, Cheyenne, WY 82001.

Results

A series of net tows, acoustic transects and CTD transects was done north of Gareloi, and north and west of Kiska Islands (Fig. 4-1, 4-2, 4-3). Sea surface records of temperature and 420 kHz ADB, integrated to 40 m depth, were gridded and contoured to document any horizontal patterns of ADB relative to surface water masses (Fig. 4-4). In addition, north-south CTD transects were plotted to document subsurface patterns of ADB relative to water mass properties (Fig. 4-5).

Distinctive frontal patterns of surface salinity and temperature were absent north of Gareloi Island (Fig. 4-4). Some patches of elevated ADB were present near the island but patches with biomass of more than 40 g m^{-2} were not observed. Most of the ADB was concentrated in the upper 40 m above the pycnocline and below 100 m depth (Fig. 4-5a, b). Some of the scattering below 100 m resulted from animals not taken in the plankton nets. Cold Intermediate Bering Sea Water, with temperatures

below 4.0°C beneath the pycnocline, was generally absent from the region north of Gareloi Island. Chlorophyll concentrations were under 1 $\mu g\ l^{-1}$, except in a small warm region between 52.0 and 52.1° N. ADB above the pycnocline averaged 13.7 $g\ m^{-2}$ (Table 4-1).

The Bering Sea front near Kiska Island in late July 1993 was expressed at the surface by relatively dense packing of isothermal lines between 52° and 52° 15' N. (Fig. 4-4b). ADB integrated to 40 m depth was elevated in the frontal regions. The average ADB for Kiska was lower than values at Gareloi Island (Table 4-1). The surface mixed layer north of Kiska was separated from the Bering Sea intermediate layer by a fairly intense pycnocline at about 35 m depth (Fig. 4-5c). Bering Sea Intermediate Water with temperatures below 4°C, was present south to 52.25° N. near the north end of Kiska. Most of the ADB detected by the 200 kHz echosounder was in a secondary halocline at about 100 to 160 m depth (Fig. 4-5a, 4-5c). The patches of intense scattering in the deep halocline were probably not from zooplankton, as they could not be accounted for by net samples through the layer. In contrast, thermal stratification north of Kiska during June, 1992, was much weaker, chlorophyll concentrations were higher, most of the biomass detected by the 200 kHz

system was in the mixed layer above the pycnocline (Fig. 4-5d), and mean ADB in the upper 45 m was more than twice as high as in July 1993 (Table 4-1).

Analysis of variance on the six most abundant taxa in net tows above the pycnocline revealed significant differences in the abundance of *Eucalanus bungii* stages IV, V, adult males and adult females between water masses and regions (Table 4-2). Abundances of late stage *Eucalanus bungii* were lower in Bering Sea water relative to Pacific water in the Gareloi Island region and south of Kiska Island. *Neocalanus* stage IV was higher in Bering Sea water than in Pacific water near Kiska. There were significantly fewer *Oikopleura* in Bering Sea water than in the Pacific groups and all three groups were significantly different with respect to abundance of *Limacina helicina* (Table 4-2).

Canonical correlation analysis relating physical variables to abundance of the most abundant taxonomic groups near Gareloi Island revealed significant correlations for the first canonical variable (Table 4-3). The group one scores of the first canonical variable were positively correlated with fluorescence and negatively correlated with sigma-t and depth. *Neocalanus plumchrus/flemingeri, Calanus pacificus* and *Limacina*

helicina were positively correlated, and *Neocalanus cristatus* and euphausiid furcilia were negatively correlated with the group 2 scores (Table 4-3). The above correlations indicate that *Neocalanus plumchrus/flemingeri, Calanus pacificus* and *Limacina helicina* were more abundant in shallower conditions with lower water density and elevated fluorescence and *Neocalanus cristatus* and euphausiid furcilia were more abundant in deeper layers, where density was higher and fluorescence lower. No significant correlation occurred for analyses on data from Bering Sea water to the north and west of Kiska Island.

The region north of Gareloi and Kiska Islands had differences in the vertical distribution of zooplankton in the upper 45 m. Highest ADB occurred in the upper 40 m near Gareloi (Fig. 4-6). Thermal stratification was fairly weak and fluorescence levels were low. The layer at 80 m depth (Fig. 4-6) had elevated concentrations of *Eukrohnia hamata, Dimophyes arctica* and *Eucalanus bungii.*

In contrast to Gareloi, the pycnocline north of Kiska Island was strong (Fig. 4-7). Substantial thermal and halo-discontinuities were observed at 30 to 50 m depth and fluorescence in the pycnocline was elevated relative to the overlaying mixed layer. Zooplankton north of Kiska

Island were patchily distributed, both vertically and horizontally. When present, elevated ADB and zooplankton densities were commonly observed in the pycnocline. Sound scattering above the pycnocline was often close to background levels. Zooplankton in the pycnocline scattering layer consisted primarily of *Neocalanus plumchrus* and *Eucalanus bungii*. The scattering layer below 120 m depth contained *Thysanoessa longipes, Eukrohnia hamata, Neocalanus cristatus, Metridia pacifica* and *Dimophyes arctica*.

Discussion:

Mean ADB computed for north of Kiska in June 1992, was lower than means computed from net tows (Chapter 2) for two reasons. Since nets were used primarily to scale the acoustics and document prey concentrations where auklets were foraging, tow locations were not random and the mean of the net samples may have overestimated regional zooplankton biomass. Conversely, ADB estimates in excess of 7 g m^{-3}, the maximum value from net tows, were considered artifact and dropped from the analysis. Therefore, ADB is a conservative measure and may underestimate actual zooplankton biomass since nets did not necessarily sample regions of maximum zooplankton

abundance. If all ADB values from Bering Sea water are incorporated into the average, the mean ADB estimate for Bering Sea water north of Kiska during June, 1992, was 35 g m^{-2}.

Lower abundances of late stage *Eucalanus bungii* from the Bering Sea water north and west of Kiska relative to Pacific water south of Kiska and near Gareloi Island suggest that the successional stage of the zooplankton community in Bering Sea water was retarded relative to that of Pacific water.

Elevated zooplankton abundance in four of the six tows from north and west of Kiska occurred in dense patches near the pycnocline at 15-50 m depth. Due to the presence of cold intermediate Bering Sea water north of Kiska, the pycnocline was more intense than north of Gareloi. The stronger pycnocline was apparently associated with a deeper chlorophyll maximum and deeper distribution of zooplankton patches than in waters north of Gareloi, where zooplankton abundance and biomass were usually greatest in the surface and declined gradually with depth. Foraging auklets were absent north of Kiska, possibly because the zooplankton forage was too deep. In contrast, small flocks of least auklets were observed north of Gareloi and were associated with regions of elevated

surface scattering (Hunt, personal com.). Foraging conditions relative to water mass types were therefore reversed compared to the prevailing pattern in June, 1992, when foraging least auklets were observed primarily in Bering Sea water. The presence of Bering Sea Intermediate Water may have enhanced foraging conditions for nesting auklets early in the season by retarding the descent of their primary prey to overwintering depths but inhibited foraging later in the season by restricting the remaining forage to the pycnocline layer below the range of diving least auklets. Least auklets dive to about 15 m depth (Hunt, personal com.).

Although auklets were present north of Gareloi Island, they occurred over sparsely scattered surface patches of *Neocalanus* stage V. Foraging auklets were much more abundant in Delarov Pass and off the south end of Kiska Island, where small-scale tidally - generated turbulence and currents were influencing prey distributions. The final two chapters examine the potential influence of tidal currents on the prey distribution of least auklets in the Delarov Islands and southern Kiska Island and artifacts which may be introduced into acoustic data by turbulence.

Table 4-1. Mean acoustic biomass (g m^{-2}) in the upper mixed layer from north of Kiska Island in June 1992 and July 1993, from north and south of the Bering Sea front near Buldir Island in June 1992, and from north of Gareloi Island in July 1993. SK = skewness, KR = kurtosis, UC = Upper 95% confidence limit, LC = lower 95% confidence limit.

Location	Mean	SK	KR	UC	LC
N. Kiska 1993	6.8	-0.75	1.51	9.7	2.1
N. Gareloi 1993	13.7	-0.03	-0.03	21.4	6.5
N. Kiska 1992	24.2	0.95	-0.21	45.3	13.1
N. Buldir 1992	18.9	0.58	-0.28	30.9	10.2
S. Buldir 1992	13.3	0.41	-0.94	23.7	6.1

Table 4-2. Analysis of variance on the six most abundant species in any tow at stations grouped by region and water mass type. Samples were collected in July 1993 from south and north of both Gareloi and Kiska Islands. P is the probability of equal means.

Group 1 (Pacific Water south of Kiska): Tows 17, 18, 19, 20, 21
Group 2 (Bering Sea Water north and west of Kiska): Tows 14, 15, 16, 22, 23, 24
Group 3 (Pacific Water north and south of Gareloi): Tows 1, 2, 3, 4, 7, 8

	Group Number			
Taxa	1	2	3	P
EUCALANUS BUNGII I	1.15	1.53	0.00	0.260
EUCALANUS BUNGII II	6.49	6.84	2.99	0.476
EUCALANUS BUNGII III	24.66	43.65	26.06	0.191
EUCALANUS BUNGII IV	20.14	16.66	52.48	0.002*
EUCALANUS BUNGII V	28.18	5.78	27.80	0.000*
EUCALANUS BUNGII AM	22.91	6.07	32.81	0.000*
EUCALANUS BUNGII AF	7.35	1.17	2.99	0.002*
NEOCALANUS II	1.21	1.08	0.00	0.405
NEOCALANUS III	12.76	19.20	13.74	0.623
NEOCALANUS IV	14.06	42.49	23.66	0.038*
NEOCALANUS V	18.88	25.31	21.68	0.738
NEOCALANUS CRISTATUS II	2.28	1.72	1.12	0.032*
NEOCALANUS CRISTATUS III	2.57	2.00	2.22	0.851
NEOCALANUS CRISTATUS IV	4.76	1.34	1.96	0.096
NEOCALANUS CRISTATUS V	1.96	1.14	2.48	0.204
CALANUS MARSHALLAE V	2.27	0.00	1.62	0.394
CALANUS PACIFICUS V	1.27	1.22	1.14	0.705
CALANUS PACIFICUS AF	1.36	1.06	1.04	0.082
METRIDIA PACIFICA IV	1.19	1.78	0.00	0.292
METRIDIA PACIFICA V	4.04	3.26	3.37	0.942

Table 4-2. Continued.

Taxa	Group Number 1	2	3	P
METRIDIA PACIFICA AF	3.12	1.05	0.00	0.012*
ACARTIA LONGIREMIS V	0.00	0.00	1.04	0.357
ACARTIA LONGIREMIS AF	1.22	0.00	0.00	0.107
PSEUDOCALANUS 2 MM AF	1.85	0.00	1.13	0.034*
SCOLECITHRICELLA OVATA V	0.00	1.57	0.00	0.465
EUPHAUSIID CALYPTOPIS	1.19	1.03	1.04	0.018*
EUPHAUSIID FURCILIA	3.93	2.48	7.73	0.000*
THYSANOESSA JUVENILES	1.79	1.31	2.68	0.277
THYSANOESSA LONGIPES	1.39	1.57	0.00	0.163
HIPPOLYTIDAE ZOEA	1.03	1.06	1.08	0.482
PARATHEMISTO PACIFICA	9.12	8.04	4.13	0.075
BARNACLE CYPRID	1.05	0.00	1.04	0.097
SAGITTA ELEGANS	5.08	7.16	4.41	0.348
EUKROHNIA HAMATA	5.18	1.69	1.08	0.001*
OIKOPLEURA SP.	3.61	1.17	4.21	0.002*
LIMACINA HELICINA	3.68	1.31	2.48	0.000*
DIMOPHYES ARCTICA	1.02	1.01	1.01	0.477

Table 4-3. Canonical correlation analysis on MOCNESS tows from north and south of Gareloi Islands in July 1993. Tows: 1, 2, 3, 4, 7, 8.

Physical variables used:

1. **Acoustically determined biomass (420 kHz).**
2. **Sigma-t.**
3. **Depth of net (m) normalized for volume filtered.**
4. **Fluorescence normalized for volume filtered.**

Biological variables = abundances (no m^{-3}) of following groups:

1. *Neocalanus* **IV & V**
2. *Neocalanus cristatus* **V**
3. *Neocalanus cristatus* **IV**
4. *Eucalanus bungii* **adult**
5. *Metridia pacifica* **adult**
6. *Calanus pacificus* **V**
7. **Euphausiid furcilia**
8. *Parathemisto pacifica*
9. *Limacina helicina*

*** Canonical Correlations Statistics ***

	Canonical Correlations	Wilks Lambda	Raos F	Num. df	Denom df	Prob. of Larger F
1	0.8536	0.0691	1.999	36	69.2	0.0068
2	0.8130	0.2547	1.398	24	55.7	0.1514
3	0.4648	0.7512	0.439	14	40.0	0.9509
4	0.2043	0.9582	0.153	6	21.0	0.9864

Table 4-3. Continued

Correlations Between the Group One Variables and the Group One Canonical Scores

	1
1	-0.1123
2	-0.7932
3	-0.7976
4	0.4994

Correlations Between the Group Two Variables and the Group Two Canonical Scores

	1
1	0.4796
2	-0.5323
3	-0.6279
4	-0.0560
5	0.2613
6	0.4472
7	-0.3959
8	0.0583
9	0.8224

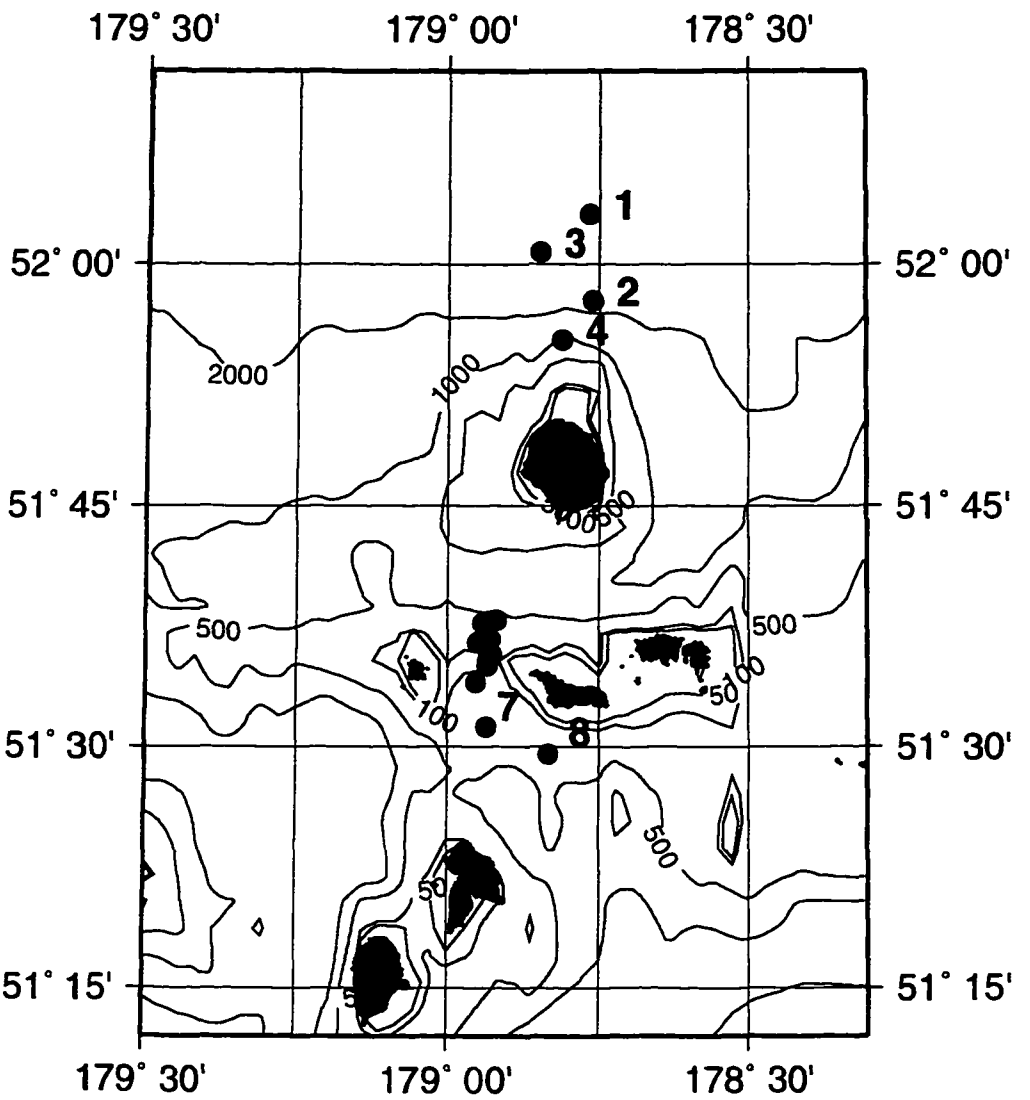

Figure 4-1a. Locations of net tows taken north of Gareloi Island and south of Delarov Pass, July 1993. Bathymetry in meters.

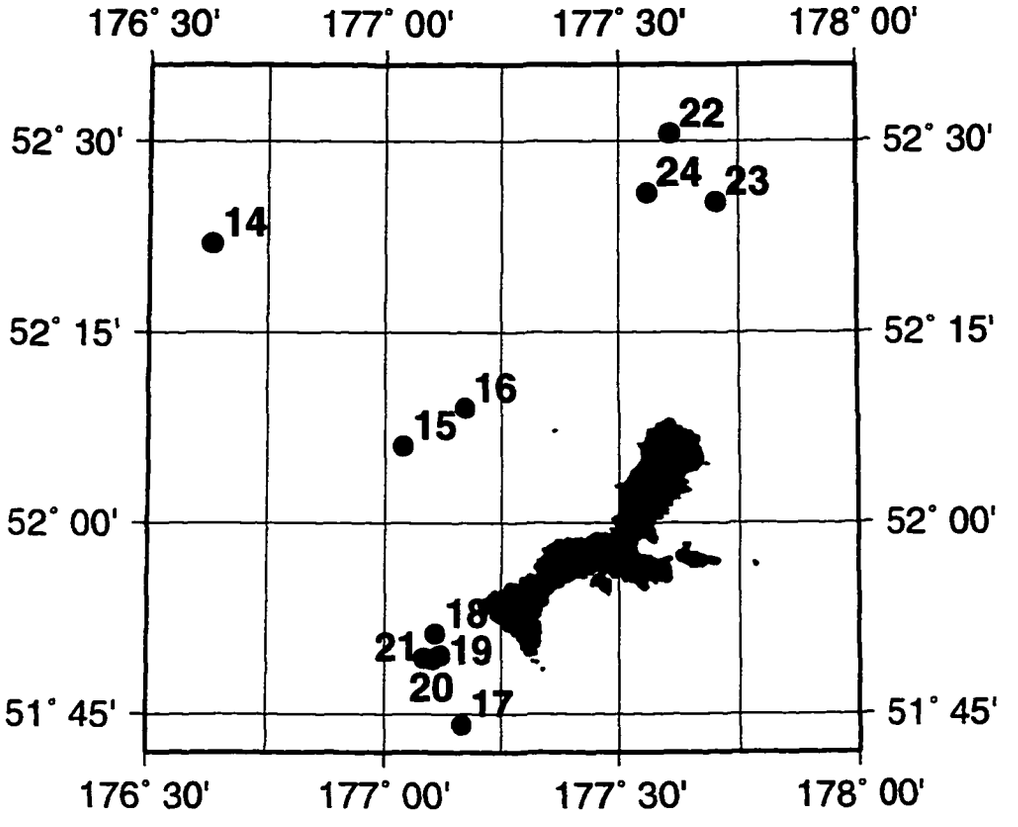

Figure 4-1b. Locations of net tows taken in the Kiska region, July-August 1993.

Figure 4-2. CTD and acoustic transects taken north of Gareloi (left) and Kiska (right) Islands, July 1993.

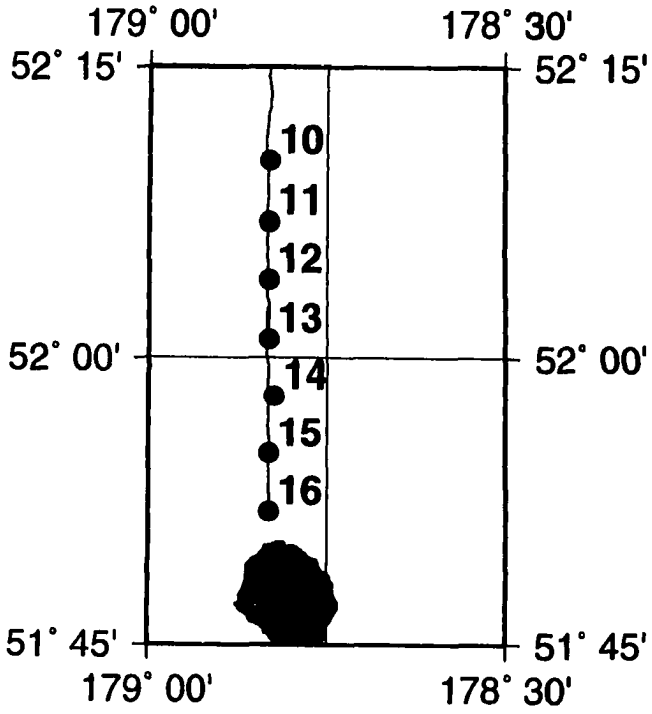

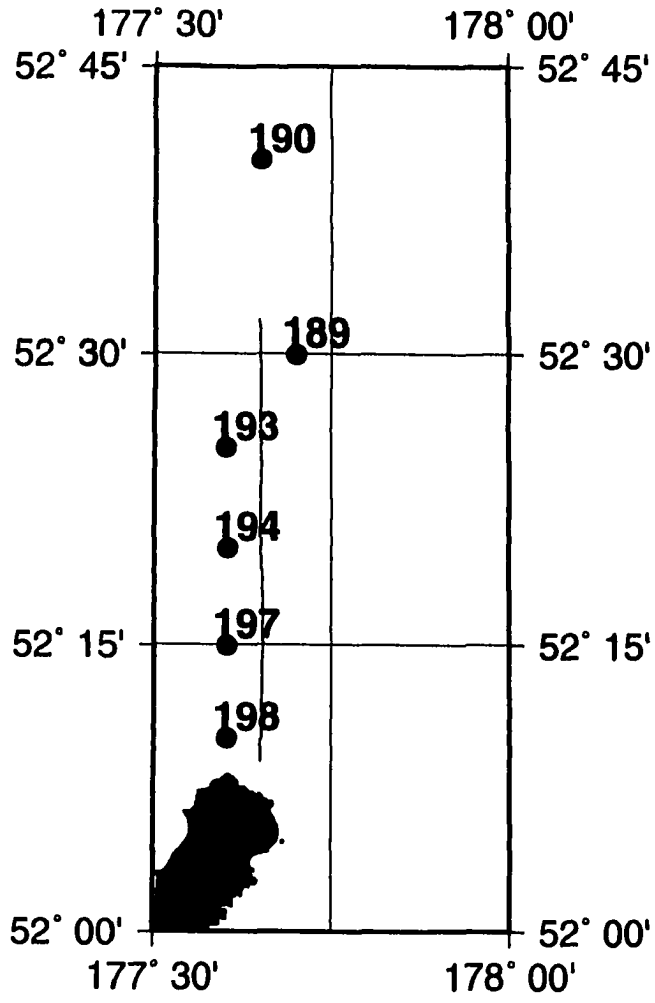

Figure 4-3. Acoustic transect run north of Gareloi Island, 9-12 July 1993 (left) and north and west of Kiska Island, 22-25 and 28-29 July 1993 (right).

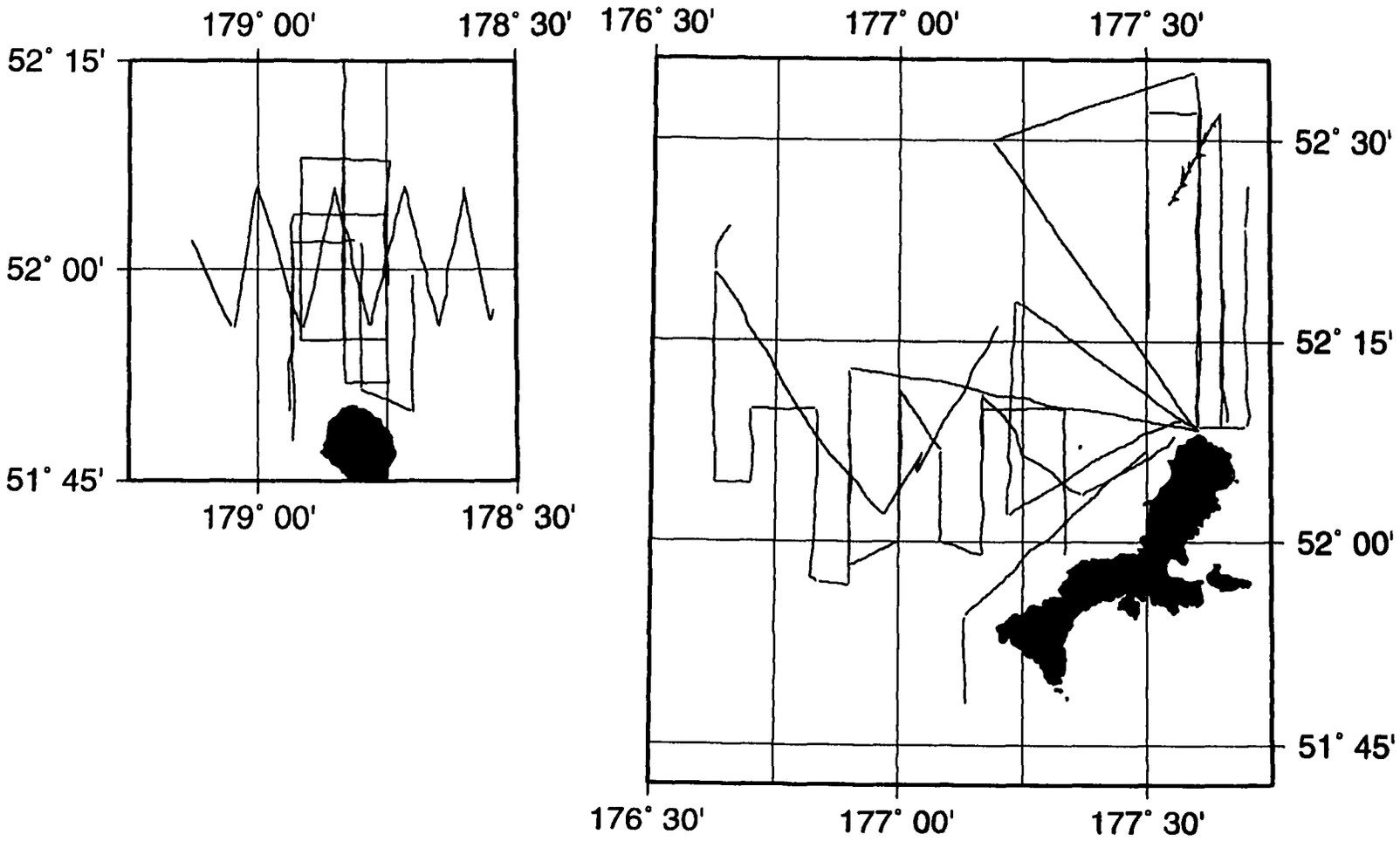

Figure 4-4. Acoustic biomass (g m^{-2}) integrated to 40 m depth and contours of sea surface temperatures (°C, contour interval 0.4) from transect data taken north of Gareloi Island, 9-12 July 1993 (left), and from north and west of Kiska, 22-25 and 28-29 July 1993 (right).

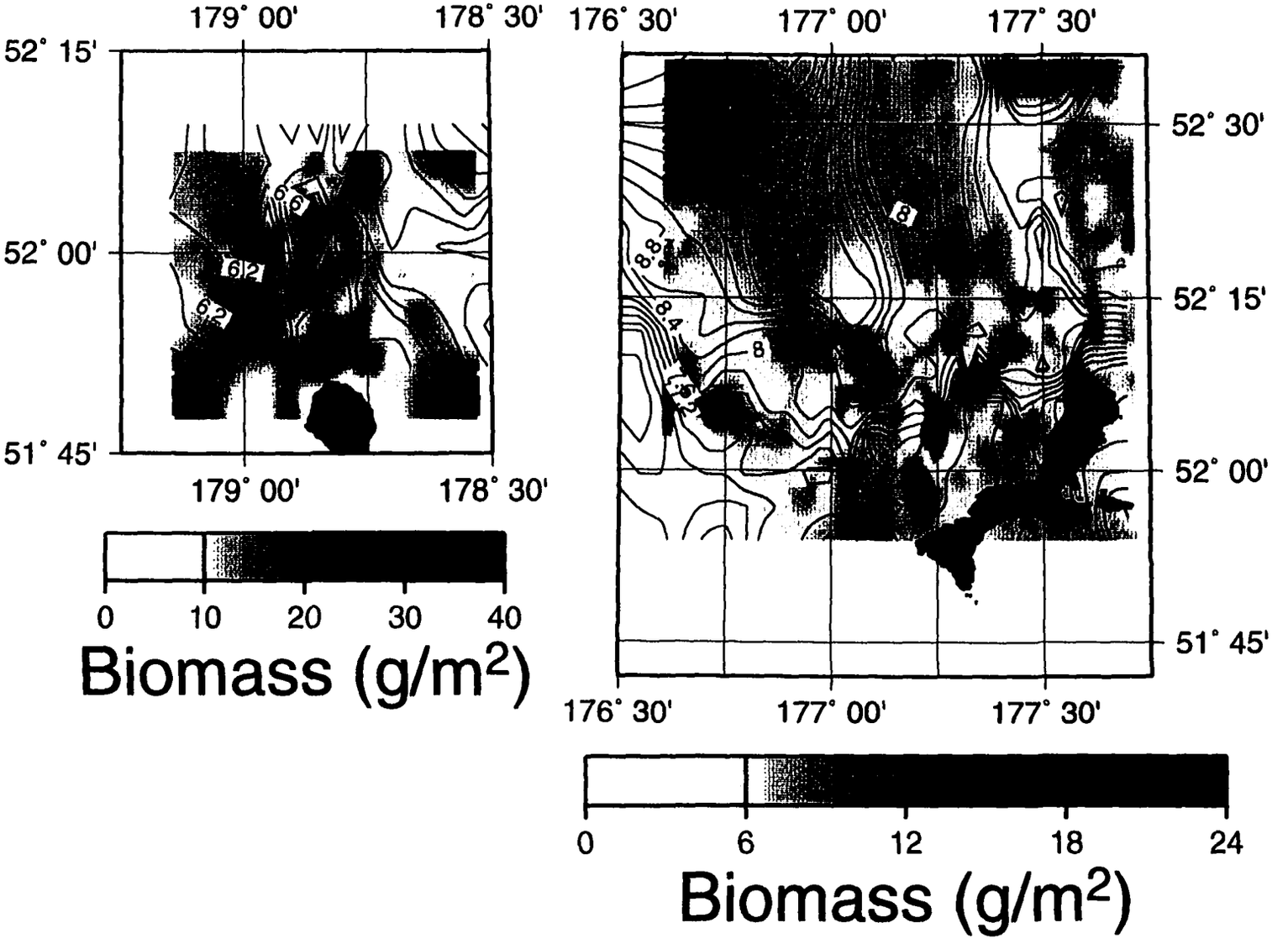

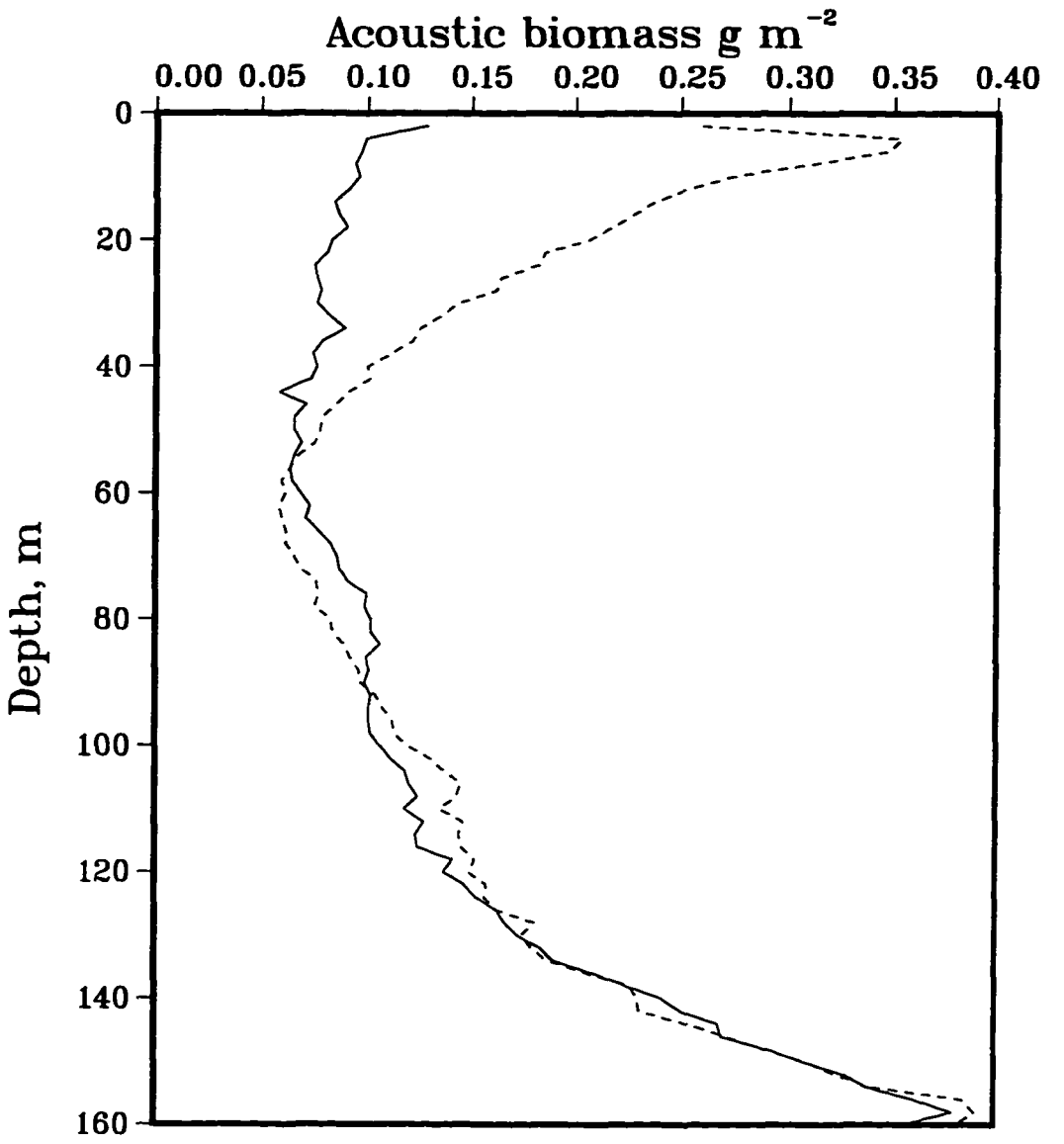

Figure 4-5a. Average acoustic biomass (420 kHz) from north of Gareloi Island (solid line) and from north and west of Kiska Island (dashed line), July 1993.

Figure 4-5b. Profiles of temperature, salinity, chlorophyll and acoustic biomass (g m^{-3}) taken north of Gareloi Island. Triangles along upper axes mark CTD station locations. Transect locations in Fig. 4-2. Horizontal axes on upper and lower figures aligned.

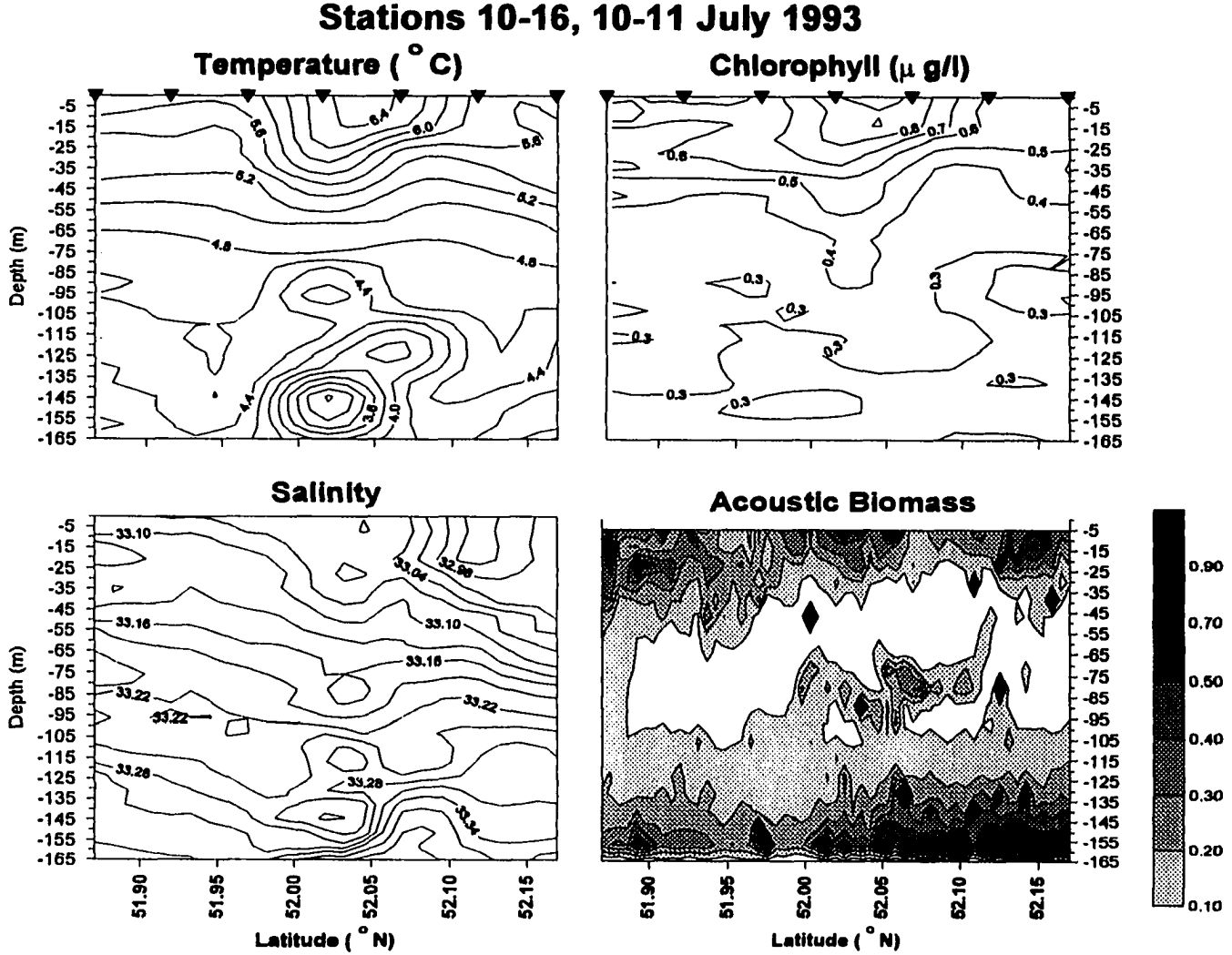

Figure 4-5c. Profiles of temperature, salinity, chlorophyll and acoustic biomass (g m^{-3}) taken north of Kiska Island. Triangles along upper axes mark CTD station locations. Transect locations in Fig. 4-2. Horizontal axes on upper and lower figures aligned.

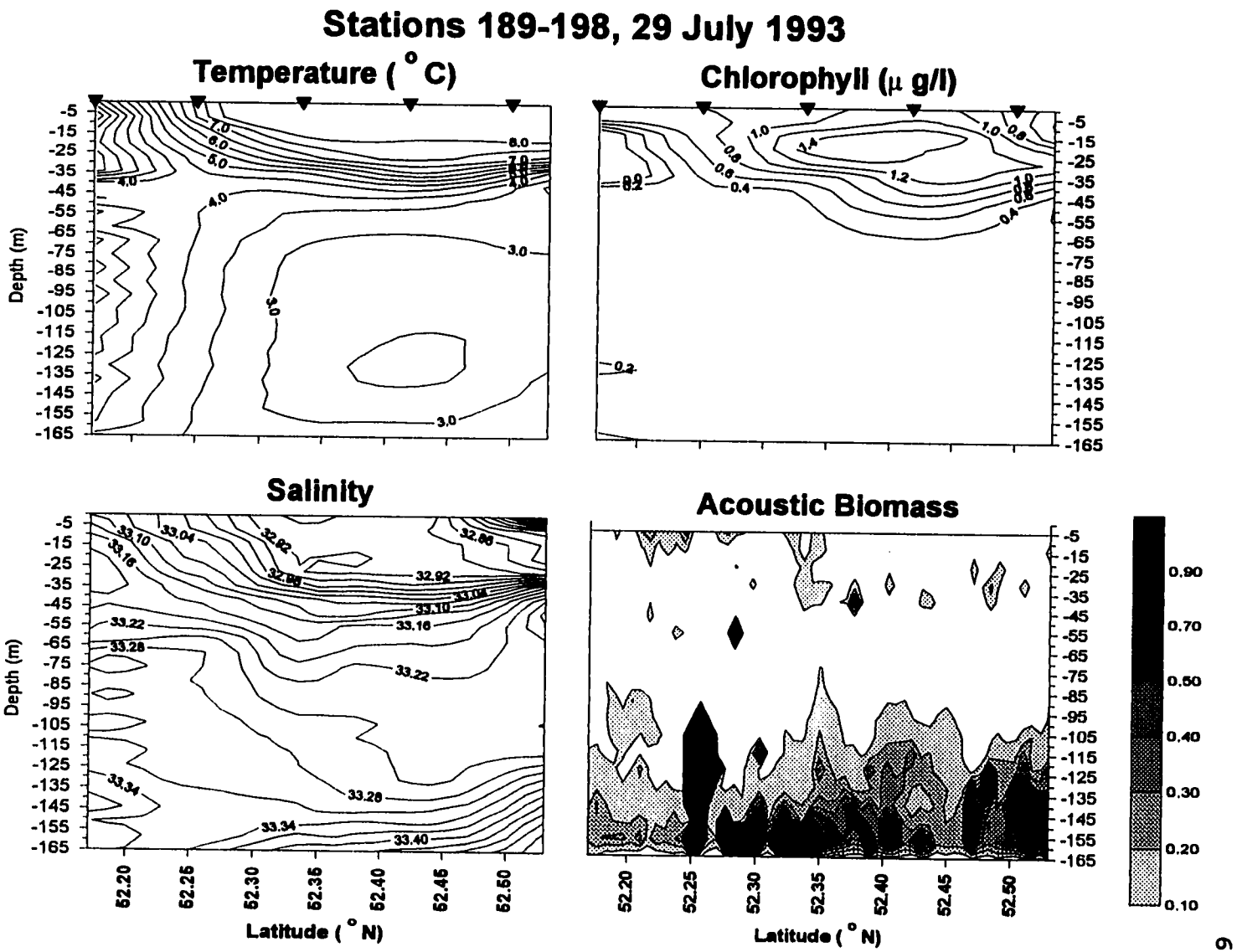

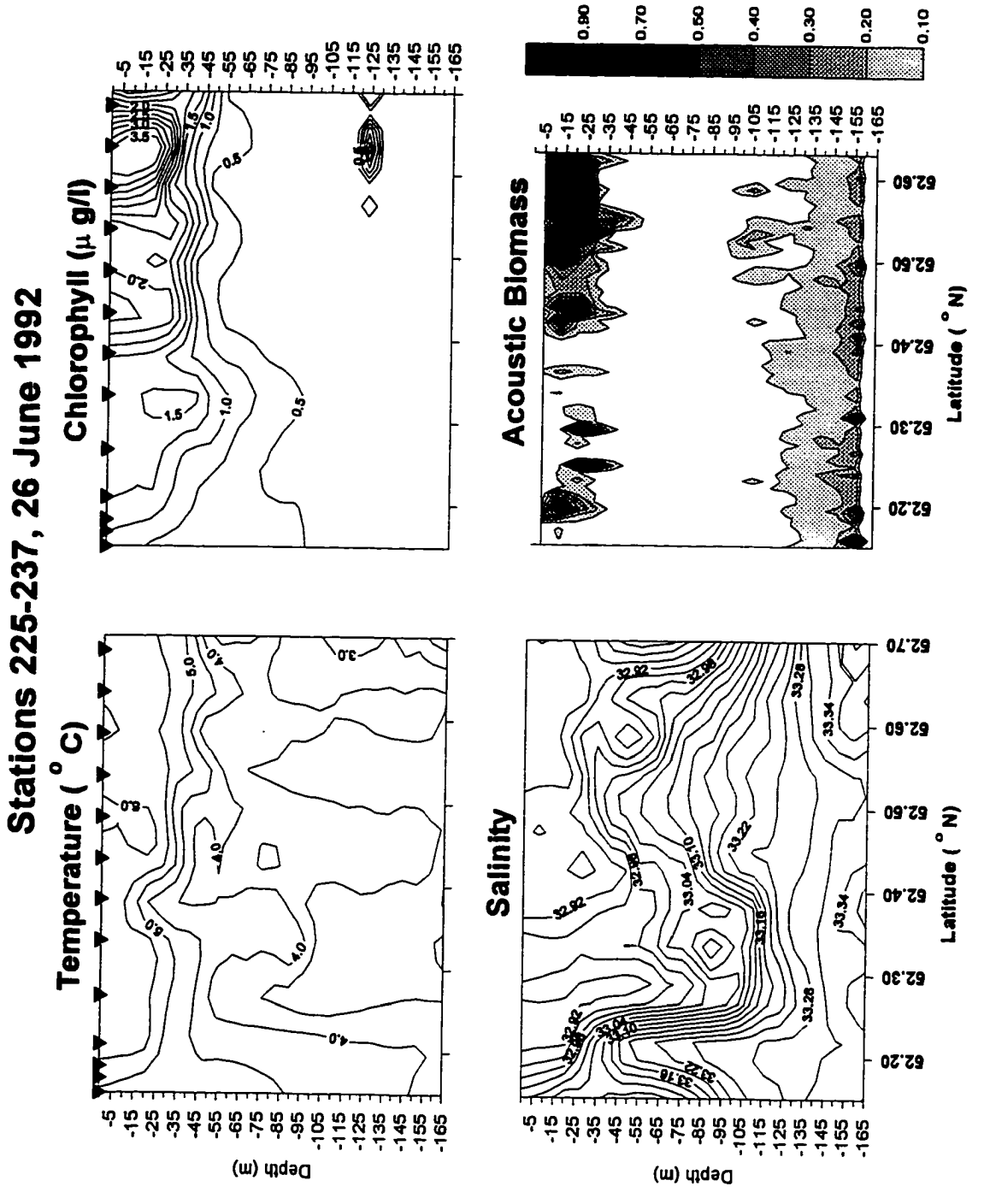

Figure 4-5d. Profiles of temperature, salinity, chlorophyll and acoustic biomass (g m^{-3}) taken north of Kiska Island. Triangles along upper axes mark CTD station locations. Transect locations in Fig. 2-2 (upper right). Horizontal axes on upper and lower figures aligned.

Figure 4-6. Zooplankton wet weight biomass (upper left), abundance (upper right), acoustic biomass (g m^{-3}; lower left), and temperature (°C), salinity and fluorescence (relative units) from MOCNESS Tow 1, taken north of Gareloi Island, 10 July 1993.

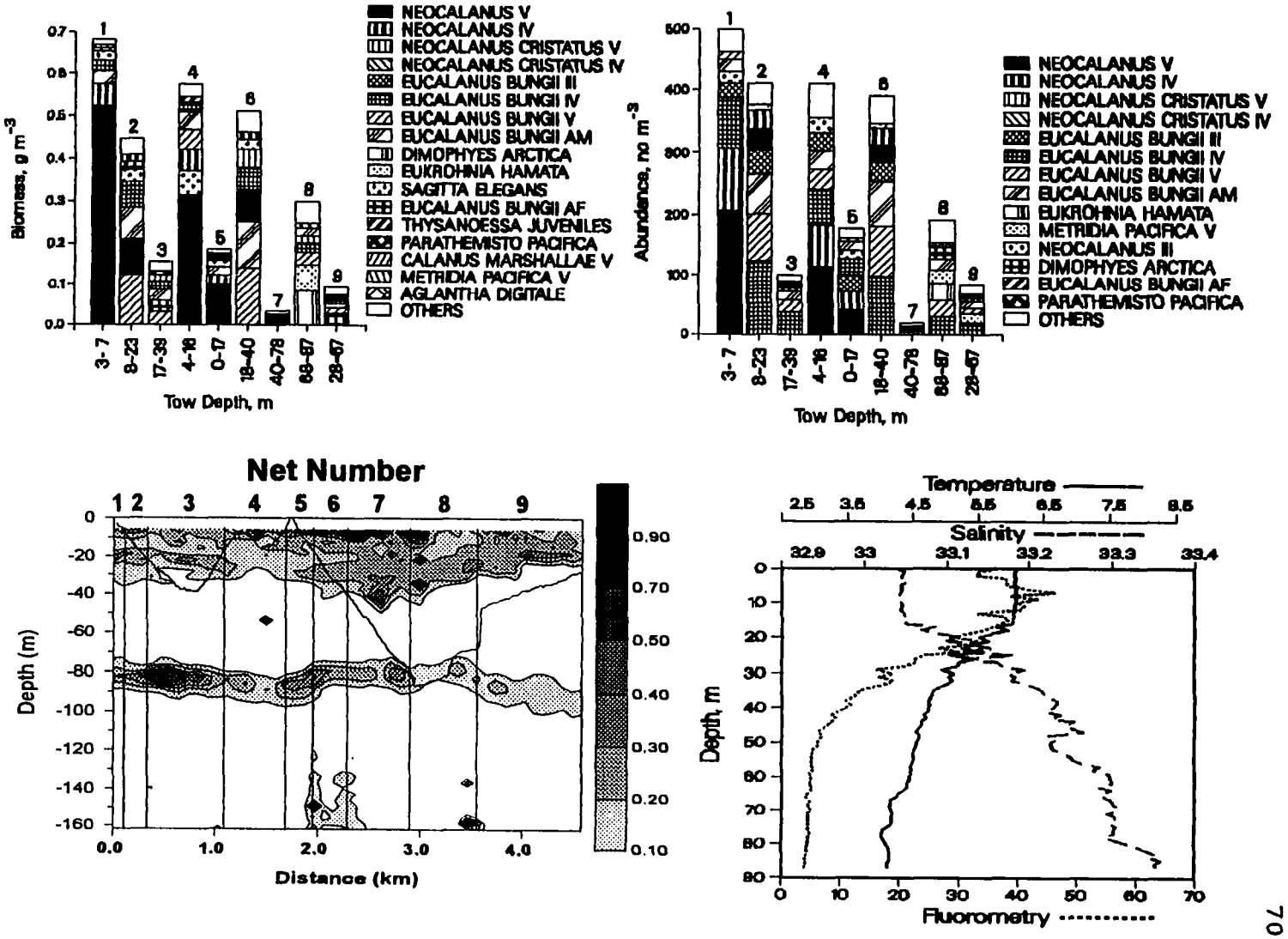

Figure 4-7. Zooplankton wet weight biomass (upper left), abundance (upper right), acoustic biomass (g m^{-3}; lower left), and temperature (°C), salinity (PPT) and fluorescence (relative units) from MOCNESS Tow 22, taken north of Kiska Island, 28 July 1993.

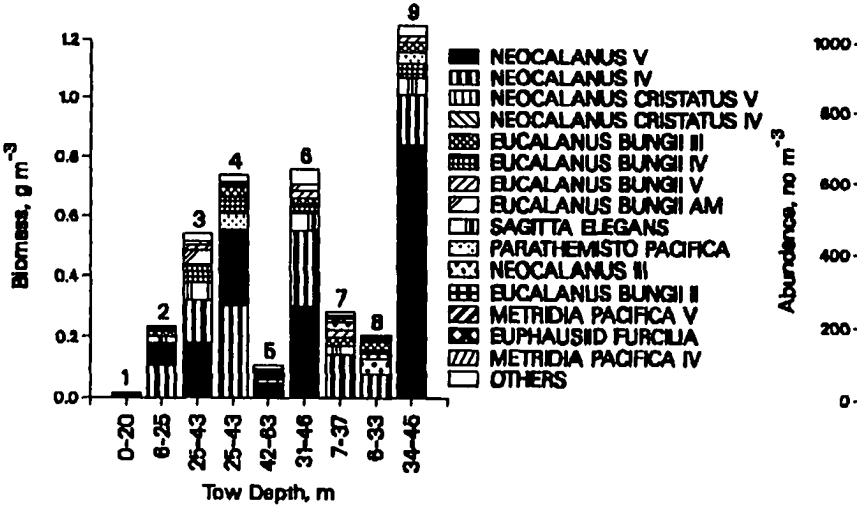

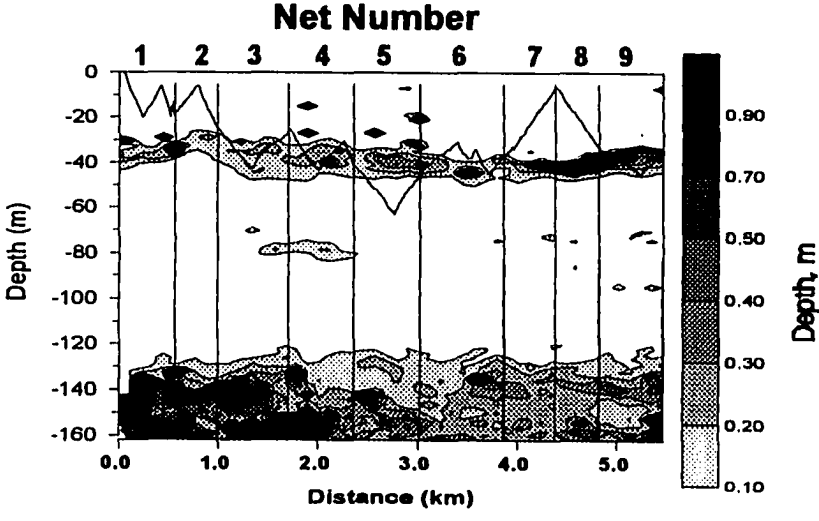

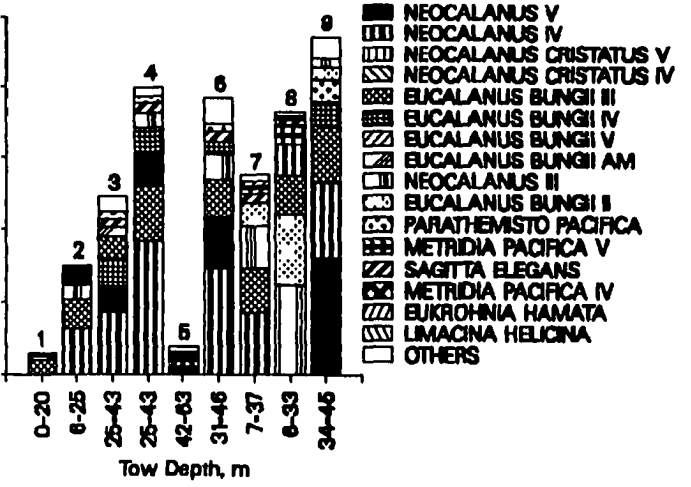
NEOCALANUS V
NEOCALANUS IV
NEOCALANUS CRISTATUS V
NEOCALANUS CRISTATUS IV
EUCALANUS BUNGII III
EUCALANUS BUNGII IV
EUCALANUS BUNGII V
EUCALANUS BUNGII AM
NEOCALANUS II
EUCALANUS BUNGII II
PARATHEMISTO PACIFICA
METRIDIA PACIFICA V
SAGITTA ELEGANS
METRIDIA PACIFICA IV
EUKROHNIA HAMATA
LIMACINA HELICINA
OTHERS
1
2
3
4
5
6
7
8
9
0-20
6-25
25-43
25-43
42-63
31-46
7-37
6-33
34-45
Tow Depth, m

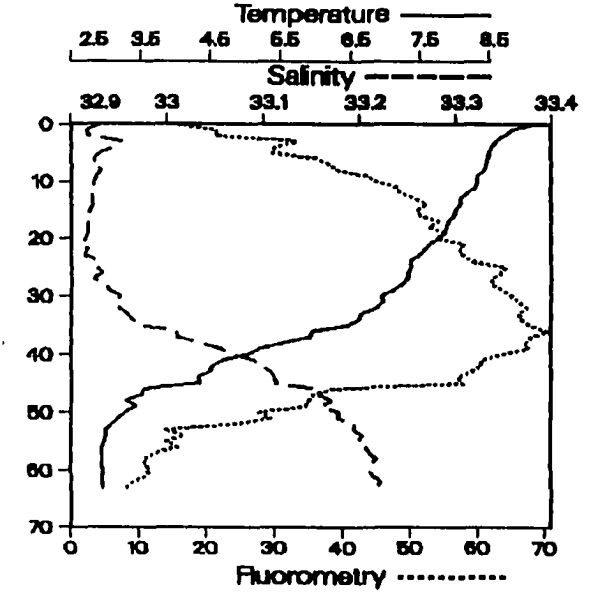
Temperature
2.5
3.5
4.5
5.5
6.5
7.5
8.5
Salinity
32.9
33
33.1
33.2
33.3
33.4
0
10
20
30
40
50
60
70
Fluorometry

5. The effect of tidally generated convergence on zooplankton distribution and acoustic data.

Since least auklets are limited to foraging mainly in the upper 15 m, the descent of their major prey taxa to greater depths substantially limited their foraging habitat relative to earlier in the season. Auklet distributional data collected during July, 1993, indicated that they were foraging primarily where physical phenomena actively transported the food taxa to the surface or where fronts or eddies concentrated the prey relative to the surrounding habitat. The above constraints on auklets limited their major feeding activity to the passes between the islands and to shallow regions around the islands where tidal currents upwelled or concentrated the food taxa. For the above reasons, the major focus of the Aleutian Bird study shifted from the open ocean regions north of the Aleutian archipelago to an un-named pass (hereafter referred to as Delarov Pass) between Unalga and Kavalga Islands in the Delarov Island group (Fig. 5-1).

Interpretation of acoustic data from the pass and shelf habitats around the islands presented additional problems not encountered in the more quiescent, deeper regions of the Bering Sea. The intense tidal flows

through the passes sometimes entrained bubbles into the surface layers, which produced strong acoustic signals and contaminated the data. In addition, schools of fish tended to be more common among the islands than over the deep ocean during the day. Therefore, additional care was required to avoid interpreting scattering from fish schools or turbulence as zooplankton targets. In this section, zooplankton and acoustic data from Delarov Pass are interpreted with respect to water column structure and currents measured with the ADCP. Specific examples of artifact from turbulence and fish schools are presented.

Sampling regime

Delarov Pass was sampled twice during the 1993 sampling season, July 13 - 20, and August 5-6. Tows 9-12 and 30-31 were taken during flood and ebb tides along a standard transect run through the pass on 178° 56' W during the first and second sampling periods respectively (Fig. 5-1a). Tows 5-6 and 32-33 were shorter tows taken north of the pass outside the region of maximum convergence, which usually occurred within the 100 m depth contour. CTD data were collected along the standard line (Fig. 5-1b).

The tidal cycle at Ogliuga Island, just to the east

of Kavalga Island on the east side of the pass, was primarily diurnal during both sampling periods (Fig. 5-2). Low water slack occurred at around noon and high water slack around midnight. Thus, ebb tides occurred in the morning and flood in the afternoon. The highest high tides were about +120 cm and the lowest lows were about -30 cm. The tide would ebb from high to low in about 7 hours but required 12 hours to flood. High water slack lasted about 4 hours and low water slack about 2 hours. Sun rise occurred around 0700 and sunset around 2300 Alaska daylight time. Therefore, most auklet foraging activity was observed during flood tide, when water flowed northward through Delarov Pass. Tidal currents through the pass exceed 200 cm sec^{-1} during the height of flood and ebb and produce 3-5 foot standing waves in the pass, making it impractical to run CTD transects. Therefore, the CTD transects were done during slack tides.

Results

The upper 20 m of the water column in the Delarov region was highly stratified, with a tidally generated frontal regions to the south or north of the ridge, depending on the phase of the tidal cycle. Stations 106-114 (Fig. 5-3) were taken along the standard transect on

July 19 from 0115 to 0440 hours, during high water slack and the early stages of ebb tide. At that time the front was to the north of the ridge, between 51.60 and 51.62° N latitude and the stratified side of the front extended southward over the sill. The water column north of the front had weak stratification and low chlorophyll concentrations, typical of conditions where Tows 5-6 and 32-33 were taken. An earlier time series taken on the standard transect line at 51.61° between 2120 and 0034 hours on 18-19 July showed the same front drifting southward during highwater slack (Fig. 5-4). A pocket of warm, brackish water with elevated chlorophyll concentration occurred in the frontal region to depths of about 30-40 m. The frontal region was pushed northward or southward over the sill with flood and ebb tide respectively. Thus, the position of the front relative to the sill was a function of the stage in the diurnal tidal cycle.

Canonical correlation analysis was done on the dominant taxonomic groups to relate abundance to physical oceanographic conditions. Results for the July data from Delarov Pass revealed significant correlations between abundance of the dominant zooplankton taxa and a complex of four physical oceanographic measurements (Table 5-1).

The first two canonical correlations were highly significant and correlations between the first two sets of canonical scores and the physical and biological variables are tabulated (Table 5-1). The first canonical variable was positively correlated to convergence and fluorescence and negatively correlated with sigma-t and depth. Positive correlations between abundances of Taxa 1, 4, 6 and 9 and the Group 1 canonical scores for canonical variable 1 indicate that *Neocalanus* stages IV and V, *Eucalanus bungii* adults, *Calanus pacificus* V and *Limacina helicina* were more abundant in shallow samples with elevated fluorescence and convergence intensity. In contrast, *Neocalanus cristatus* stage IV and *Metridia pacifica* adults were more abundant at greater depths where convergence intensity and fluorescence were depressed. The above results suggest that density, depth and fluorescence are the primary factors influencing the distribution of the major zooplankton taxa in the pass, while convergence intensity was of secondary importance. Correlations between the second canonical scores in Group 1 and the Group 2 variables suggest that abundance of *Neocalanus cristatus* stage V was negatively influenced by elevated convergence and fluorescence.

The above relationships revealed by canonical

correlation analysis between the physical variables and zooplankton abundance are illustrated by several transects run through the pass during flood tide. Elevated abundance of zooplankton in the convergence zones downstream of the pass is illustrated in plots of zooplankton abundance relative to physical variables (Figs. 5-5, 5-6). The convergence occurred in regions of declining north-south current velocities and were accompanied by elevated acoustic scattering in the surface layers north of the ridge and by high amplitude oscillations in salinity and temperature. Volume scattering in the convergence zones exceeded -68 dB and was apparently not the result of zooplankton alone, which produce volume scattering below -68 dB at concentrations measured in the nets (Appendix II).

In contrast, lowest zooplankton densities were observed primarily in regions of divergence, where water velocities over the ridge where accelerating or over 200 cm sec^{-1} (Fig. 5-5, 5-6, Net 2; Fig. 5-7, Nets 2-6). Tow 10, taken across the ridge when maximum current velocities exceeded 240 cm s^{-1} and strong convergences were present north of the ridge (Fig. 5-7), had zooplankton densities under 175 indiv. m^{-3} during the entire tow. The TS profile from the MOCNESS system showed elevated salinities

and depressed temperatures to less than 5 m depth and no sign of mixing. The deeper water mass had essentially been upwelled almost to the surface, pressing the warmer water mass into a thin layer less than 5 m thick. Although the tow fished as shallow as 3 m depth, none of the nets contained elevated zooplankton densities characteristic of convergence zones during Tows 11 and 12. Elevated densities of zooplankton did not occur in the convergence zone in the absence of a warmer brackish layer.

Elevated scattering consistently occurred below the pycnocline over the ridge during flood and ebb tides. Although Nets 2-4 of Tow 9 fished through a scattering layer above the bottom on the ridge (Fig. 5-8), the plankton densities were not elevated relative to subpycnocline regions outside the scattering layer. Euphausiids in the samples consisted primarily of furcilid stages with a few calyptopis and post furcilids. Adult and juvenile euphausiids did not appear in any of the samples taken during July. Zooplankton densities tended to be lower downstream of the convergences, where tilting of isothermals and isohalines are indicative of the mixing regime typical of the north side of the ridge during flood tide (Fig. 5-9).

Oscillations in the temperature salinity record from tows in the convergence zones suggest the presence of internal waves in the pycnocline layers (Fig. 5-5, 5-6). Some of the oscillations may be related to small changes in the depth of the MOCNESS as it was pushed up and down in the convergences and divergences. Sound scattering in the convergence zone appeared as a series of very narrow vertical streaks on the echograms, each streak lasting for one to several sweeps (Fig. 5-10). Small-scale features in the convergence zones were not recorded in the acoustic files or by the plankton samples, both of which integrated over the length of a number of individual waves.

The CTD transect taken during August indicated that a frontal system was present (Fig. 5-11). Although marked stratification was present south of the front, canonical correlation on the August data revealed weaker relationships between the Group 1 variable and depth, density and convergence intensity (Table 5-2). The first canonical variable was negatively correlated with fluorescence and positively correlated with sigma-t and depth. However, the depth correlation was much weaker than in July. Negative correlations between abundance of Taxa 1, 4, 8 and 9 and the Group 1 canonical scores for

canonical variable 1 indicate that *Neocalanus* stages IV and V, *Eucalanus bungii* adults, *Metridia pacifica* adults, *Parathemisto pacifica* and *Limacina helicina* were more abundant in regions of high fluorescence and low sigma-t values. The positive correlation of Taxa 2 with the Group 1 canonical scores indicates that *Neocalanus cristatus* stage V was more abundant in regions of higher water density and lower fluorescence.

Highest densities of *Neocalanus plumchrus* stage V in August occurred in a convergence zone during ebb tide where southward current velocities declined from 80 to 30 cm sec^{-1} and temperatures rapidly increased from 5.8 to 6.5°C (Fig. 5-12). In contrast, *Limacina helicina* dominated in a strong convergence zone north of the ridge, where temperatures increases from 5.3 to 7.5°C, salinity dropped below 32.9 and north-south current velocities decreased from 100 to 20 cm s^{-1} (Fig. 5-13). Marginal increases in zooplankton density were observed in the convergence zone during Tow 33, where current velocities declined from 140 to 60 cm s^{-1}, temperatures increased from 5.3 to 6.5°C and salinity declined from 33.1 to 32.9 psu (Fig. 5-14). In all three cases elevated zooplankton densities occurred either in the convergence zones or on the warm side of the convergence relative to other samples

from the same tow taken on the cold side of the convergence. In contrast to July, the August samples included *Thysanoessa longipes* and *Thysanoessa inspinata*, important food items for crested auklets.

Discussion

The zooplankton data from the Delarov region indicate the presence of two core zooplankton assemblages: a shallow community in the warm, low-salinity surface layer dominated by late stage interzonal copepods, including important prey taxa for auklets, and a subpycnocline community having much lower densities of essentially the same taxa. Regions with intermediate zooplankton densities apparently reflect the physical mixing of the shallow and deep water masses by tidal energy. Although elevated zooplankton densities occurred in samples outside the pass, auklets concentrated their foraging in the pass in convergence regions during flood or ebb tides. Auklets may prefer to forage in the pass when tidal currents are strong for several reasons. Mixing processes in the convergence zones may be concentrating prey from the warmer surface layer or somehow increasing the contact rate between auklets and their copepod prey. In addition, the pass may provide a region where surface plankton

aggregates are consistently flushed through, thus relieving the birds of the need to actively search out aggregates over a wider expanse of ocean.

Although the convergence zones in the presence of a warm surface layer were apparently regions of elevated zooplankton densities and foraging activity by auklets, the scale of individual plankton patches within the convergence zones is unknown because the net samples undoubtedly integrated through discrete patches, as indicated by temperature-salinity oscillation in the TS trace for individual net samples. Nevertheless, data from Tow 30, for example, suggest that densities of the dominant prey organism, *N. plumchrus* stage V, within discrete patches is probably at least several times greater than average values outside convergence. The exact mechanism concentrating zooplankton within the convergence zones is not known. However, recent detailed studies of flow patterns within a convergence in Haro Strait in the San Juan Islands (Farmer *et al.*, 1995) may offer some insights.

The convergence zone in the Delarov region consisted of a series of internal waves or boils, similar to those described in Farmer *et al.* (1995). Boils in Haro Strait consisted of 175 m wide patches of smooth upwelled water

surrounded by 15 m wide rings of rough water indicating regions of intense downwelling (Farmer *et al.*, 1995). The internal waves or boils in the Delarov region appeared as temperature and salinity spikes in the TS trace from the MOCNESS tows and as dark streaks in the echograms. The length of the boils or internal waves varied from about 50 to 150 m, as estimated from the distance between temperature peaks as computed by temperature and flow meter data from the MOCNESS. However, the zone of most intense downwelling, as indicated from dark streaks on the echograms, was much narrower, probably on the order of 15 m, as suggested from the Haro Strait data (Farmer *et al.*, 1995). The simple vertical displacement of surface zooplankton to greater depths is unlikely to enhance foraging conditions for auklets. In all probability, the enhancement mechanism involves small scale processes within the shear zone dividing the upwelling and downwelling water masses within the convergence. If the above is correct, then auklets may be seeking out individual patches of zooplankton on the order of 10 to 20 m in width.

Unfortunately, we had no way of measuring zooplankton densities within the shear zones. Due to entrainment of bubbles from surface turbulence, acoustic data in the

shear zones were more a function of downwelling velocity (eg. Farmer *et al.*, 1995) than a reflection of zooplankton densities. In addition, the intense physical turbulence in the shear zones is also a potential source of acoustic backscatter (Stanton 1994). We therefore consider the acoustic data from the convergence regions as indicative of downwelling rather than zooplankton densities. Reduced densities of *Neocalanus plumchrus* in surface waters during August was probably due to their migration to greater depths after their feeding cycle which ends in July and August (Miller and Clemmons, 1988). By August the least auklets were probably experiencing reduced food abundance, even in regions like Delarov Pass, where hydrographic conditions apparently produce plankton aggregates. Only one sample from August contained copepod densities similar to those encountered commonly in the warm regions and convergence zones in July.

Table 5-1. Canonical correlation analysis relating four physical oceanographic variables to nine groups of the dominant zooplankton taxa in Delarov Pass, July 13-20 1993.

Physical variables used:

1. Sound scattering measure of convergence intensity.
2. Sigma-t.
3. Depth of net normalized for volume filtered.
4. Fluorescence normalized for volume filtered.

Biological variables = abundances of following groups:

1. Neocalanus IV & V
2. Neocalanus cristatus V
3. Neocalanus cristatus IV
4. Eucalanus bungii adult
5. Metridia pacifica adult
6. Calanus pacificus V
7. Euphausiid furcilia
8. Parathemisto pacifica
9. Limacina helicina

*** Canonical Correlations Statistics ***

	Canonical Correlations	Wilks Lambda	Raos F	Num. df	Denom. df	Prob. of Larger F
1	0.9031	0.0371	5.054	36	129.2	0.0000
2	0.8403	0.2011	3.142	24	102.1	0.0000
3	0.5017	0.6843	1.074	14	72.0	0.3948
4	0.2926	0.9144	0.577	6	37.0	0.7460

Table 5-1. Continued.

Correlations Between the Group One Variables and the Group One Canonical Scores

	1	2
1	0.3786	-0.4030
2	-0.9696	-0.0731
3	-0.7782	-0.1943
4	0.9127	-0.3442

Correlations Between the Group Two Variables and the Group One Canonical Scores

	1	2
1	0.4690	-0.2518
2	-0.0036	0.6489
3	-0.4472	-0.0276
4	0.5144	-0.4288
5	-0.5588	-0.3122
6	0.3876	-0.2822
7	-0.2868	-0.3400
8	0.2359	0.0463
9	0.6577	-0.3777

Table 5-2. Canonical correlation analysis relating four physical oceanographic variables to nine groups of the dominant taxa in Delarov Pass, August 5-6, 1993.

Physical variables used:

1. Sound scattering measure of convergence intensity.
2. Sigma-t.
3. Depth of net normalized for volume filtered.
4. Fluorescence normalized for volume filtered.

Biological variables = abundances of following groups:

1. Neocalanus IV & V
2. Neocalanus cristatus V
3. Neocalanus cristatus IV
4. Eucalanus bungii adult
5. Metridia pacifica adult
6. Calanus pacificus V
7. Euphausiid furcilia
8. Parathemisto pacifica
9. Limacina helicina

*** Canonical Correlations Statistics ***

	Canonical Correlations	Wilks Lambda	Raos F	Num. df	Denom. df	Prob. of Larger F
1	0.8317	0.0844	1.698	36	65.4	0.0314
2	0.6809	0.2737	1.239	24	52.8	0.2536
3	0.5723	0.5103	1.085	14	38.0	0.4003
4	0.4911	0.7588	1.059	6	20.0	0.4185

Table 5-2. Continued.

Correlations Between the Group One Variables and the Group One Canonical Scores

	1
1	0.1120
2	0.6103
3	0.3219
4	-0.8899

Correlations Between the Group Two Variables and the Group One Canonical Scores

	1
1	-0.4352
2	0.5823
3	0.2164
4	-0.5237
5	-0.4771
6	-0.1145
7	-0.1428
8	-0.3202
9	-0.3491

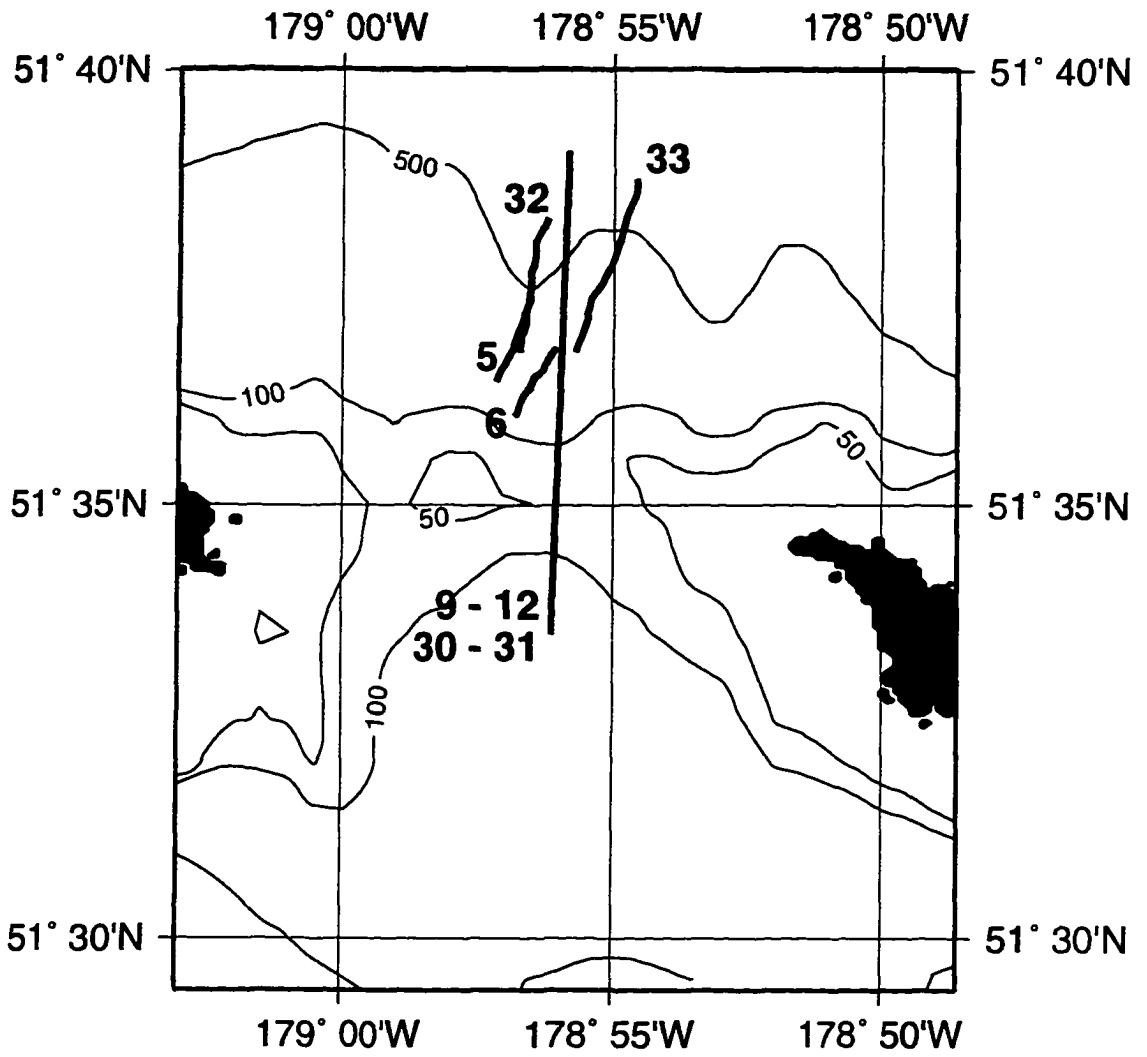

Figure 5-1a. Location of MOCNESS tows in Delarov Pass, July-August 1993. Tows 9 through 12 and 30 and 31 were taken on the standard transect line.

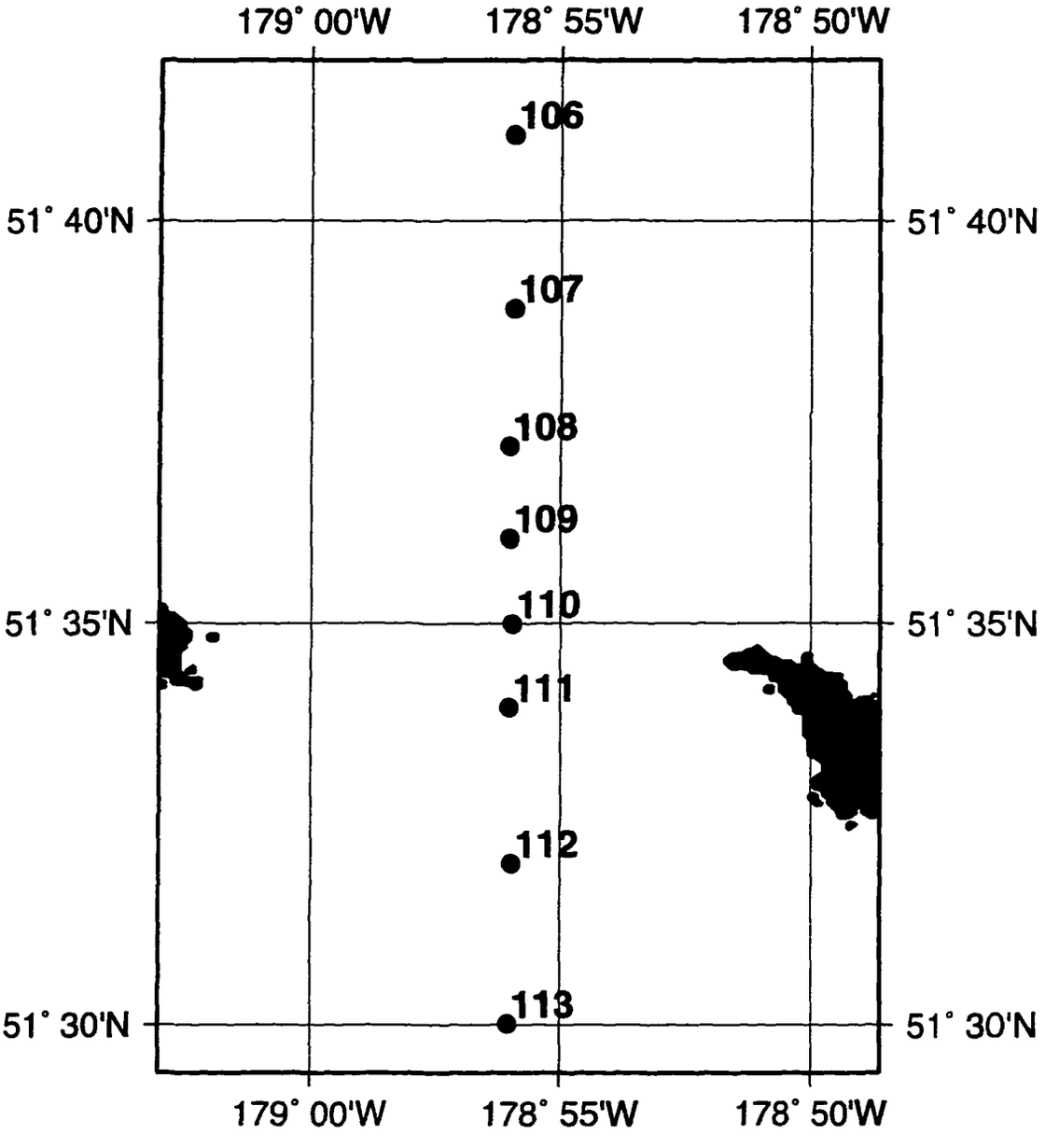

Figure 5-1b. CTD stations along standard line through Delarov Pass, 19 July 1993.

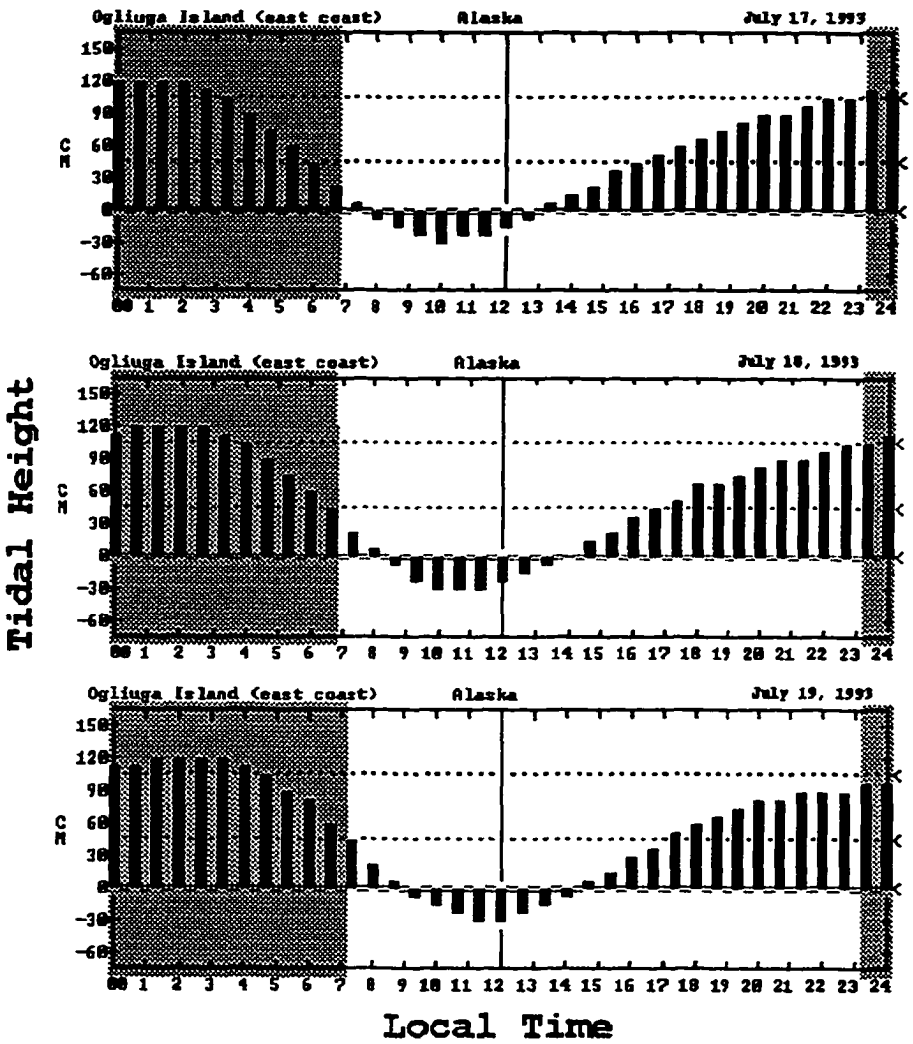

Figure 5-2. The tidal cycle at Ogliuga Island (Delarov group), western Aleutian Islands, 17-29 July 1993. Shaded area indicates night. Figure modified from the NOAA tides program.

Figure 5-3. CTD transect taken on the standard transect line through Delarov Pass, 0115-0440 hours (Station locations in Fig. 5-1b). Solid triangles indicate station locations. Horizontal axes on upper and lower figures aligned.

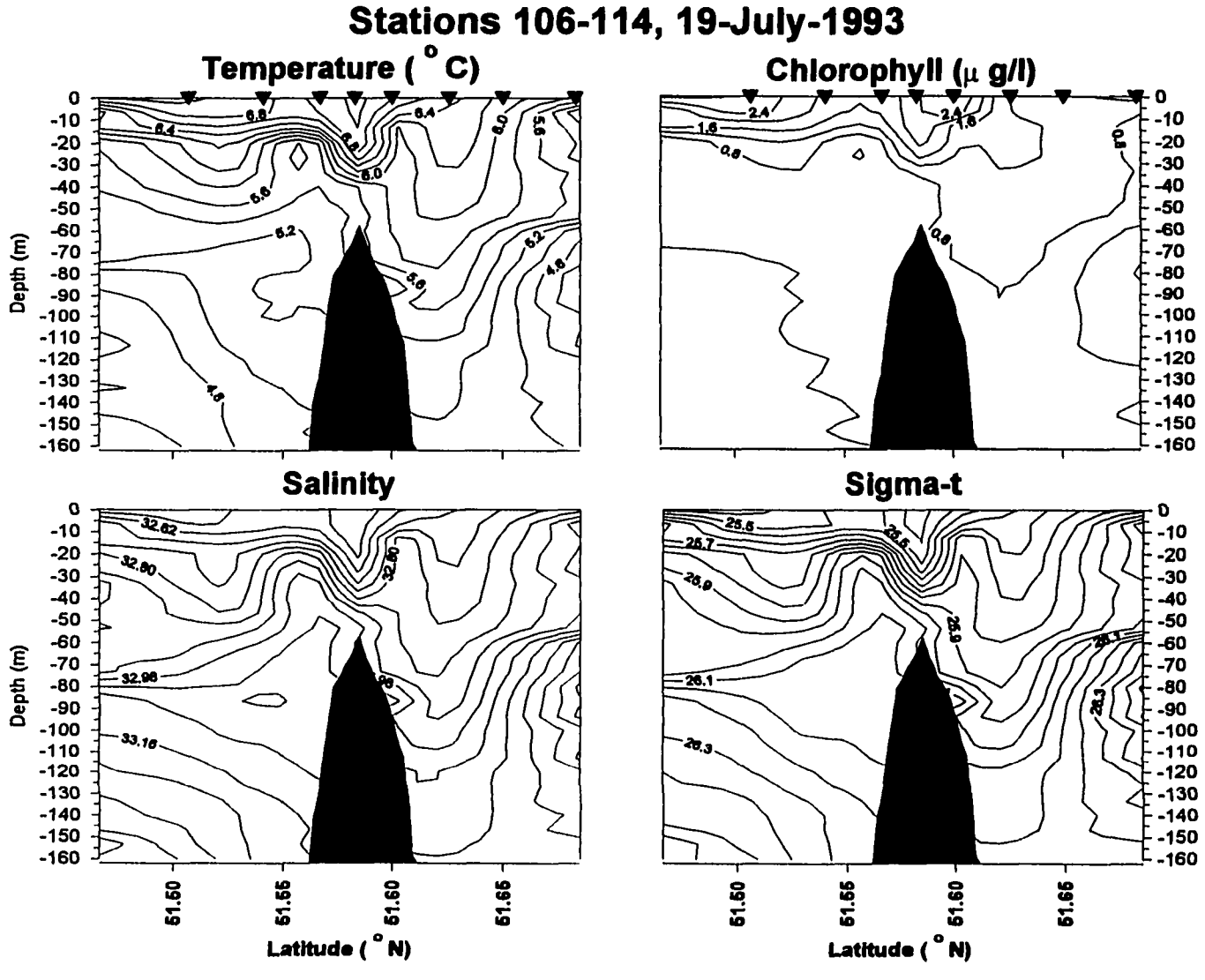

Figure 5-4. CTD time series taken on the standard transect line through Delarov Pass, western Aleutian Islands, at 51.61° N. Lat. between 2120 and 0034 hours, 18-19 July 1993. Samples taken at about 10 minute intervals. Horizontal axes on upper and lower figures aligned.

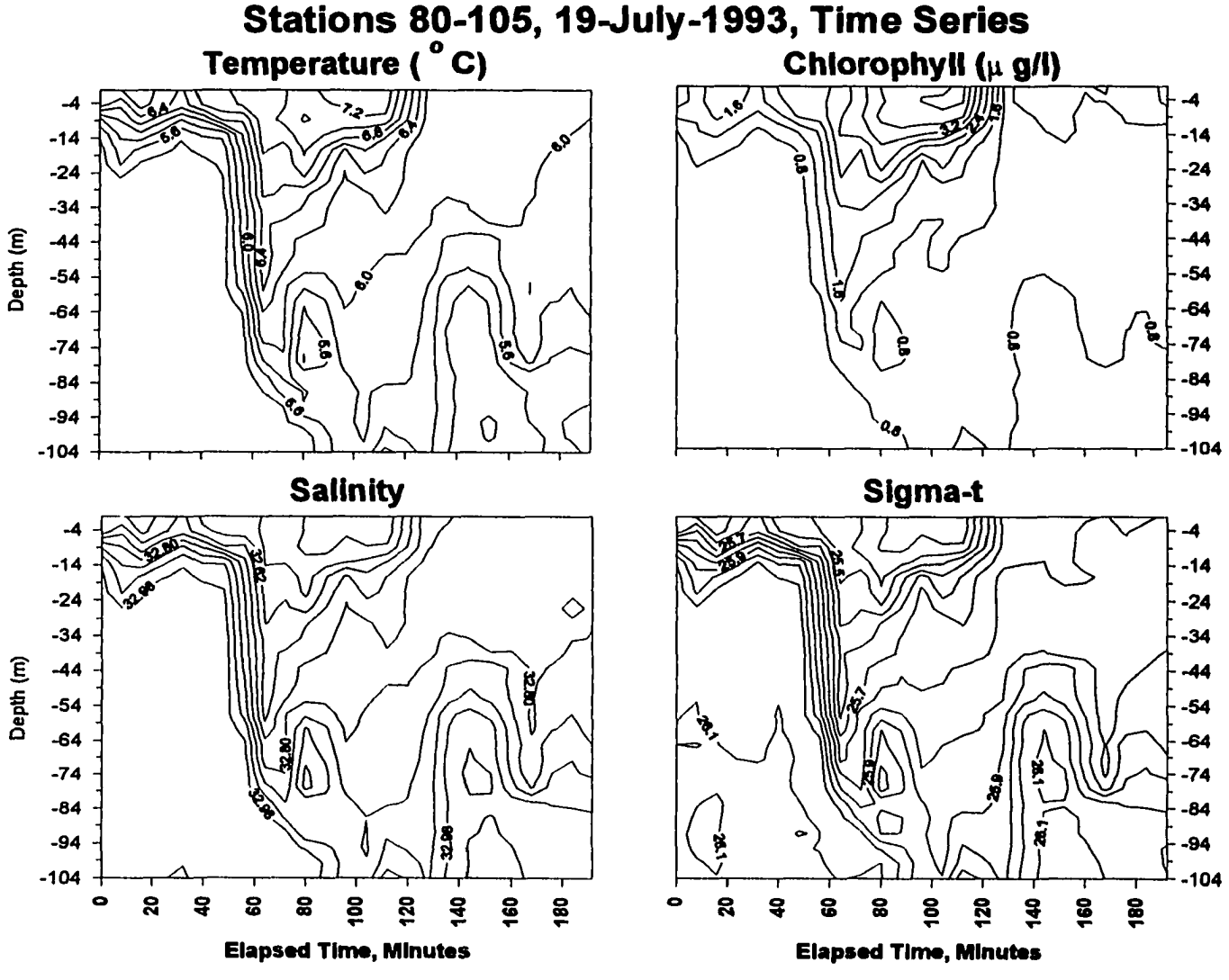

Figure 5-5. MOCNESS Tow 11, taken through Delarov Pass, 18 July 1993. Upper left: north-south component of current velocity; lower left: Acoustic backscattering intensity, volume scattering in dB (Solid line indicates net track, vertical bars are net cycles); Upper left: Salinity - temperature trace from MOCNESS sensors; Lower left: abundance of seven major taxa in each sample. Horizontal axes (latitude) on upper and lower figures aligned.

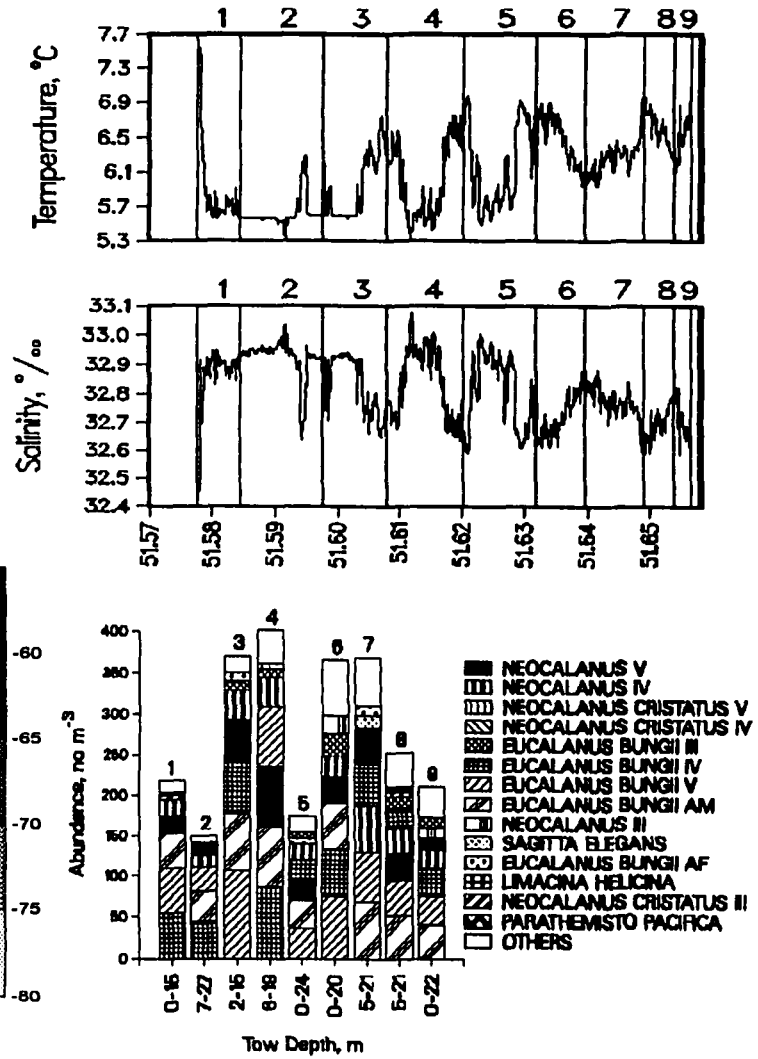
Temperature, °C
7.7
7.3
6.9
6.5
6.1
5.7
5.3
1 2 3 4 5 6 7 8 9
Salinity, °/₀₀
33.1
33.0
32.9
32.8
32.7
32.6
32.5
32.4
1 2 3 4 5 6 7 8 9
51.57
51.58
51.59
51.60
51.61
51.62
51.63
51.64
51.65
-60
-65
-70
-75
-80
Abundance, no m⁻³
400
350
300
250
200
150
100
50
0
1
2
3
4
5
6
7
8
9
0-15
7-27
2-15
8-18
0-24
0-20
5-21
5-21
0-22
Tow Depth, m
NEOCALANUS V
NEOCALANUS IV
NEOCALANUS CRISTATUS V
NEOCALANUS CRISTATUS IV
EUCALANUS BUNGII III
EUCALANUS BUNGII IV
EUCALANUS BUNGII V
EUCALANUS BUNGII AM
NEOCALANUS II
SAGITTA ELEGANS
EUCALANUS BUNGII AF
LIMACINA HELICINA
NEOCALANUS CRISTATUS II
PARATHEMISTO PACIFICA
OTHERS

Figure 5-6. MOCNESS Tow 12, taken through Delarov Pass, 18 July 1993. Upper left: north-south component of current velocity; lower left: Acoustic backscattering intensity, volume scattering in dB (Solid line indicates net track, vertical bars are net cycles); Upper left: Salinity - temperature trace from MOCNESS sensors; Lower left: abundance of seven major taxa in each sample. Horizontal axes (latitude) on upper and lower figures aligned.

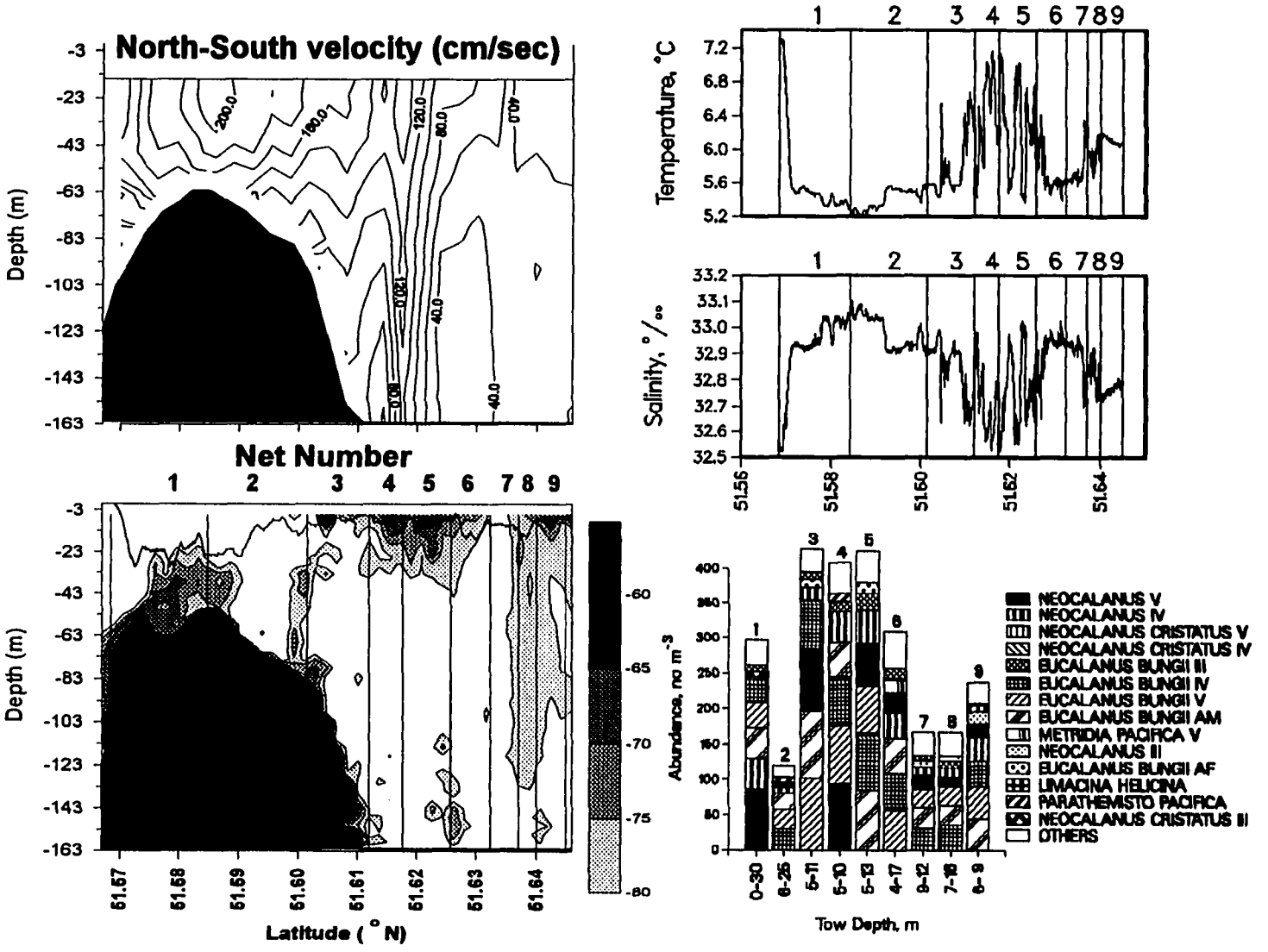

Figure 5-7. MOCNESS Tow 10, taken through Delarov Pass, 18 July 1993. Upper left: north-south component of current velocity; lower left: Acoustic backscattering intensity, volume scattering in dB (Solid line indicates net track, vertical bars are net cycles); Upper left: CTD trace from MOCNESS sensors, values averaged for each 1 m depth interval, solid line: temperature (°C), dashed line: salinity (ppt), dotted line: fluorescence (relative units); Lower left: abundance of seven major taxa in each sample. Horizontal axes (latitude) on upper and lower figures aligned.

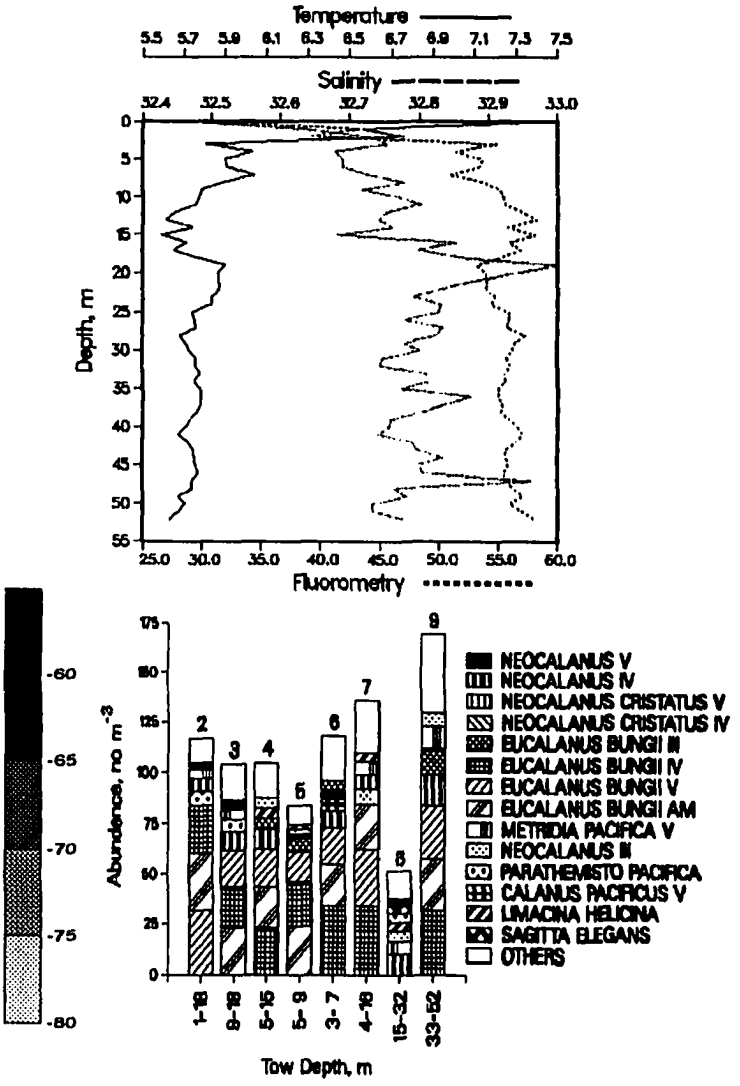
Temperature
5.5 5.7 5.9 6.1 6.3 6.5 6.7 6.9 7.1 7.3 7.5
Salinity
32.4 32.5 32.6 32.7 32.8 32.9 33.0
Depth, m
0 5 10 15 20 25 30 35 40 45 50 55
25.0 30.0 35.0 40.0 45.0 50.0 55.0 60.0
Fluorometry
-60
-65
-70
-75
-80
Abundance, no m-3
175 150 125 100 75 50 25 0
2 3 4 6 7 9 5
1-18 8-18 5-15 5-9 3-7 4-16 15-32 33-62
Tow Depth, m
NEOCALANUS V
NEOCALANUS IV
NEOCALANUS CRISTATUS V
NEOCALANUS CRISTATUS IV
EUCALANUS BUNGII III
EUCALANUS BUNGII IV
EUCALANUS BUNGII V
EUCALANUS BUNGII AM
METRIDIA PACIFICA V
NEOCALANUS III
PARATHEMISTO PACIFICA
CALANUS PACIFICUS V
LIMACINA HELICINA
SAGITTA ELEGANS
OTHERS

Figure 5-8. MOCNESS Tow 9, taken through Delarov Pass, 14 July 1993. Upper left: abundance of seven major taxa in each sample; lower left: Acoustic backscattering intensity, volume scattering in dB (Solid line indicates net track, vertical bars are net cycles); Right: CTD trace from MOCNESS sensors, values averaged for each 1 m depth interval, solid line: temperature (°C), dashed line: salinity (ppt), dotted line: fluorescence (relative units).

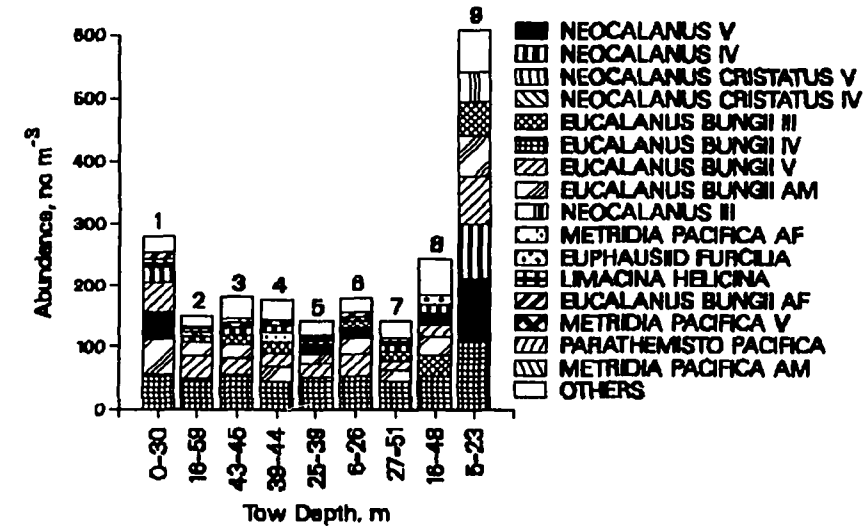

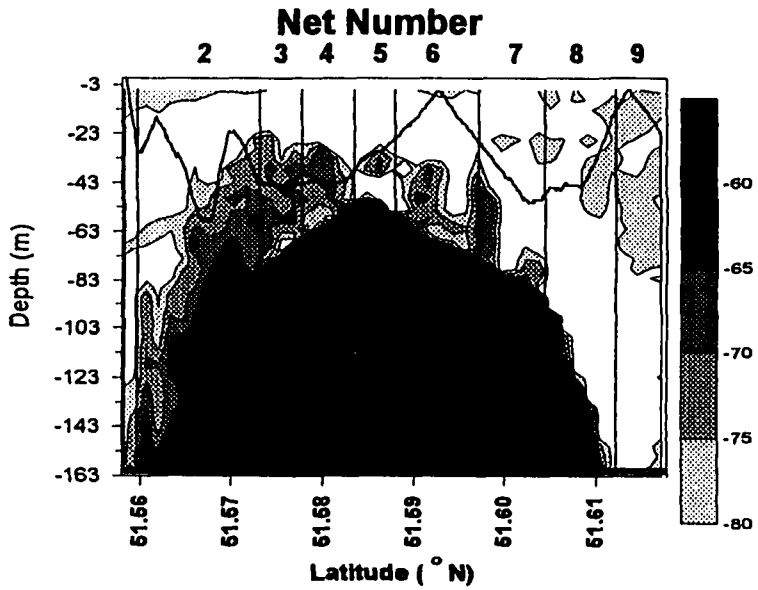

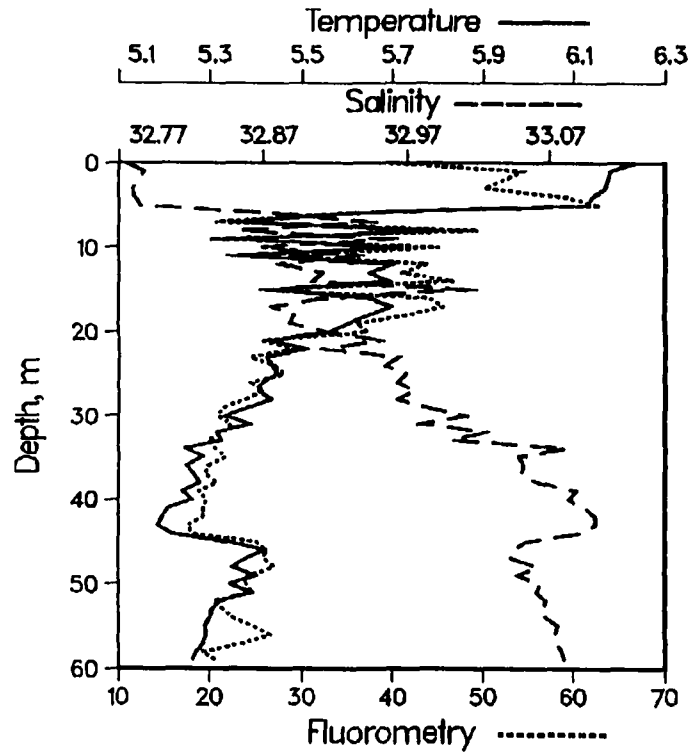

Figure 5-9. Tow 5, taken in Delarov Pass, July 13, 1993. Upper: Temperature salinity profiles from MOCNESS trace; lower left: acoustically determined biomass (g m^{-3}) (Solid line indicates net track, vertical bars are net cycles); Lower left: abundance of seven major taxa in each sample. Horizontal axes (latitude) on upper and lower figures aligned.

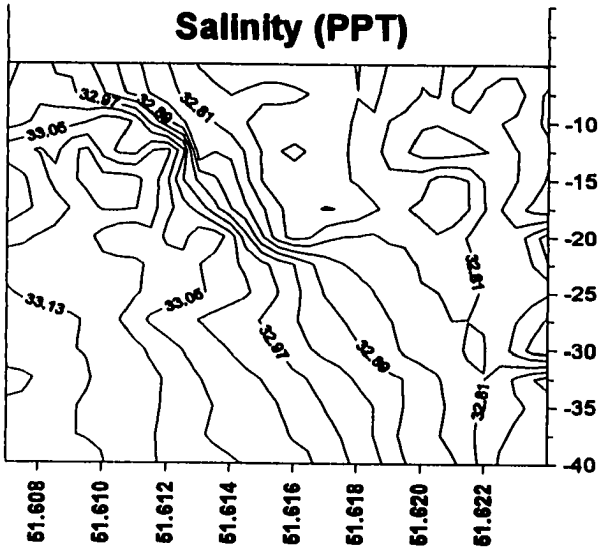
Salinity (PPT)
32.87
32.89
32.81
33.05
33.13
33.05
32.87
32.89
32.81
32.81
-10
-15
-20
-25
-30
-35
-40
51.608
51.610
51.612
51.614
51.616
51.618
51.620
51.622

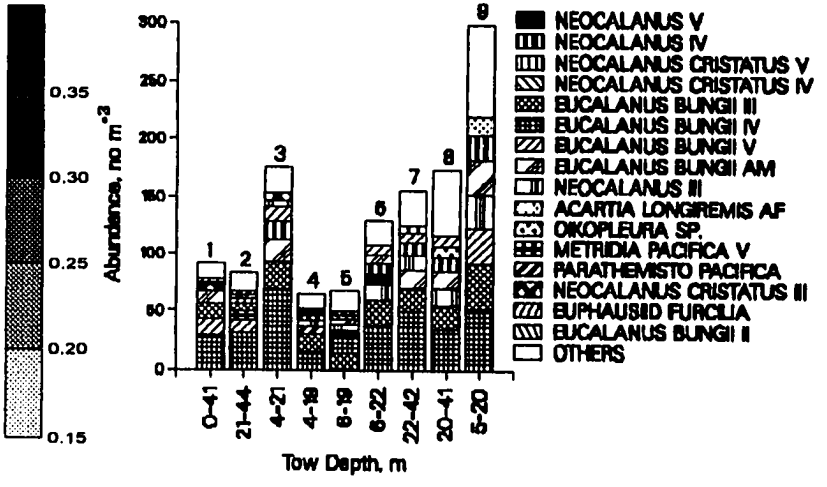
0.35
0.30
0.25
0.20
0.15
Abundance, no m-3
300
250
200
150
100
50
0
1
2
3
4
5
6
7
8
9
0-41
21-44
4-21
4-18
8-19
6-22
22-42
20-41
5-20
Tow Depth, m
NEOCALANUS V
NEOCALANUS IV
NEOCALANUS CRISTATUS V
NEOCALANUS CRISTATUS IV
EUCALANUS BUNGII III
EUCALANUS BUNGII IV
EUCALANUS BUNGII V
EUCALANUS BUNGII AM
NEOCALANUS III
ACARTIA LONGIREMIS AF
OIKOPLEURA SP.
METRIDIA PACIFICA V
PARATHEMISTO PACIFICA
NEOCALANUS CRISTATUS III
EUPHAUSIID FURCILIA
EUCALANUS BUNGII II
OTHERS

Figure 5-10. Echogram, taken through Delarov Pass during southward flowing tide, 1028-1301 hrs, 19 July 1993. Black vertical lines (arrows) in initial part of record indicate convergence zones.

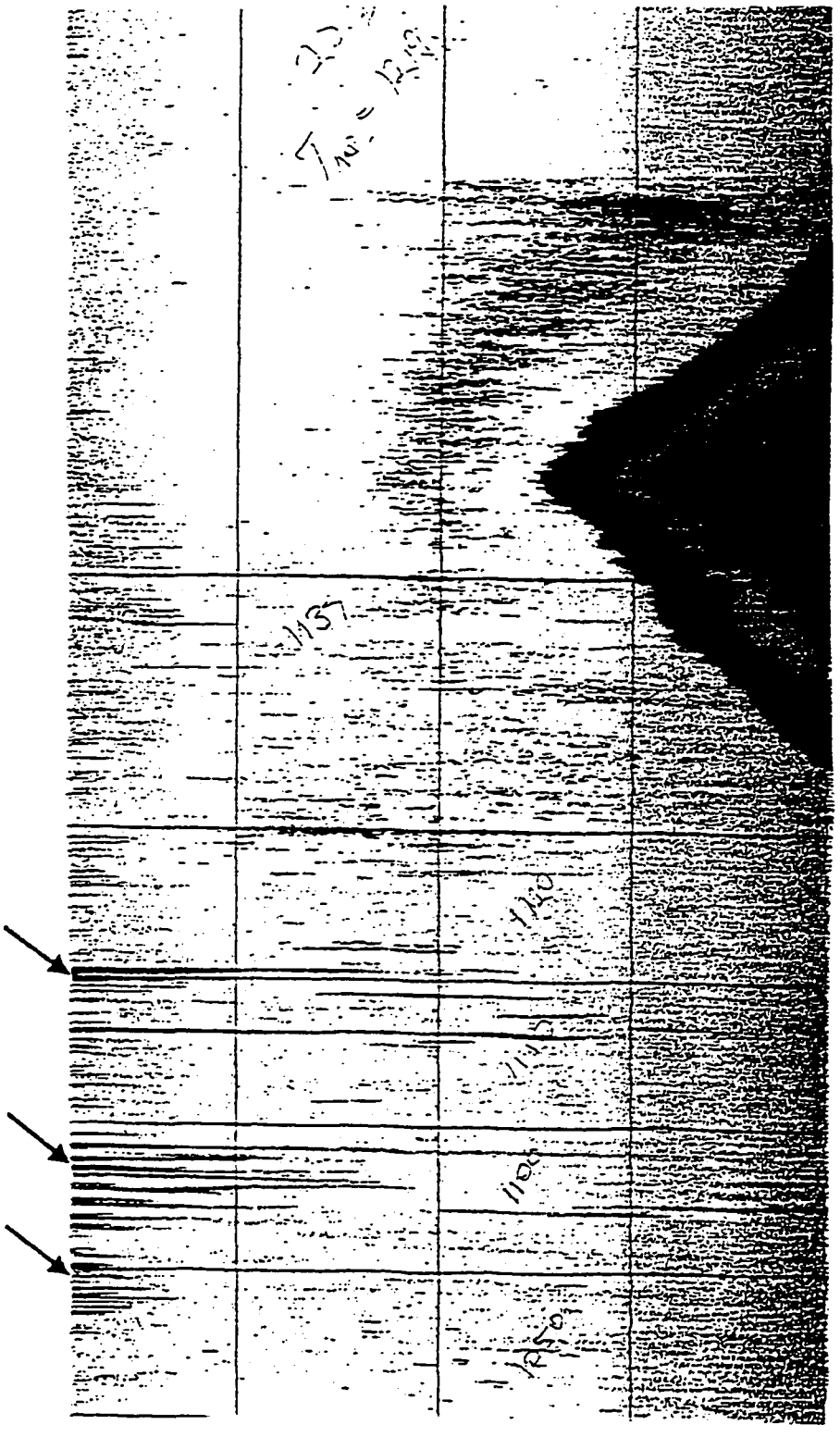

Figure 5-11. CTD transect taken on the standard transect line through Delarov Pass. Solid triangles indicate station locations. Horizontal axes (latitude) on upper and lower figures aligned.

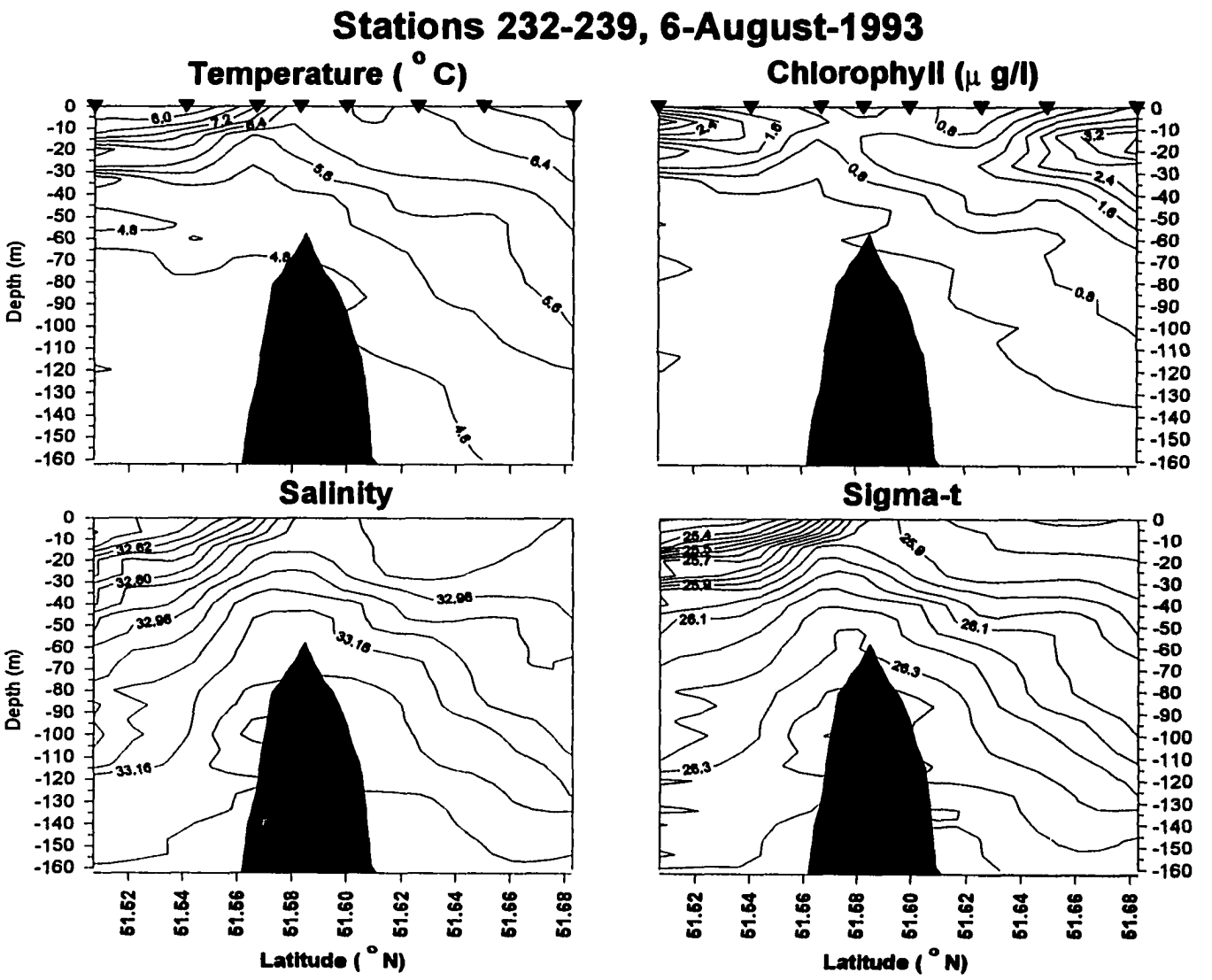

Figure 5-12. MOCNESS Tow 30, taken through Delarov Pass, 5 August 1993. Upper left: north-south component of current velocity; lower left: Acoustic backscattering intensity, volume scattering in dB (Solid line indicates net track, vertical bars are net cycles); Upper left: Salinity - temperature trace from MOCNESS sensors; Lower left: abundance of seven major taxa in each sample. Horizontal axes (latitude) on upper and lower figures aligned.

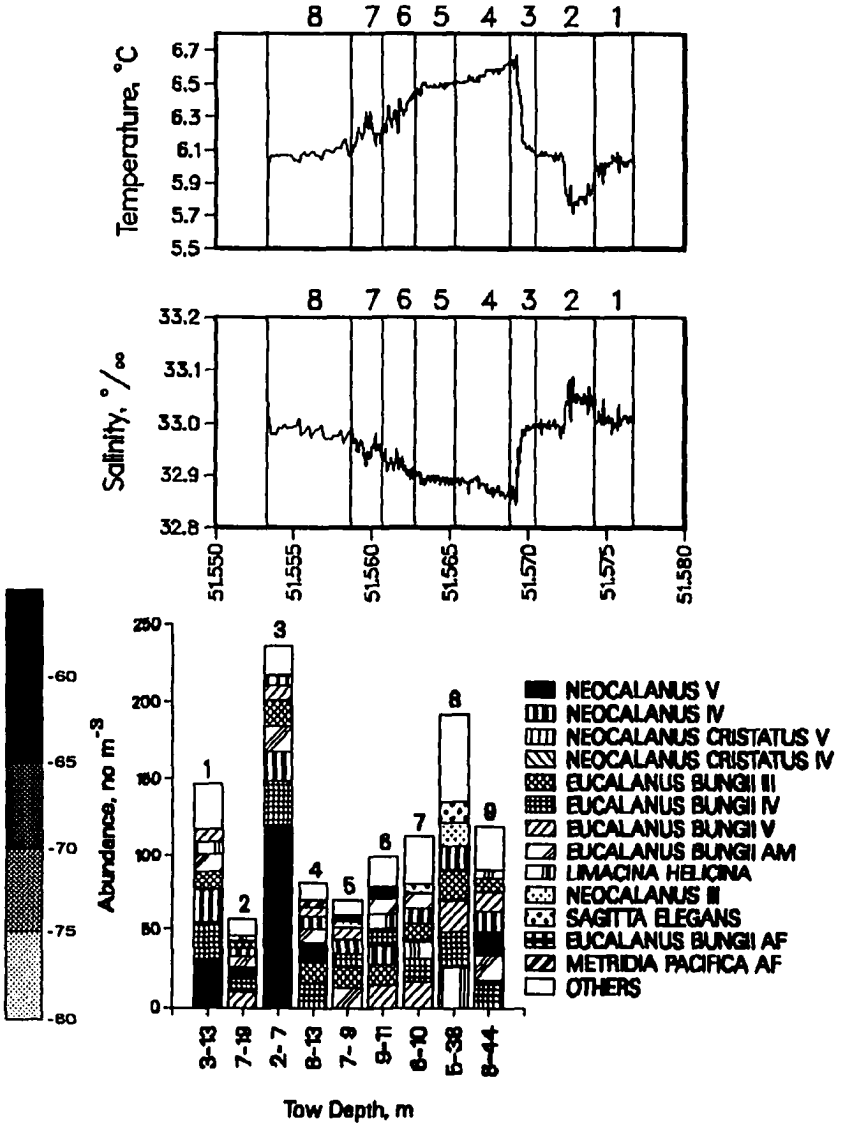
8 7 6 5 4 3 2 1
Temperature, °C
6.7
6.5
6.3
6.1
5.9
5.7
5.5
8 7 6 5 4 3 2 1
Salinity, °/∞
33.2
33.1
33.0
32.9
32.8
51.550
51.555
51.560
51.565
51.570
51.575
51.580
-60
-65
-70
-75
-80
Abundance, no m-3
250
200
150
100
50
0
1
2
3
4
5
6
7
8
9
3-13
7-19
2-7
8-13
7-9
9-11
8-10
5-38
8-44
Tow Depth, m
NEOCALANUS V
NEOCALANUS IV
NEOCALANUS CRISTATUS V
NEOCALANUS CRISTATUS IV
EUCALANUS BUNGII II
EUCALANUS BUNGII IV
EUCALANUS BUNGII V
EUCALANUS BUNGII AM
LIMACINA HELICINA
NEOCALANUS III
SAGITTA ELEGANS
EUCALANUS BUNGII AF
METRIDIA PACIFICA AF
OTHERS

Figure 5-13. MOCNESS Tow 31, taken through Delarov Pass, 5 August 1993. Upper left: north-south component of current velocity; lower left: Acoustic backscattering intensity, volume scattering in dB (Solid line indicates net track, vertical bars are net cycles); Upper left: Salinity - temperature trace from MOCNESS sensors; Lower left: abundance of seven major taxa in each sample. Horizontal axes (latitude) on upper and lower figures aligned.

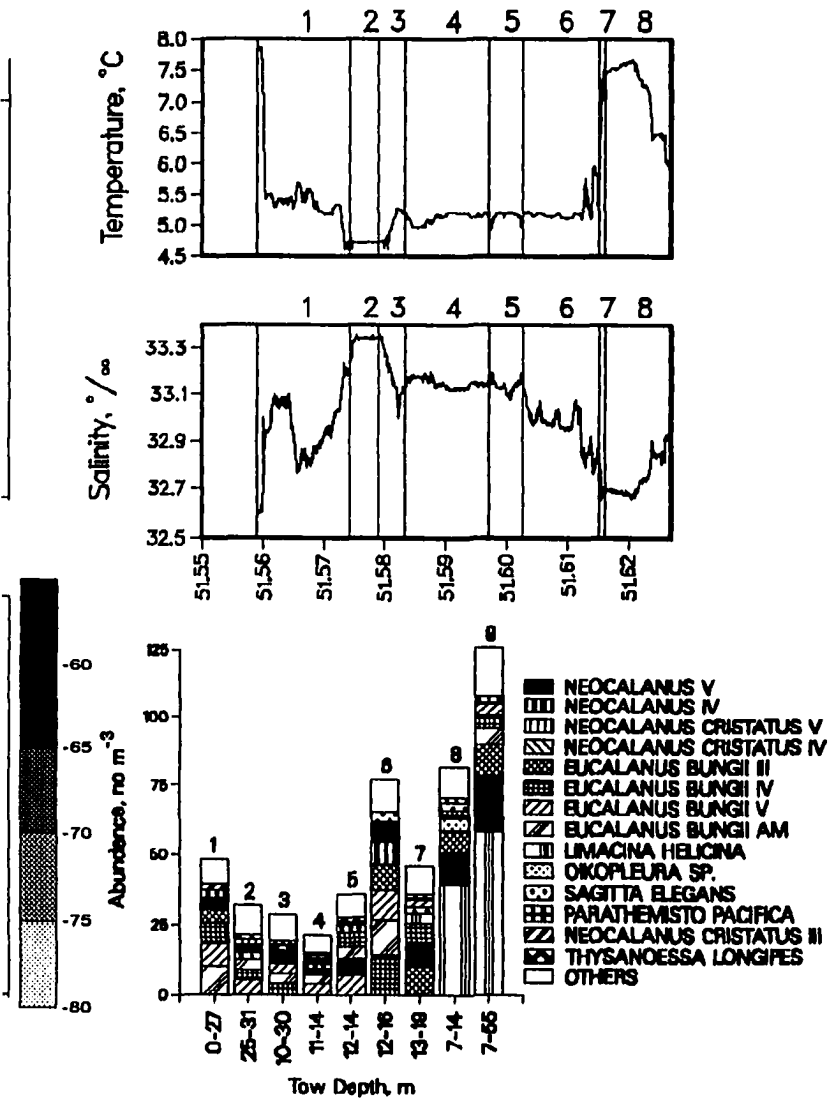
1 2 3 4 5 6 7 8
Temperature, °C
8.0
7.5
7.0
6.5
6.0
5.5
5.0
4.5
1 2 3 4 5 6 7 8
Salinity, °/∞
33.3
33.1
32.9
32.7
32.5
51.55
51.56
51.57
51.58
51.59
51.60
51.61
51.62
-60
-65
-70
-75
-80
Abundance, no m-3
125
100
75
50
25
0
1
2
3
4
5
6
7
8
9
0-27
25-31
10-30
11-14
12-14
12-16
13-18
7-14
7-65
Tow Depth, m
NEOCALANUS V
NEOCALANUS IV
NEOCALANUS CRISTATUS V
NEOCALANUS CRISTATUS IV
EUCALANUS BUNGII III
EUCALANUS BUNGII IV
EUCALANUS BUNGII V
EUCALANUS BUNGII AM
LIMACINA HELICINA
OIKOPLEURA SP.
SAGITTA ELEGANS
PARATHEMISTO PACIFICA
NEOCALANUS CRISTATUS III
THYSANOESSA LONGIPES
OTHERS

Figure 5-14. MOCNESS Tow 33, taken in Delarov Pass, 6 August 1993. Upper left: north-south component of current velocity; lower left: Acoustic backscattering intensity, volume scattering in dB (Solid line indicates net track, vertical bars are net cycles); Upper left: Salinity - temperature trace from MOCNESS sensors; Lower left: abundance of seven major taxa in each sample. Horizontal axes (latitude) on upper and lower figures aligned.

1 2 3 4 5 6 7 8 9
Temperature, °C
8.0
7.5
7.0
6.5
6.0
5.5
5.0
4.5
1 2 3 4 5 6 7 8 9
Salinity, °/₀₀
33.3
33.2
33.1
33.0
32.9
32.8
32.7
32.6
32.5
51.612
51.622
51.632
51.642
-60
-65
-70
-75
-80
Abundance, no m⁻³
175
150
125
100
75
50
25
0
1
2
3
4
5
6
7
8
9
NEOCALANUS V
NEOCALANUS IV
NEOCALANUS CRISTATUS V
NEOCALANUS CRISTATUS IV
EUCALANUS BUNGII III
EUCALANUS BUNGII IV
EUCALANUS BUNGII V
EUCALANUS BUNGII AM
LIMACINA HELICINA
PARATHEMISTO PACIFICA
EUCALANUS BUNGII II
EUKROHNIA HAMATA
SAGITTA ELEGANS
NEOCALANUS III
OTHERS
0-16
6-10
7-9
5-8
5-8
3-9
6-9
5-7
7-34
Tow Depth, m

6. The influence of tidal energy on zooplankton and auklet foraging near a ridge south of Kiska Island.

Earlier samples from north of Kiska Island during July 1993 indicated that the major zooplankton prey of least auklets were present at low densities or absent from the upper mixed layer. Nevertheless, auklets were still tending chicks in the colonies at Pt. Sirius on the northern end of Kiska Island and were therefore still limited to foraging in the vicinity of Kiska Island. The above constraints forced the auklets to shift their foraging strategy from the large-scale zooplankton layers characteristic of the Bering Sea water mass in June 1992 to small scale patches in tidally generated frontal regions south of Kiska Island. In this chapter, data are presented on the distribution of zooplankton and acoustic biomass relative to current patterns and auklet densities over a small shelf on the southern end of Kiska. The auklet data presented in this chapter was provided by Mary Beth Decker, University of California Irvine.

Sampling regime

The southern Kiska shelf extends southwest of the island and has two lateral ridges of less than 100 m depth (Fig. 6-1). Samples were taken July 26-28, 1993. Sampling on

July 26 consisted of repeated runs along a standard transect across the shelf (thick line, **Fig. 6-2**); a zig zag pattern was run across the ridge on July 27 (thin lines, **Fig. 6-2**). The tidal cycle in Gertrude Cove, Kiska Island, was primarily diurnal with a weak semidiurnal component during the sampling period (**Fig. 6-3**). The tide ebbed during night when CTD transects were done, and flooded during the day, when the bird counts, acoustic transects and net tows were taken.

Results

The longest CTD transect, run over the self from the Pacific to the west side of the ridge (**Fig. 6-1**), was taken early on 28 July. Isothermal and isohaline lines over the ridge peak showed a marked dip, suggestive of turbulence or localized up- and downwelling (**Fig. 6-4**). The isolines in three of the four CTD transects across the shelf had depth oscillations over the ridge. Currents over the ridge were consistently northward during the day; the east-west velocity component was strongest near the island in the morning (northern most transect line of **Fig. 6-2**; **Fig. 6-5**). A sharp drop in surface temperature and rise in surface salinity at km 8 along the transect occurred in a region of westward acceleration of the east-west velocity component over the shelf east of the ridge, and

rapid westward deceleration in the east-west velocity components across the shelf break, suggestive of an intense convergence over the ridge (**Fig. 6-5**). The above physical features were accompanied by elevated sound scattering from 100 m depth to the surface and a dense flock of foraging auklets (**Fig. 6-5**). Surface salinities of 33.25 and temperatures of under 5°C confirmed the presence of water from below 60 m depth on the surface. The above is the clearest example of auklets foraging in a region of upwelling from 60 m below the pycnocline to the surface.

The second transect in the north-south zig zag survey also revealed upwelling over the ridge (**Fig. 6-6**). Substantial east-west velocity convergences were still present and acoustic data still indicated upwelling from below 100 m depth. The highest surface salinity and lowest surface temperature over the ridge were 32.93 and 6.3°C (**Fig. 6-6**). The TS signature of the surface water over the ridge suggests upwelling from the base of the pycnocline, but it could also result from mixing of deeper water with surface water. Auklet flocks were densest on either side of the coldest water at km 6 along the transect. By transect 3 in the zig-zag series (**Fig. 6-2**), the east-west convergence had substantially weakened,

there were no marked surface salinity-temperature discontinuities over the ridge, and the auklets were spread to the west and east of the ridge crest (**Fig. 6-7**).

Although the above data clearly indicate feeding by auklets in upwelling regions, auklet densities were also occasionally elevated in warmer surface water. Higher temperatures and elevated surface scattering to the west of the ridge occurred with elevated auklet densities on the standard transect occupied on July 26 (**Fig. 6-8**). The lower surface temperatures around km 20 may have been due to a very weak subsurface east-west convergence as suggested by the east-west velocity components over the middle of the ridge. Lower temperatures and elevated salinity also occurred on the west end of the transect. The warmer region between km 5 and 20 may be due to a surface convergence, possibly concentrating prey organisms in the surface layer.

Five tows were done in the southern Kiska region, one south of the shelf and the others over the ridge on the west side of the shelf (**Fig. 6-9**). The *Neocalanus* over the shelf consisted primarily of *N. plumchrus* stage IV and V. Highest densities of *Neocalanus* occurred in surface tows above the pycnocline, where temperatures were over 7°C and salinities under 32.8 (**Figs. 6-10, 6-11**). The

patches of intense scattering with S_v > -68 dB, (**Fig. 6-11**) are typical of fish schools. Fluorescence above the pycnocline exceeded saturation values for the MOCNESS fluorometer. One tow was done below the pycnocline through a region where columns of intense scattering were ascending from the ridge (**Fig. 6-12**). The scattering exceeded -68 dB and was clearly not from zooplankton. Elevated zooplankton densities occurred outside regions of maximum scattering, in Nets 3 and 5. A temperature-salinity spike occurred during Net 5, apparently due to downwelling of the bottom of the pycnocline to below 15 m depth. A much smaller spike was also observed during Net 3. Overall zooplankton biomass was low, probably approaching the sensitivity threshold of the acoustic equipment.

Discussion

Flow over the southern Kiska shelf was clearly producing upwelling over the ridge and the upwelling was apparently fueling a phytoplankton bloom, as indicated by elevated chlorophyll values. Southward flow in excess of 50 cm sec^{-1} was observed over the ridge during ebb tide, while northward flow predominated during flood tide. Nevertheless, it is unclear what portion of the flow over

the shelf was tidally driven and what portion was geostrophic flow through the pass (e.g. Reed and Stabeno, 1994; Reed, 1984; Reed and Stabeno, 1993). Information on the resultant velocities over the ridge is necessary to estimate the residence time of water masses in the region and the length of time a given copepod population might experience the favorable conditions indicated by elevated chlorophyll concentrations over the shelf. However, given the obvious dynamic flow conditions in the Aleutian Passes (Reed and Stabeno, 1994), the residence time of zooplankton stocks on the ridge is probably only a small percentage of the length of the *Neocalanus* development period, about 150 days (Miller and Clemons, 1988; Miller, 1993). Therefore, elevated *Neocalanus* densities over the ridge are unlikely to be related to more favorable foraging conditions alone. In all probability, some physical mechanism is also involved in concentrating the zooplankton in regions where auklets forage.

The depth distribution of zooplankton in Bering Sea and Pacific water differed during July 1993. Averages of acoustic biomass by depth from the Gareloi and northern Kiska regions illustrate the effect of differences in stratification on the depth distribution of acoustic biomass (**Fig. 4-5a**). Pacific water had maximum average

biomass at the surface. In contrast, a distinct surface maximum in acoustic biomass was absent from Bering Sea water, where the biomass maximum varied with the depth of the pycnocline. Pacific water seemed to consist of a series of pools of warmer water, with elevated chlorophyll and *Neocalanus* concentrations, surrounded by denser water upwelled from below. These pools were periodically advected over the shelf, where mixing, convergence and divergence of the surface water masses in response to tidal forcing was apparently generating patches of elevated production and zooplankton densities. Minor changes in zooplankton depth distribution relative to light, temperature and feeding conditions in a regime with vertical flow gradients might be sufficient to produce the localized patches of elevated copepod densities observed at the boundaries between water masses over the south Kiska shelf. The least auklets were apparently able to locate and exploit those plankton patches.

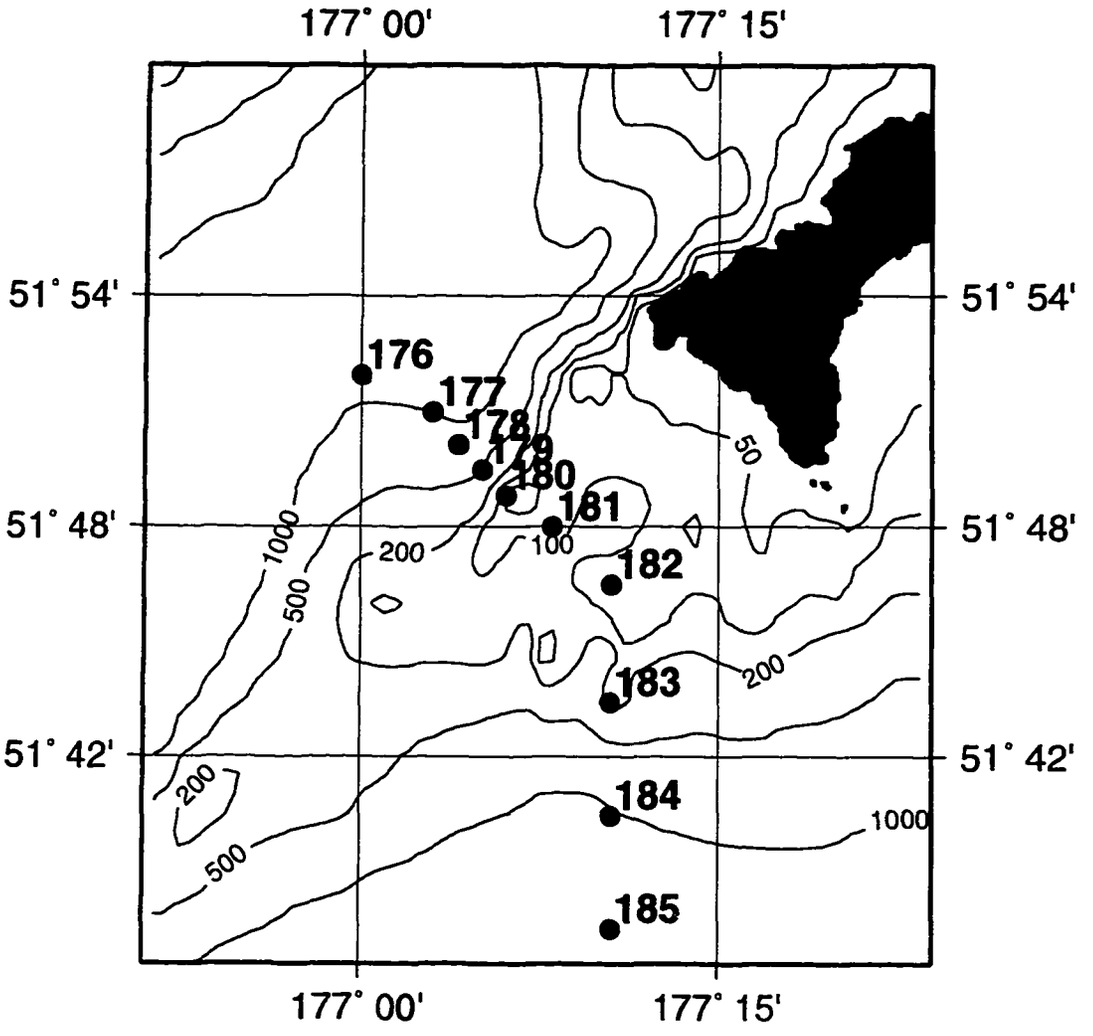

Figure 6-1. CTD stations along a transect over the shelf south of Kiska Island, taken 0018-0404 hrs., 28 July 1993.

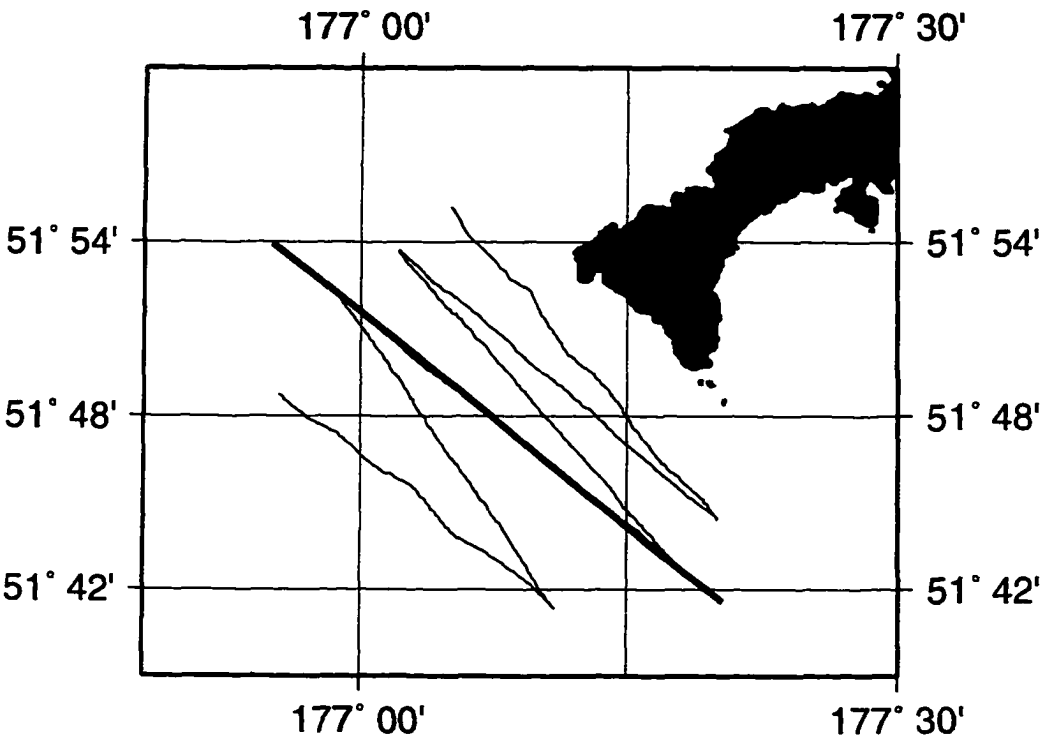

Figure 6-2. Transects run south of Kiska Island, 26-27 July 1993. Thick line: transect run 26 July; thin lines: zig zag transects run 27 July, numbered 6-1 to 6-6 from north to south.

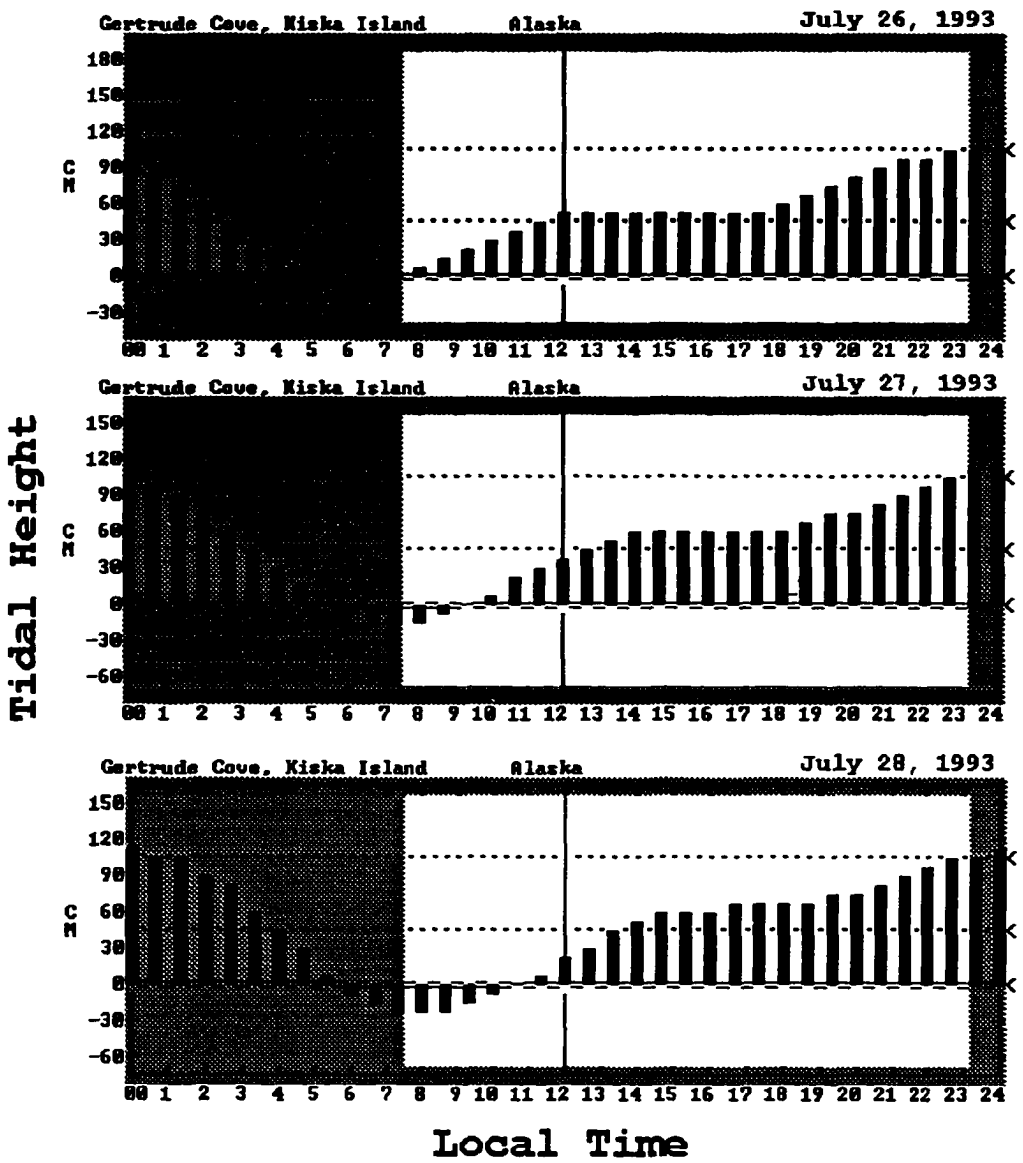

Figure 6-3. Tidal cycle in Gertrude Cove, Kiska Island, 26-28 July 1993, modified from NOAA tides program.

Figure 6-4. CTD transect taken over the shelf south of Kiska Island, taken 0018-0404 hrs, 28 July 1993. Solid triangles indicate station locations. Horizontal axes (distance) on upper and lower figures aligned.

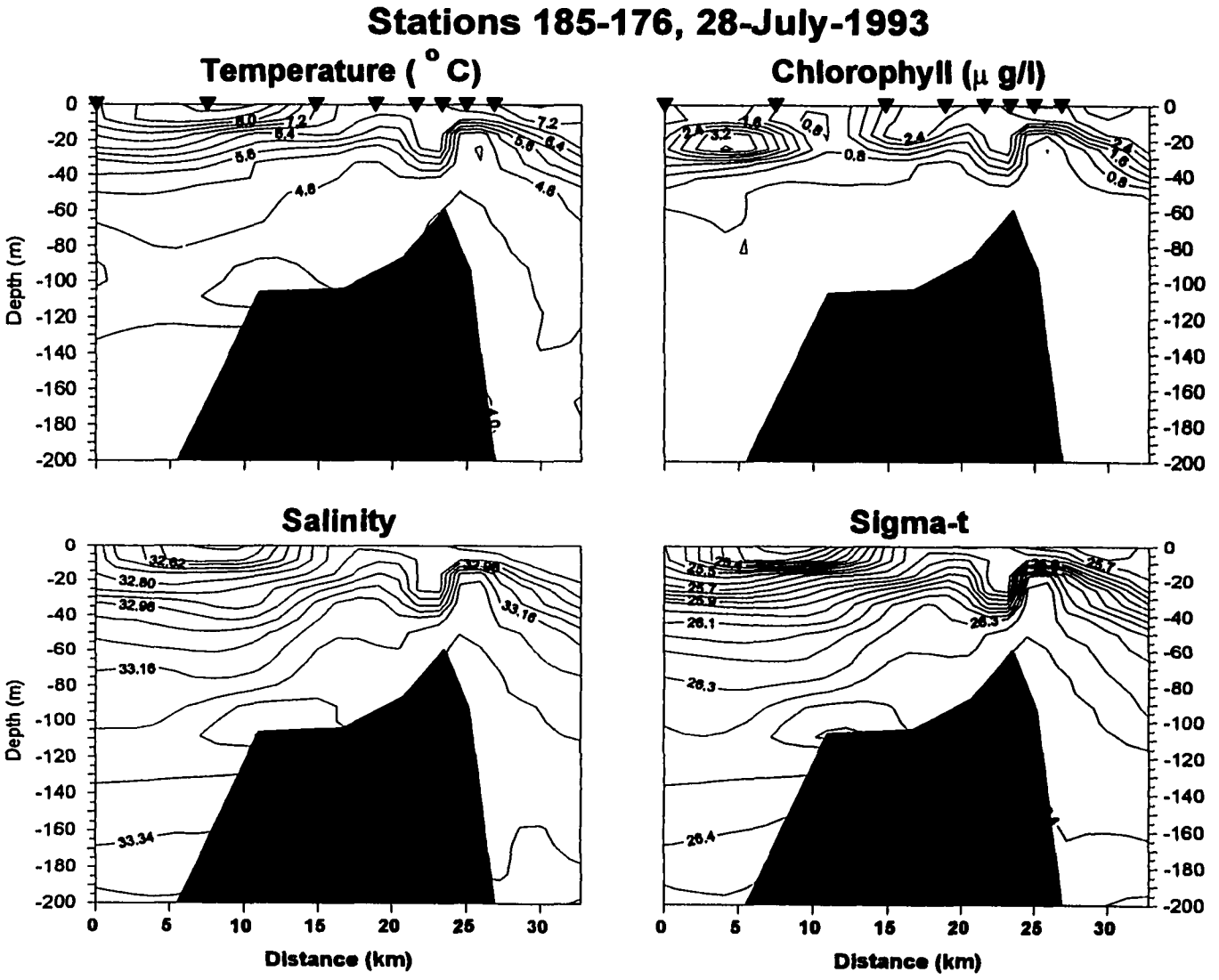

Figure 6-5. Transect 6-1 (Fig. 6-2), taken south of Kiska Island, 0839-1043 hrs, 27 July 1993. Upper and middle left: velocity components from ADCP data; Upper right: least auklet densities; Lower right: volume scattering (dB); Lower left: sea surface temperature and salinity. Horizontal axes (distance) on upper and lower figures aligned.

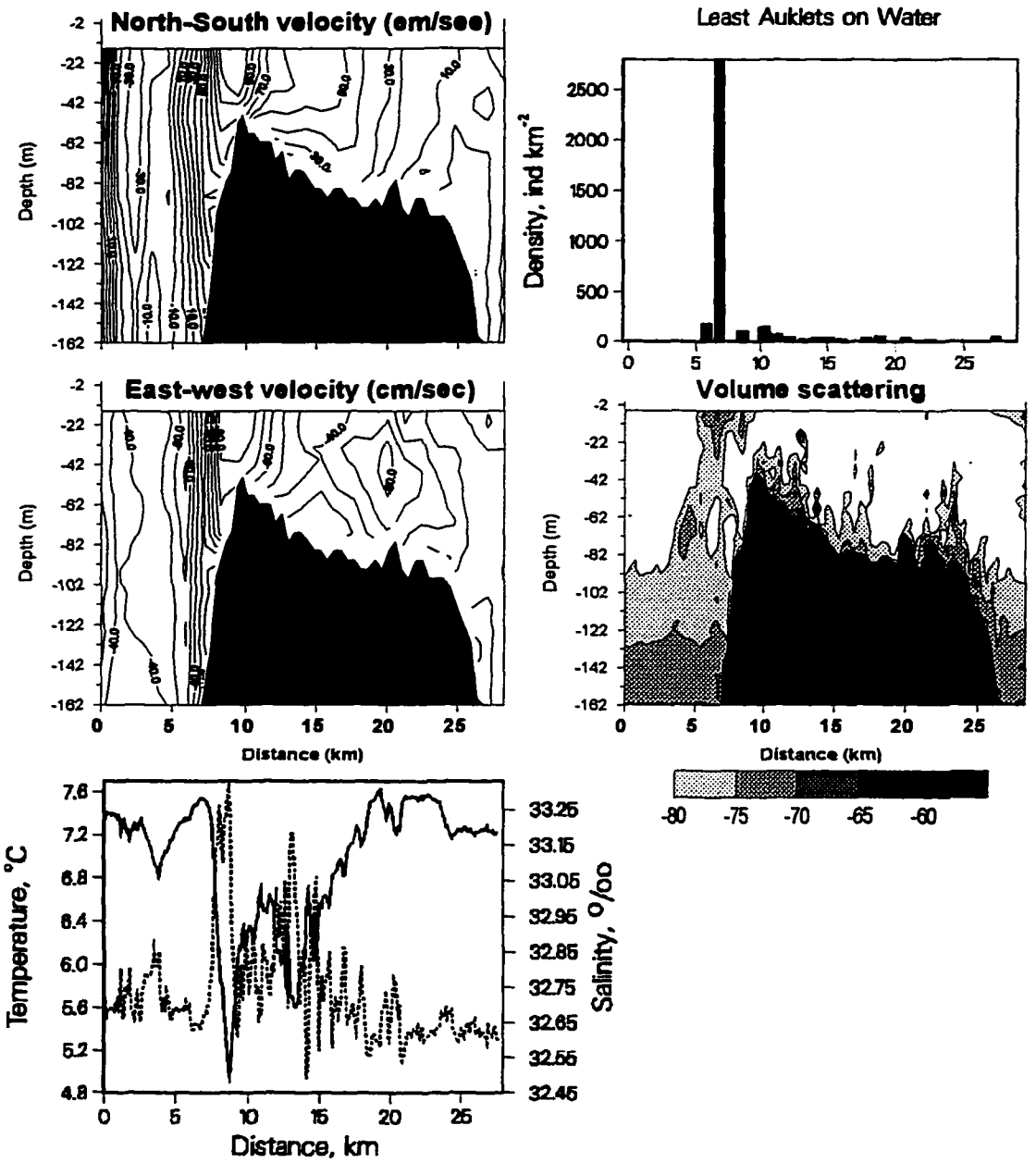

Figure 6-6. Transect 6-2 (Fig. 6-2), taken south of Kiska Island, 1044-1245 hrs, 27 July 1993. Upper and middle left: velocity components from ADCP data; Upper right: least auklet densities; Lower right: volume scattering (dB); Lower left: sea surface temperature and salinity. Horizontal axes (distance) on upper and lower figures aligned.

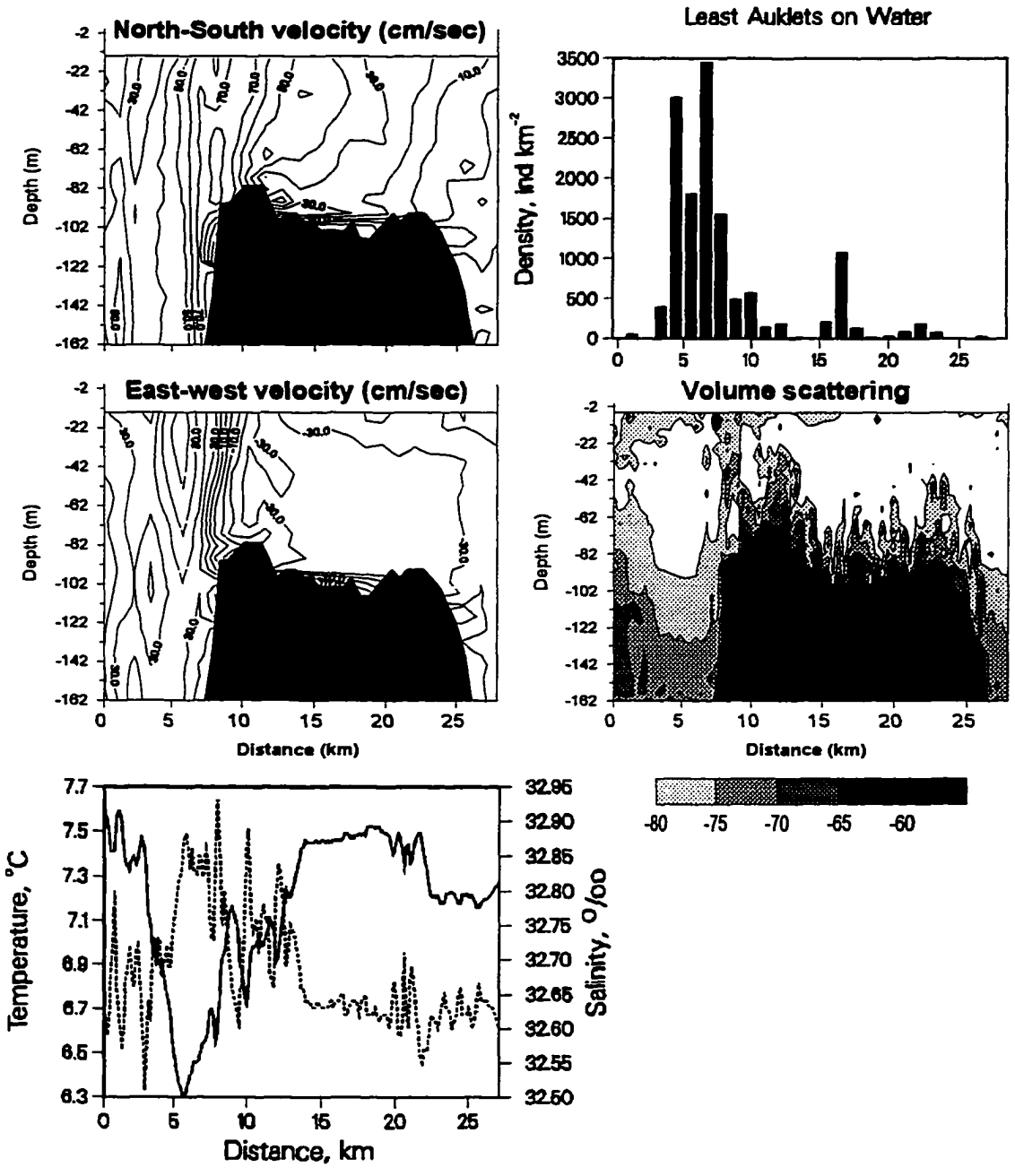

Figure 6-7. Transect 6-3 (Fig. 6-2), taken south of Kiska Island, 1227-1418 hrs, 27 July 1993. Upper and middle left: velocity components from ADCP data; Upper right: least auklet densities; Lower right: volume scattering (dB); Lower left: sea surface temperature and salinity. Horizontal axes (distance) on upper and lower figures aligned.

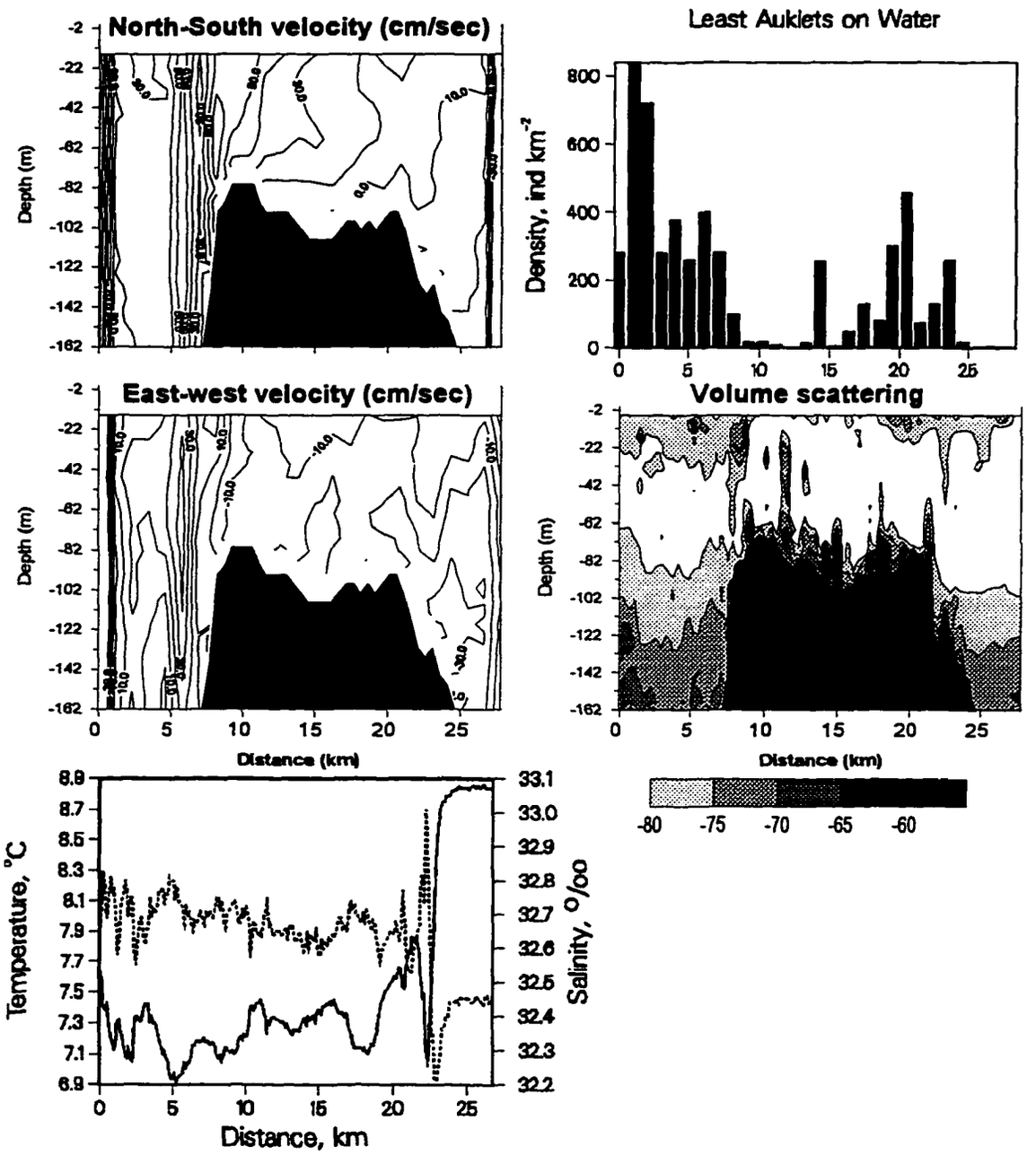

Figure 6-8. Transect 5-3, taken along the standard transect south of Kiska Island (Fig. 6-2), 1226-1445 hrs, 26 July 1993. Upper and middle left: velocity components from ADCP data; Upper right: least auklet densities; Lower right: volume scattering (dB); Lower left: sea surface temperature and salinity. Horizontal axes (distance) on upper and lower figures aligned.

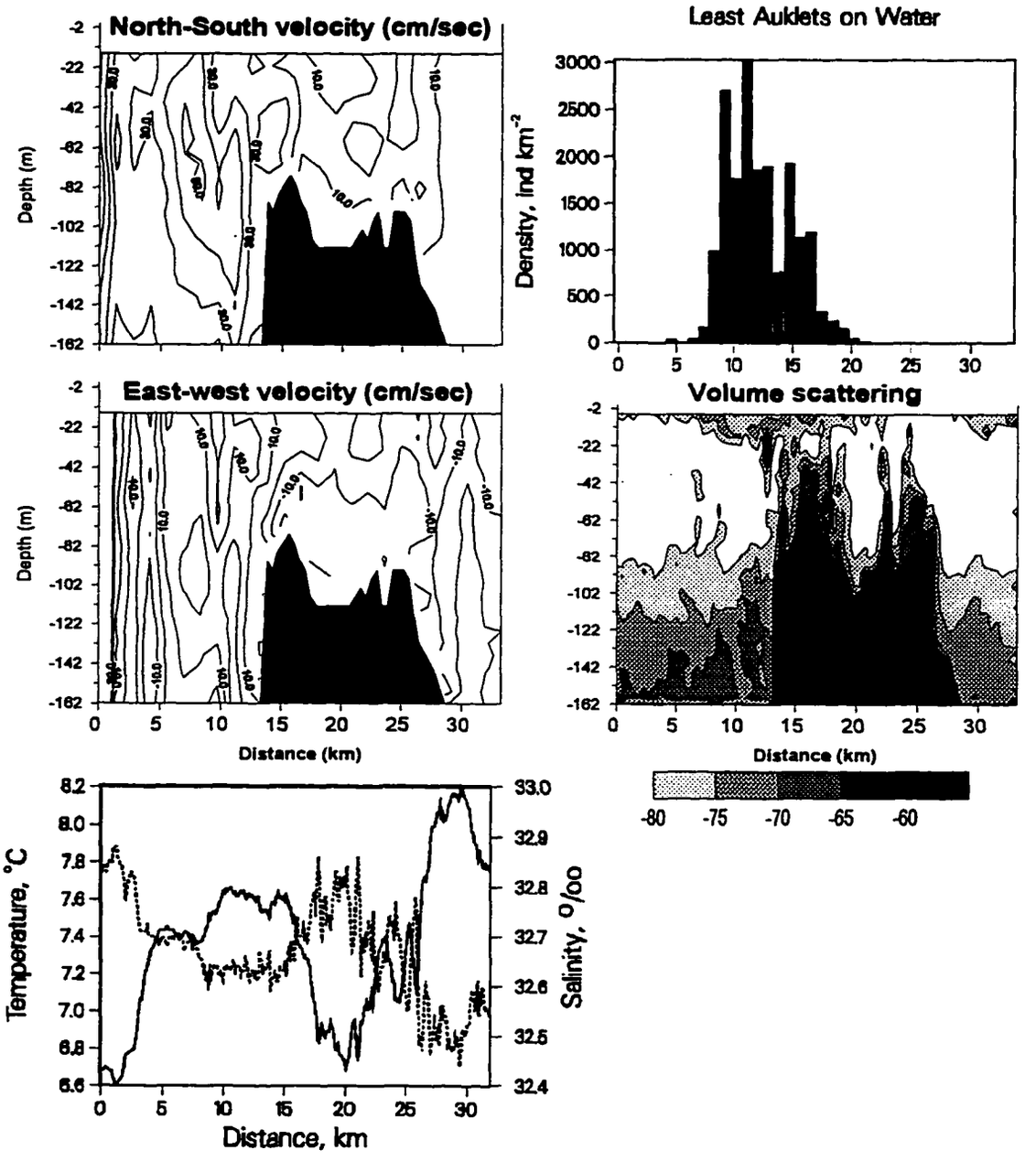

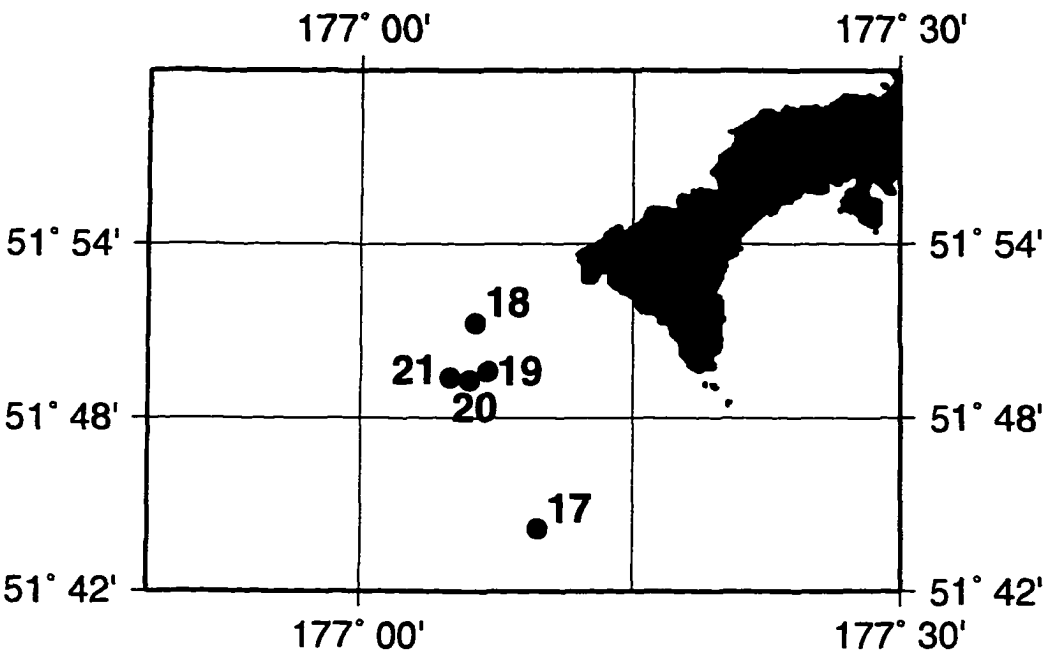

Figure 6-9. Locations of MOCNESS tows taken south of Kiska Island, 25-28 July 1993.

Figure 6-10. MOCNESS Tow 18, taken south of Kiska Island, 2030 hrs, 25 July 1993. Upper: Wet weight biomass of the upper seven taxa ranked by biomass in each net, numbers above bars are net numbers; Lower left: acoustic backscattering intensity, volume scattering in dB (Solid line indicates net track, vertical bars are net cycles); Lower right: CTD trace from MOCNESS sensors, values averaged for each 1 m depth interval, solid line: temperature (°C), dashed line: salinity (ppt), dotted line: fluorescence (relative units).

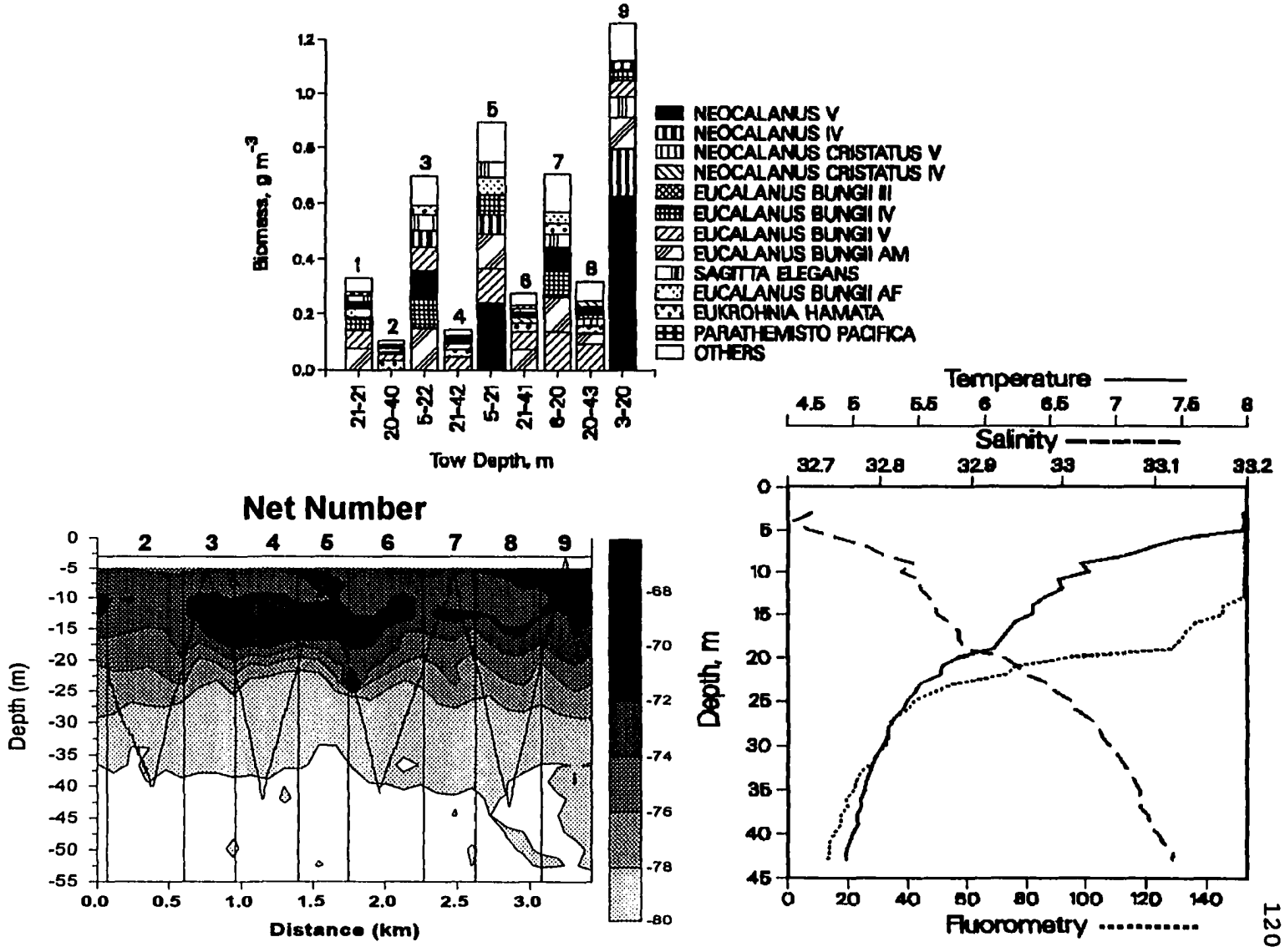

Figure 6-11. MOCNESS Tow 19, taken south of Kiska Island, 2209 hrs, 25 July 1993. Wet weight biomass of the upper seven taxa ranked by biomass in each net, numbers above bars are net numbers; Lower left: acoustic backscattering intensity, volume scattering in dB (Solid line indicates net track, vertical bars are net cycles); Lower right: CTD trace from MOCNESS sensors, values averaged for each 1 m depth interval, solid line: temperature (°C), dashed line: salinity (ppt), dotted line: fluorescence (relative units).

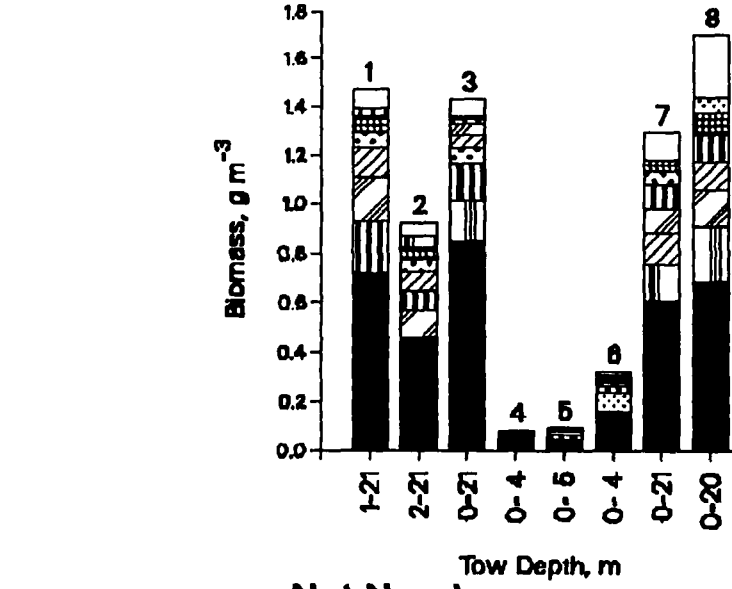

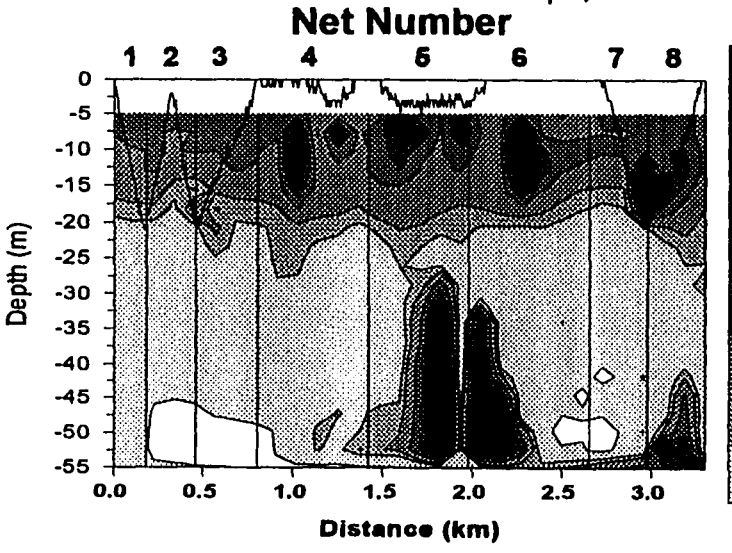

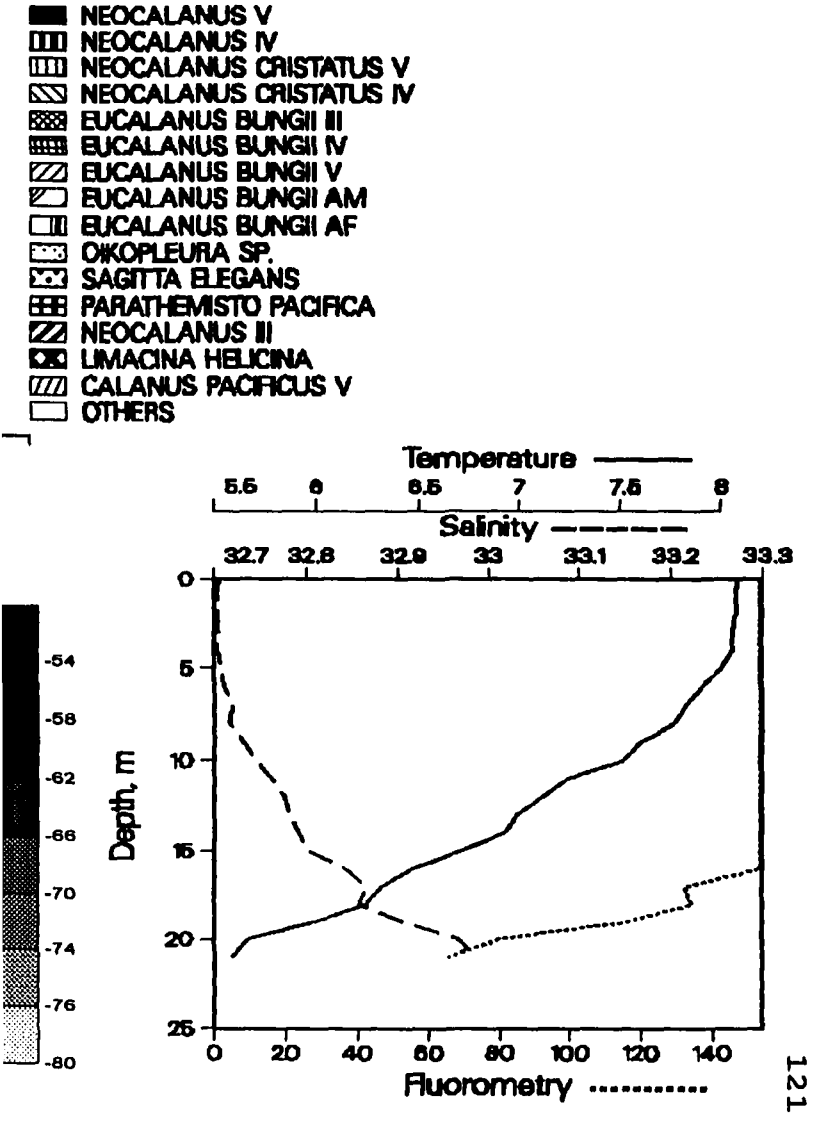
NEOCALANUS V
NEOCALANUS IV
NEOCALANUS CRISTATUS V
NEOCALANUS CRISTATUS IV
EUCALANUS BUNGII III
EUCALANUS BUNGII IV
EUCALANUS BUNGII V
EUCALANUS BUNGII AM
EUCALANUS BUNGII AF
OIKOPLEURA SP.
SAGITTA ELEGANS
PARATHEMISTO PACIFICA
NEOCALANUS III
LIMACINA HELICINA
CALANUS PACIFICUS V
OTHERS
Temperature
5.5 6 6.5 7 7.5 8
Salinity
32.7 32.8 32.9 33 33.1 33.2 33.3
0 5 10 15 20 25
Depth, m
-54 -58 -62 -66 -70 -74 -76 -80
0 20 40 60 80 100 120 140
Fluorometry

Figure 6-12. MOCNESS Tow 21, taken south of Kiska Island, 2008 hrs., July 27, 1993. Upper left: Salinity - temperature trace from MOCNESS sensors; Lower left: Acoustic backscattering intensity, volume scattering in dB (Solid line indicates net track, vertical bars are net cycles); Upper left: Wet weight biomass of the upper seven taxa ranked by biomass in each net, numbers above bars are net numbers; Lower left: abundance of seven major taxa in each sample.

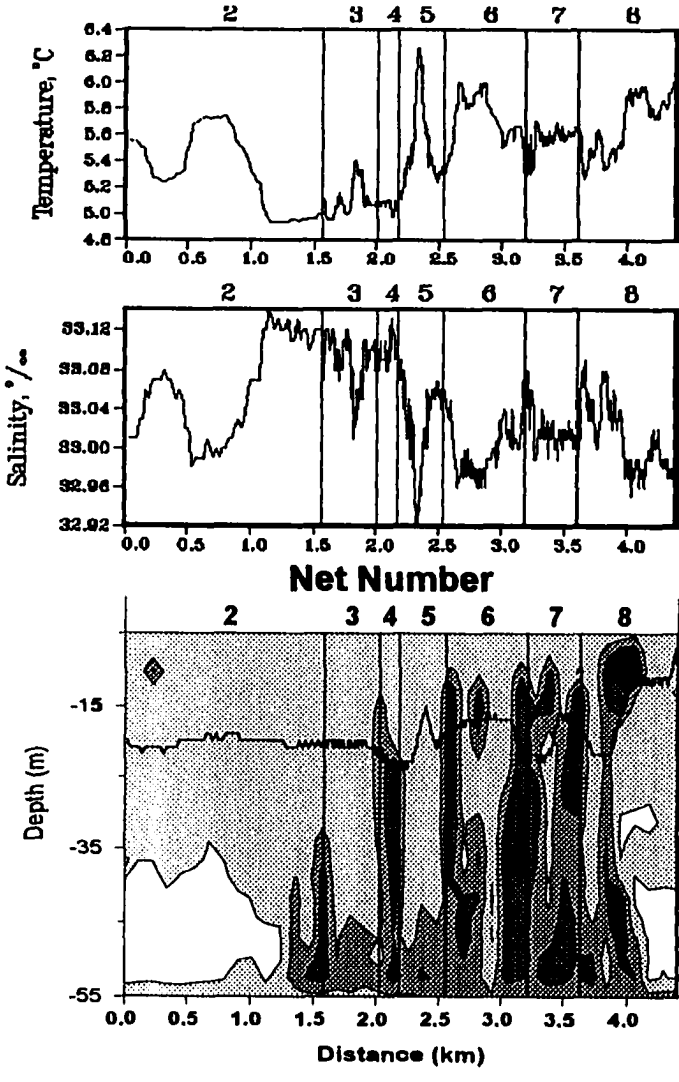

Biomass, g m-3
0.35
0.30
0.25
0.20
0.15
0.10
0.05
0.00
2
3
4
5
6
7
8
18-22
20-22
21-24
15-24
16-23
16-23
7-23
Tow Depth, m
NEOCALANUS V
NEOCALANUS IV
NEOCALANUS CRISTATUS V
NEOCALANUS CRISTATUS IV
EUCALANUS BUNGII III
EUCALANUS BUNGII IV
EUCALANUS BUNGII V
EUCALANUS BUNGII AM
EUKROHNIA HAMATA
SAGITTA ELEGANS
EUCALANUS BUNGII AF
METRIDIA PACIFICA AF
OTHERS

Abundance, no m-3
300
250
200
150
100
50
0
2
3
4
5
6
7
8
18-22
20-22
21-24
15-24
16-23
16-23
7-23
Tow Depth, m
NEOCALANUS V
NEOCALANUS IV
NEOCALANUS CRISTATUS V
NEOCALANUS CRISTATUS IV
EUCALANUS BUNGII III
EUCALANUS BUNGII IV
EUCALANUS BUNGII V
EUCALANUS BUNGII AM
EUKROHNIA HAMATA
EUCALANUS BUNGII II
METRIDIA PACIFICA V
NEOCALANUS III
NEOCALANUS CRISTATUS III
OTHERS

-40
-50
-60
-70
-80

7. Conclusions

Direct comparison of net-caught zooplankton wet weight biomass (WWB) with acoustically determined biomass (ADB) measured during MOCNESS tows indicated that ADB is a reasonable estimator of WWB in regions without intense turbulence or fish schools (Appendix II). Application of the Stanton fluid sphere model to volume scattering at 200 and 420 kHz produced ADB estimates similar to WWB in regions where zooplankton biomass was dominated by *N. cristatus*. However, target size was underestimated, possibly due to target orientation relative to the incident sound wave. Volume scattering in the mixed layer in turbulent regions was inflated by entrained bubbles and turbulent sound scattering. Intense scattering in turbulent regions was more indicative of downwelling than zooplankton biomass.

Direct comparison of zooplankton densities reported by different studies is complicated by the many different units used to express abundance and biomass, and the various gear types and sampling strategies employed. Zooplankton biomass estimates by a number of studies in the eastern Gulf of Alaska and eastern Bering Sea were recently tabulated and compared by converting the various units to mg C m^{-3} (Incze *et al.*, 1997). I have modified

the table in Incze *et al.*, (1997) to include acoustic biomass estimates from this study and estimates by Motoda and Minoda (1974) from the western Aleutian Islands (Table 7-1). Wet weight biomass in g m^{-3} was converted to g C m^{-3} using the regression equation in Weibe *et al.* (1975).

Highest zooplankton biomass was reported from Shelikov Strait and the outer shelf of the Bering Sea in May, from north of Kiska Island in June and from the Kamchatka Basin in summer (Table 7-1). Average zooplankton biomass from the upper 150 m of the central Gulf of Alaska in 1957 and 1980 (Brodeur and Ware, 1992) was 5.22 and 10.08 g C m^{-3}, respectively, when converted using the regression equation in Weibe *et al.* (1975). The biomass I measured acoustically in the western Aleutian Islands therefore falls between the high values for the Bering Sea and recent estimates for the Gulf of Alaska. If average wet weight biomass from our net tows is converted to carbon, values range from 18.5 g C m^{-3} for Pacific water south of Kiska and Buldir to 63.7 g C m^{-3} for Bering Sea water to the north of the islands. The higher biomass estimates from net tows reflect the net sampling emphasis on regions of elevated biomass where seabirds were foraging.

Two major hydrographic regimes occur around the

western Aleutian Islands (Fig. 3-16): Alaska Stream (Pacific) water to the south and resident Bering Sea water or a mixture of Bering Sea and Alaska Stream water to the north of the islands. *Neocalanus cristatus* and *Neocalanus flemingeri* occurred predominantly in Bering Sea water during June, 1992; *Neocalanus plumchrus* and *Eucalanus bungii* were dominant in Alaska Stream water. *N. plumchrus* and *N. flemingeri* occurred in the upper mixed layer and the pycnocline; *N. cristatus*, if present above 50 m depth, occurred in the pycnocline. Abundance and biomass of *N. cristatus* and *N. flemingeri* were very low or they were absent in July, 1993, when the dominant copepods in the upper mixed layer were *N. plumchrus* and *E. bungii*.

Zooplankton biomass in Bering Sea water was substantially greater than that in Alaska Stream water during June, 1992, primarily due to elevated abundances of *N. cristatus*. Zooplankton biomass was lower in all habitats during July, 1993, relative to that in Bering Sea water in June, 1992. Three factors probably caused lower biomass on the Bering Sea side of the Aleutians in 1993 relative to 1992: 1) Ontogenetic migration of *N. cristatus* and *N. flemingeri* out of the upper water column prior to July; 2) Elevated flow rates through the Aleutian passes in 1993 relative to 1992 may have pushed resident Bering

Sea zooplankton stocks northward or mixed them with the more dilute Pacific populations; 3) An anomalous flow regime from 1990 to spring 1992 (Stabeno and Reed, 1992) may have elevated zooplankton stocks north of the islands during June, 1992, by transporting zooplankton to Kiska Island from the Kamchatka Basin, where elevated zooplankton abundance and biomass has been recorded (Motoda and Minoda, 1974).

Several scale-dependent factors were influencing food availability to seabirds. Least auklets were foraging primarily north of Kiska Island in resident Bering Sea water during June, 1992. Zooplankton layers containing auklet prey occurred over hundreds to thousands of square kilometers of ocean occupied by Bering Sea water. Factors influencing the position of Bering Sea water relative to the nesting sites on Kiska and Buldir Islands may be related to long-term climate anomalies that could affect the flow of Alaska Stream water through the Aleutian Island passes. Thus, factors influencing foraging north of the Aleutians may involve events with temporal scales in years and spatial scales the size of ocean basins.

In the absence of elevated zooplankton densities north of the Aleutians, auklets were foraging in narrow passes and over shelf regions near the islands. Tidal

currents through Delarov Pass were producing convergences at size scales of tens of meters lasting for hours. Currents over a ridge south of Kiska were apparently upwelling and concentrating zooplankton on a scale of tens of kilometers. Some portion of the flow over the ridge was apparently tidally driven.

It is unclear what caused the flow anomaly through Near Strait from 1990 to 1992. Model simulations indicate that variations in wind stress can produce variations in flow rate into the Bering Sea (Overland *et al.*, 1994), although the authors did not speculate as to exactly what climatic conditions elevate or depress northward flow. Stabeno and Reed (1992) speculated that the anomaly may have been caused by inertial effects which displaced the Alaska Stream southward, rather than from wind stress. In the absence of a long-term data set on flow through Near Pass, the frequency and magnitude of depressed flow rates through the pass are unknown.

Long-term zooplankton data sets from north and south of the Aleutian Islands indicate persistent elevated zooplankton densities on the Bering Sea side of the islands relative to the Pacific side (Motoda and Minoda, 1974). Therefore, elevated northward flow through the passes would depress zooplankton densities north of the

Aleutian Islands.

In addition to variations in transport, decadal variations in zooplankton production may affect overall zooplankton density. A steady decline in zooplankton densities in the North Atlantic persisted from the 1940s to the late 1970s, followed by a reverse trend in the 1980s (Colebrook, 1985, 1986). The decline in zooplankton abundance in the Atlantic correlated with a 20 year increasing trend in northerly winds and depressed temperatures associated with the Atlantic oscillation (Mann and Lazier, 1991).

Decadal variations in zooplankton density and distribution over the Gulf of Alaska may have resulted from decadal variation in wind intensity and overall primary production rates (Brodeur and Ware, 1992). Highest positive correlations have been observed between the annual average zooplankton densities and surface salinities (Frost, 1983), suggesting that elevated mixing of nutrients into the photic zone may have enhanced primary production and elevated zooplankton production. Thus, interannual, climate-mediated differences in zooplankton production are superimposed on variations in transport to produce differences in local zooplankton distribution and abundance in any given year.

Although depressed flow through Near Pass probably results in higher densities of forage for auklets near Kiska and Buldir Islands, it is unclear if higher food densities affect the chick rearing success of least auklets nesting on the islands. I have no data on the long-term fledging success of auklets on the islands, nor do I have data on variations in fledgling success relative to flow rates through the passes or zooplankton densities near the islands. Food is only one of many possible factors influencing the growth and survival of chicks. Other possible factors include a limitation of suitable nest sites, nest predation and predation on chicks after fledging. Therefore, although temporal and spatial differences in prey distribution affected the distribution of foraging auklets during the breeding season, I have no evidence that such differences affect chick survival or overall auklet population levels.

Table 7-1. Comparison of zooplankton biomass estimates from the Gulf of Alaska and Bering Sea (modified from Incze *et al.*, 1996).

Location	Month	Year	Biomass	Depth (m)	Original Source
Station P	May	1956-1980	2.0	0-150	Fulton (1983)
Prince Willaim Sound	Early April	1976	3.3	0-700	Damker (1977)
	Late May	1976	3.6	0-700	Damker (1977)
Kachemak Bay	Early April	1976	0.8	0-72	Damker (1977)
	Early May	1976	17.5	0-72	Damker (1977)
	Late May	1976	3.7	0-72	Damker (1977)
	Early July	1976	1.6	0-72	Damker (1977)
Lower Cook Inlet	Early April	1976	2.2	0-25	Damker (1977)
	Early May	1976	7.5	0-25	Damker (1977)
	Late May	1976	5.5	0-25	Damker (1977)
	Early July	1976	20.4	0-25	Damker (1977)
Shelikof Strait	Late April	1987-1989	11.5	0 to Bottom	Incze *et al.* (1997)
	Early May	1985,1986 1989	21.0	0 to Bottom	Incze *et al.* (1997)
	Late May	1986-1987	42.8	0 to Bottom	Incze *et al.* (1997)

Table 7-1. (Continued)

Location	Month	Year	Biomass	Depth (m)	Source
Bering Slope	April	1980	1.7	0-1200	Vidal & Smith (1986)
	May	1980	12.3	0-1200	
Outer Shelf	April	1980	15.4	0-150	Vidal & Smith (1986)
	May	1980	30.8	0-150	
Middle Shelf	April	1980	21.4	0-70	Vidal & Smith (1986)
	May	1980	21.4	0-70	
North of Kiska & Buldir	Early-Mid Summer	1950s-1960s	19.2	0-80	Motoda & Minoda (1974)
South of Kiska & Buldir	Early-Mid Summer	1950s-1960s	10.6	0-80	Motoda & Minoda (1974)
Kamchatka Basin	Early-Mid Summer	1950s-1960s	35.8	0-80	Motoda & Minoda (1974)
North of Kiska	June	1992	30.6	0-50	This study
North of Buldir	June	1992	22.7	0-50	This study
South of Buldir	June	1992	14.8	0-50	This study
North of Gareloi	July	1993	15.3	0-50	This study
North of Kiska	July	1993	6.5	0-50	This study

Appendix I. Applied Marine Acoustics - Theoretical Considerations

The basic principles of sound scattering by zooplankton have been outlined in recent publications (Holliday, 1980; Green and Weibe, 1990; Smith *et al.*, 1992). The following discussion summarizes much of the information in the above references.

Active acoustics functions by transmission of a sound pulse at specific frequencies and detection of the reflected echoes from distant targets. It originated as a weapons system to detect submarines. Knowledge of the speed of sound in seawater and the time lag between transmission and detection permits estimation of the range (distance) of the target from the transducer. In addition, the intensity of the incoming signal is an indication of the size and concentration of the targets.

Quantitative acoustics involves conversion of the signal to a voltage and measurement of the voltage peak heights as a function of range from the transducer. The incoming signal must be corrected for signal loss due to geometric spreading, 20Log(R) or 40Log(R) for volume scattering or discrete targets respectively (Urick, 1975), where R is the target range from the transducer. The signal must also be corrected for absorption of sound by

seawater ($2\alpha R$), where α is the absorption coefficient in dB/m; a series of equations relate α to salinity, temperature and transmitted sound frequency (Urick, 1975). The incoming signal is amplified with respect to range to correct for the above losses, so that signal intensity is a function of target characteristics, not range from the transducer. The signal voltage can then be expressed as:

$$V^2 = k\sigma_{bs} b^2(\theta,\phi),$$

where k is a calibration coefficient, σ_{bs} is the back-scattering cross section of the target, as outlined below, and $b^2(\theta,\phi)$ is the beam pattern factor of the transducer. The beam pattern factor is the ratio of the transmitted intensity (I) at angular coordinates (θ,ϕ) to the intensity on the acoustic axis of the transducer (i.e. $b(\theta,\phi) = I(\theta,\phi)/I(0,0)$). It is essentially a measure of the receiving sensitivity of the transducer relative to the position of the target in the sound cone with respect to the acoustic axis.

The relative intensity of the returned signal is computed by summing the individual voltage peaks from discrete depths over a given number of transmissions (pings) during echo integration:

$$RD_{ir}=\frac{\sum V^2_{ir}}{PP_r x N_i},$$

where RD_{ir} is the relative intensity of the returned signal in depth stratum i and record number r, V_{ir} is the signal voltage in stratum i of report r, PP_r is the number of processed pings for the report interval and N_i is the number of targets per ping in stratum i. Absolute abundance is

$$AD_{ir}=RD_{ir} x A_i,$$

where AD_{ir} is absolute abundance and A_i is a constant containing the back-scattering cross-section of the targets, calibration values and the beam pattern factor:

$$A=\frac{1}{\pi \tau c \sigma_{bs} p_o^2 g_x^2 b_{av}^2(\theta,\phi)},$$

where τ is the pulse width in seconds, c is the speed of sound in m/sec, p_o^2 is transmitted pressure level in μPa

at one meter from the transducer, g_x^2 is the system gain in V/μPa, and $b_{av}^2(\theta,\phi)$ is the mean squared beam pattern factor of the transducer.

The target back-scattering cross-section is the most difficult of the parameters in the A constant to measure and a great deal of effort has been devoted to its empirical and theoretical determination. The volume scattering strength is defined as:

$$S_v = 10\log\left(\frac{I_s}{I_i}\right),$$

where I_s is the back scattering intensity at one meter from a unit volume containing the scatters and I_i is the intensity incident on the volume (e.g. Greenlaw, 1979). The back scattering cross section (σ_{bs}) is related to S_v by the equation (Greenlaw, 1979):

$$S_v = 10\log\left(\frac{\sigma_{bs}}{4\pi}\right).$$

The target strength is defined as (e.g. Wiebe *et al.*, 1990):

$$TS=10\log(\sigma_{bs}).$$

Thus, the target strength of an animal is its back scattering cross-section expressed in decibels.

The fundamental assumption governing quantitative acoustics is that the total scattering intensity from a given volume of water is equal to the sum of the scattering by each individual randomly-distributed target within the volume. However, the target strength of an individual target is a function of its physical aspect relative to the direction of the incident sound wave. When converting relative signal intensity to absolute abundance or biomass, it is assumed that the animals are randomly distributed within the insonified volume and that a sufficient number of measurements will produce an unbiased mean value of S_v, which can then be used to estimate σ_{bs}.

Two of the most commonly applied techniques to estimate σ_{bs} are direct measures using dual or split beam technology and theoretical computations based on sound scattering models.

The target strength of any discrete target in a given

depth stratum can be computed from the returned voltage if the position of the target in the beam relative to the acoustic axis can be determined. Dual beam and split beam technologies permit measurement of σ_{bs} by insonifying the target with two sound beams simultaneously. With dual beam, a wide beam is superimposed over a narrow beam transmission and the acoustic axes of the two beams are aligned. The voltages returned by each transducer are then expressed by:

$$V^2_n = k_n \sigma_{bs} b^2_n(\theta,\phi),$$

$$V^2_w = k_w \sigma_{bs} b_n(\theta,\phi)\, b_w(\theta,\phi),$$

where the subscripts n and w denote the narrow and wide beams, respectively, and b_n and b_w are the beam pattern factors. If b_w/b_n is known or the wide beam is designed such that the beam pattern factor is 1 over the main lobe of the narrow beam, then the ratio of the squared voltages on the two transducers is:

$$\frac{V^2_n}{V^2_w} = \frac{k_n b_n(\theta,\phi)}{k_w}.$$

When this equation is solved for $b_n(\theta,\phi)$ and the result substituted into the above equation for V^2_n, the equation can be solved for σ_{bs} and all the variables measured

directly.

Dual beam is not often used for direct measures of zooplankton target strength with subsurface transducers because of the difficulty in detecting discrete small targets within a given stratum of the sound cone at reasonable ranges from the transducer. However, dual beam has been used from submersibles to measure the size composition of individuals in euphausiid swarms (Green *et al.*, 1989) and for measurement of σ_{bs} on individual targets in the laboratory (Wiebe *et al.*, 1990). Target strength of an individual species or life stage can vary by over 10 dB, depending on the orientation of the target in the sound cone. Therefore, the average target strength from numerous measurements is preferred.

Sound scattering models can be used to estimate target strength from differences in the volume scattering at different frequencies (Greenlaw, 1979; Holliday and Pieper, 1980; Greenlaw and Johnson, 1983; Pieper and Holliday, 1984; Pieper *et al.*, 1990). Essentially, sound scatters off any target if the density and speed of sound in the propagating medium and the target differ. The

back scattering coefficient is defined as:

$$C_b = \frac{\rho_1 c_1 - \rho_o c_o}{\rho_1 c_1 + \rho_o c_o},$$

where ρ_o and ρ_1 and c_o and c_1 are the densities and speed of sound in the medium and target. As the difference between $\rho_o C_o$ and $\rho_1 c_1$ increases, the sound scattering capability of the target increases and C_b approaches 1. With zooplankton, the ratios ρ_1/ρ_o (defined as g) and c_1/c_o (defined as h) approach 1 so they are very weak sound scatterers.

In addition to g and h, the intensity of sound scattering by a target is a function of the sound frequency and the size and shape of the target. If the size of the scatterer is held constant and the frequency is increased, the intensity of the scattering will initially increase monotonically through a frequency interval called the Rayleigh scattering region; here increases in σ_{bs} are proportional to $(ka)^4$ where k is the wave number of the sound wave $(\lambda/2\pi)$, λ is the wave length in m and *a* is the radius (mm) of the target sphere. The upper limit of the Rayleigh region occurs when ka approaches 1.4 and the wave length is roughly equal to the equivalent spherical radius (ESR) of the target. Increases in frequency above the upper limit of the

Rayleigh region produce acoustic resonance within the target, leading to marked irregularities in σ_{bs} with increasing frequency. At yet higher frequencies, the geometric optics region, σ_{bs} is constant with respect to increases in frequency. Sound scattering models exploit this difference in target strength relative to frequency to estimate the size of targets from volume scattering data.

One of the earlier models of sound scattering by organisms is the fluid sphere model (Anderson, 1950; Greenlaw, 1979). A simplified version of the fluid sphere scattering model was used to estimate the abundance and size of euphausiids (Greenlaw 1979). However, application of this simplified model to abundance of large calanoids from the subarctic Pacific produced gross underestimates of the biomass as compared with net estimates (this study). Several potentially useful scattering models are now available, including another version of the fluid sphere model (Stanton, 1989). I applied the Stanton (1989) version of the fluid sphere model to *Neocalanus cristatus* populations north of the Aleutian Islands with mixed results (**Chapter 3**). All of the models attempt to estimate target size from differences in σ_{bs} measured at different frequencies. Stanton's (1989) fluid sphere

equation is:

$$\sigma = \frac{a^2 (ka)^4 \alpha^2 G}{1 + [4 (ka)^4 \alpha^2] / (R^2 F)},$$

where the wave number k is related to frequency by k = $2\pi f/c$, c is the speed of sound and f the frequency, a is the equivalent spherical radius of the target, α is defined as:

$$\alpha = \frac{1 - gh^2}{3gh^2} + \frac{1 - g}{1 + 2g}$$

and g and h are defined above. R is a plane-wave-plane-interface reflection coefficient to account for penetrability of the target by the wave and is defined as:

$$R = \frac{(gh - 1)}{(gh + 1)}.$$

The G and F terms are heuristic functions to account for irregular geometries and resonance. When applying the model to two frequencies, f_{HI} and f_{LO}, the ratio of σ_{bs} at the two frequencies is computed ($\sigma_R = \sigma_{bs}(f_{Hi}) / \sigma_{bs}(f_{Lo})$), and the model equations for σ_{bs} at the two frequencies are substituted into the ratio. The resulting equation can be

solved for the target radius. The solution to the above equation is:

$$a^4 = \frac{R^2(K_H^4 - \sigma_R K_L^4)}{4K_L^4 K_H^4 \alpha^2 (\sigma_R - 1)}.$$

K_L and K_H are the wave numbers at the lower and higher frequencies respectively. I omitted the G and F terms from the equations because they do not permit unique solutions for the radius.

The ESR value computed from the above equation can be inserted back into the model equation to estimate σ_{bs}, which can be used in the A constant to estimate absolute abundance. A complete presentation of the high-pass fluid sphere model, along with models for prolate spheroids, straight cylinders and bent cylinders is available (Stanton, 1989a, 1989b). At first glance, the prolate spheroid model might seem more appropriate to copepods, however, this formulation assumes that the incident and scattered sound waves are normal to the long axis of the spheroid (Stanton, 1989a), an assumption which is probably rarely met. The straight and bent cylinder models are probably more appropriate to euphausiids or shrimp than to copepods.

The fluid sphere model, or truncated fluid sphere

model, (Pieper and Holliday, 1984)has also been used with multiple frequencies to estimate the size distribution of zooplankton (Holiday and Pieper, 1980; Greenlaw and Johnson, 1983; Costello *et al.*, 1989; Pieper *et al.*, 1990). To explain the multifrequency technique, the acoustic equations are expressed as outlined in Greenlaw and Johnson (1983). The total echo intensity from a given volume, corrected for calibration, sound cone spreading and attenuation loss, is expressed as

$$I_T \propto I_o \sum_{i=1}^{S} N(a_i) R(f, a_i),$$

where I_o is the incident sound intensity, $N(a_i)$ is the number of scatters of ESR a_i, $R(f,a_i)$ is the scattering characteristics of a target of ESR a_i and S is the number of size categories. If N is large and the animals do not occur in discrete size categories, the sum can be expressed as the integral

$$I_T \propto I_o \int_0^{\infty} R(f, a) N(a) \, da$$

Given the relative scattering intensity ($I_r = I_T/I_o$) from a given volume at a fixed range at F frequencies, the above summation can be expressed by the following set of

equations:

$$
\begin{aligned}
I_r(f_1) &= N(a_1)R(f_1,a_1) + N(a_2)R(f_1,a_2) + \ldots + N(a_s)R(f_1,a_s) \\
I_r(f_2) &= N(a_1)R(f_2,a_1) + N(a_2)R(f_2,a_2) + \ldots + N(a_s)R(f_2,a_s) \\
&\vdots \\
I_r(f_F) &= N(a_1)R(f_F,a_1) + N(a_2)R(f_F,a_2) + \ldots + N(a_s)R(f_F,a_s)
\end{aligned}
$$

The values for R(f,a) are computed using data on the size categories of zooplankton from net tows, the frequencies of the acoustic measurements and the appropriate sound-scattering models. The above set of equations can then be solved by a least squares technique, regularization methods or inversion methods (Holliday, 1980; Greenlaw and Johnson, 1983). However, if the matrix of R(f,a) values is singular or nearly singular, solutions to the above series of equations will not exist or will be unstable. Thus, the scattering coefficients in the matrix must be independent of one another. A careful selection of the frequencies to be used and the solution methods may minimize inherent instabilities in the solutions. If the model is verified using net tows, plankton pumps or other sampling devices concurrently with acoustic measurements, then it can be applied to acoustic data to estimate the size the scattering organisms and convert relative back-scattering intensity to absolute abundance or biomass.

Back-scattering models with up to 21 frequencies have been used to estimate zooplankton size distribution (Costello *et al.*, 1989; Pieper *et al.*, 1990). The equipment required to simultaneously gather data at 21 frequencies is complex and cost- prohibitive for most studies. In addition, it is lowered on a hydrographic wire with the vessel stationary and therefore lacks the sampling density possible with a towed transducer array. Nevertheless, when the size composition of the zooplankton community is very diverse, multiple frequency sampling may be the only way to obtain reliable acoustic density estimates. However, if the zooplankton community is dominated by one or two species, two or three acoustic frequencies may provide reliable biomass estimates. If frequencies greater than 420 kHz can be avoided, a range of at least 60 m from the transducer can be achieved, and the transducers can feasibly be towed beside the vessel near the surface and still permit sufficient depth penetration to produce a reasonable data set for the upper mixed layer. Such a configuration can result in high enough sample densities to permit examination of zooplankton biomass distribution over a sufficiently wide range of spatial and temporal scales so that the trophic questions currently posed in many research and management

studies can be addressed.

Appendix II: Converting volume scattering to biomass

Although acoustic techniques are one of the most effective methods for measuring the spatial distribution of zooplankton, care must be exercised to insure that quantitative results are an accurate representation of abundance or biomass. Acoustic measurements are especially sensitive to misinterpretation due to the broad range of reflected sound intensity relative to the size, shape and orientation of the targets in the sound cone. Wiebe *et al.* (1990) measured the target strength of a broad size range of zooplankters and micronekters from large copepods to shrimp and found target strengths ranging from -93 to -43 dB/animal, a range equivalent to five orders of magnitude.

The three most common approaches to scaling volume scattering (S_v) to zooplankton biomass or abundance are the following: 1) direct comparison using net tows or plankton pumps (Pieper, 1979, 1983; Simmard *et al.*, 1986; Simard and Mackas, 1989); 2) application of scattering models with multiple frequencies (Holliday and Pieper, 1980; Pieper *et al.*, 1990; Cockrane *et al.*, 1991; Napp *et al.*, 1993); 3) direct measurement of scattering using dual beam or split beam technology (Greene *et al.*, 1988, 1989, 1991). Deployment of dual beam or high frequency

equipment for zooplankton surveys requires submersibles, remotely operated vehicles or a variable depth towed instrument package because of the short effective range of the highest frequencies. However, if the community is dominated by large zooplankton or micronekton, frequencies of up to 420 kHz can be employed using a towed surface transducer, thus permitting greater survey speeds and larger areal coverage. In such cases S_v can be scaled with concurrently collected net samples using regression analysis or by applying target strength corrections from the literature or from model calculations (Coyle *et al.*, 1992; Coyle and Cooney, 1993, Macaulay *et al.*, 1995). Volume scattering in this study has been scaled using direct measures of zooplankton from net tows. Also, application of the fluid sphere model by Stanton (1989b) for two frequencies was explored.

In addition to zooplankton, sound energy can be scattered by fish, bubbles and turbulence. Bubbles scatter sound at much higher intensity than zooplankton because of the large differences in the density of air and water. Fish also have a much higher target strength than zooplankton because of their gas bladders (e.g. Love, 1977; Foote and Traynor, 1988). Thus, intense sound scattering can sometimes indicate the presence of fish or

bubbles rather than zooplankton. Also, turbulence can produce echoes similar to those of zooplankton (Stanton *et al.*, 1994). Therefore, S_v from regions with high current velocity may include scattering from turbulence and entrained air bubbles.

Results:

Regression analysis was used to relate S_v to wet weight biomass (WWB) determined from net tows. Direct regression of S_v against WWB did not produce the best fit because S_v is a logarithmic scale and biomass an arithmetic scale. The best fit was derived when S_v was converted to biomass using a default scaler of -74 dB/g, chosen to produce ADB estimates within an order of magnitude of the corresponding WWB estimates.

Regression analysis was then used to refine the default scaler to optimize the fit between ADB and WWB. Regression of ADB against WWB was conducted for the 420 kHz ADB taken in 1992 and 1993 (Table 3-1). Maximum zooplankton biomass recorded by net samples was 7 g m^{-3}. Furthermore, biomass of over 1.5 g m^{-3} occurred only in regions where zooplankton wet weight was dominated by *Neocalanus cristatus*. Volume scattering in excess of -61 dB in 1992 and -68 dB in 1993 lowered the regression

coefficients due to excessive scattering relative to net caught biomass. Scattering from bubbles or fish appear as distant outliers in scatter plots of S_v against net-caught zooplankton biomass and therefore provided a standard by which signals could be interpreted as scattering from zooplankton rather than fish or bubbles (see triangles, Fig. 3-1). Since some of the tows included nets from layers with and without excessive scattering, some of the triangles in Fig. 3-1 occur within the range of zooplankton biomass. Nevertheless, I consider S_v from regions of excessive turbulence to be an unreliable measure of zooplankton biomass. In such cases the entire tow, including nets outside the layer of excessive scattering, were removed from the regression analyses. The net tow data were therefore the final standard for maximum acoustic biomass estimates, and they are conservative. Tows used in the regression analyses are listed in Table 3-1. Transects with scattering in excess of -61 and -68 dB are reported as volume scattering in dB and interpreted as fish or bubbles. All acoustic data scaled to biomass had volume scattering under the above limits.

The fluid sphere models of both Greenlaw (1979) and Stanton (1989b) were used as a second, independent measure

of target strength for the 1992 S_v estimates. Both equations produced ESR estimates (equivalent spherical radius, see introduction) of 0.4 to 1.0 mm (Fig. 3-2), averaging 0.69 and 0.54 mm (Greenlaw and Stanton models respectively). Regression analysis was undertaken to compare WWB with biomass computed from both models using 200 kHz and 420 kHz volume scattering. Both models are sensitive to g (ratio of the target density to water density) and h (ratio of the speed of sound in the animal to the speed of sound in water). Both g and h could be adjusted to produce regression slopes of about 1.0. However, the r^2 for the regression using the Greenlaw model equation was only 0.1 while the r^2 from the Stanton equation was 0.53. Changing g in the Stanton equation altered the slope of the regression but left the r^2 value unchanged. A regression slope of 1.006 was attained when h = 1.027, the average value for *Calanus* spp. from the Arctic (Kogeler *et al.*, 1987) and g = 1.055. The very rapid increase in acoustic biomass at about 0.5 mm equivalent spherical radius (ESR) (Fig. 3-2) is characteristic of regions where *Neocalanus cristatus* dominated in the scattering layers. Nevertheless, the above average ESR values were 2 to 3 times below the ESR for *N. cristatus*, computed from its wet weight biomass and

density values equal to 1.048, the value of g which produced ADB which most closely approximated WWB.

Discussion:

Linear regression of net-caught and acoustic estimates of biomass or abundance has produced r^2 values between 0.23 and 0.93 in other studies (Pieper, 1983, 1979; Simard and Mackas, 1989; Simmard *et al.*, 1986), with most values around 0.5. A similar range of r^2 values was obtained when comparing net-caught abundance data with abundance estimates using an optical plankton counter (Huntley *et al.*, 1995). The values obtained in this study (0.26 - 0.61) are therefore fairly typical. The r^2 value for the 200 kHz data from 1993 was low because zooplankton biomass was close to or below the detection threshold of the 200 kHz system.

In addition to direct comparison, the 1992 acoustic data in this study were scaled using a dual frequency scattering model. Sound-scattering models are sometime preferred because they can be more readily extended to regions where net tows are not available. However, scattering models are sensitive to small variations in the g and h parameters. Direct measurements on Arctic zooplankton produced a range of values from < 1.0 to 1.078

and 1.021 to 1.044 for g and h respectively (Kogeler *et al.*, 1987). Such a range of values could result in differences in biomass estimates of an order of magnitude or more. I obtained highest correlations between net caught and acoustic biomass estimates using the Stanton (1989b) fluid sphere model equations with g and h values of 1.055 and 1.027, respectively. The latter is the average value obtained for *Calanus hyperboreus* and *C. finmarchicus* (Kogeler *et al.*, 1987). Some of the variation in g and h appears to be related to the season, physiological state of the target animals or the life history stage of the animals (Kogeler *et al.*, 1987). Other authors have also selected g and h to maximize correlations between acoustic and net or plankton pump size and biomass estimates (Holliday and Pieper, 1980; Cochrane *et al.*, 1991).

Even when model estimates of acoustic biomass closely approximated net-caught biomass estimates, the equivalent spherical radius of the targets in this study was apparently substantially underestimated by the model equations. The ESR value for *Neocalanus cristatus* copepodid stage V, the dominant zooplankton in most samples, is 1.44 mm when computed from an average wet weight biomass of 13.9 mg/animal, measured on specimens

from our net samples. Thus, direct measures of ESR are about 2-3 times greater than the model estimates, averaging 0.55 mm. Part of the cause for the discrepancy between predicted and measured ESR may relate to the mixture of zooplankton in the scattering layers. Although the biomass in the layers was dominated by *Neocalanus cristatus*, the majority of animals were smaller copepodid stages of *N. plumchrus/flemingeri* and other taxa. If the smaller taxa were transparent to the 200 kHz sounder but detected by the 420 kHz sounder, the volume scattering ratios and estimated ESR would be biased. However, given the overwhelming dominance of *N. cristatus* biomass in the layers, the bias is probably minimal.

An additional source of error may relate to the shape assumptions inherent in the fluid sphere model, which assumes the targets are spherical when they clearly are not. The sound scattering model for a prolate spheroid might initially seem more appropriate to estimate copepod biomass, however, the equation solutions assume that the incident sound wave is normal to the long axis of the spheroid (Stanton, 1989a), an assumption which is probably rarely met. In fact, there is some evidence that copepods of the family Calanidae under natural conditions hang with their antennules extended horizontally and the long axis

of the body vertical (Mackas *et al.*, 1983; Landry and Fagerness, 1988; Dagg, 1993a). Under such conditions, the long axis of the target would be parallel to an incident sound wave propagating from a surface towed transducer. The above target-sound wave aspect ratio would probably result in an underestimate of the sound scattering cross section and an underestimation of ESR when using the fluid sphere model.

The model predicted an average target strength for areas dominated by *N. cristatus* of -100 dB/animal. Direct measures of target strength by dual beam on single specimens of *N. cristatus* yielded average values of -76 to -79 dB/animal for 10-12 mg individuals (Wiebe *et al.*, 1990). The lower target strength predicted by the fluid sphere model is probably due to violations of the assumed aspect ratio of the incident sound wave to the long axis of the copepod body. Despite the above caveats, the fluid sphere model provided an additional confirmation that scattering was from zooplankton rather that fish or bubbles, as scattering from the latter produce unreal numbers or computation violations due to violation of the assumed values of g and h.

Table AII-1. Regression statistics for comparison of net-caught zooplankton biomass and ADB from the western Aleutian Islands, 1992-1993.

June 1992

420 kHz data, calibration done on tows 1-7, 9, 11, 13-15, 17-24, 26-27.

Slope: 0.33
Intercept: 0.067
r^2: 0.61
Acoustic mean biomass: 1.692
Net mean biomass: 0.623
Standard error of the intercept: 0.069
Standard error of the slope: 0.025
Biosonics calibration data for HX162 420 kHz:
Correction factor for acoustic data: 545
Scaler for acoustic data: -69.6 dB/g

200 kHz data, calibration done on Tows 1-7, 9, 14, 15, 17,18,two nets of 19, 21-24, and 27.

Slope: 0.71
Intercept: 0.18
r^2: 0.50
Acoustic mean biomass: 0.66
Net mean biomass: 0.64
Standard error of the intercept: 0.08
Standard error of the slope: 0.07.
Correction factor for acoustic data: 1082
Scaler for acoustic data: -72.5 dB/g

Table AII-1. Continued.

July-August 1993

420 kHz data, calibration done on Tows 1-8, 13-18, 24-27 (excluding Net 2, Tow 17).

Slope: 0.51
Intercept: 0.09
r^2: 0.50
Acoustic mean biomass: 0.64
Net mean biomass: 0.42
Standard error of intercept: 0.03
Standard error of slope: 0.05
Correction factor for acoustic data: 777
Scaler for acoustic data: -71 dB/g

200 kHz: Calibration done on Tows 1-9,13,15-17,22-28.
Slope: 0.63
Intercept: 0.2
r^2: 0.26
Acoustic mean biomass: 0.28
Net mean biomass: 0.37
Standard error of the intercept: 0.04
Standard error of the slope: 0.1
Correction factor for acoustic data: 965
Scaler for acoustic data: -72 dB/g

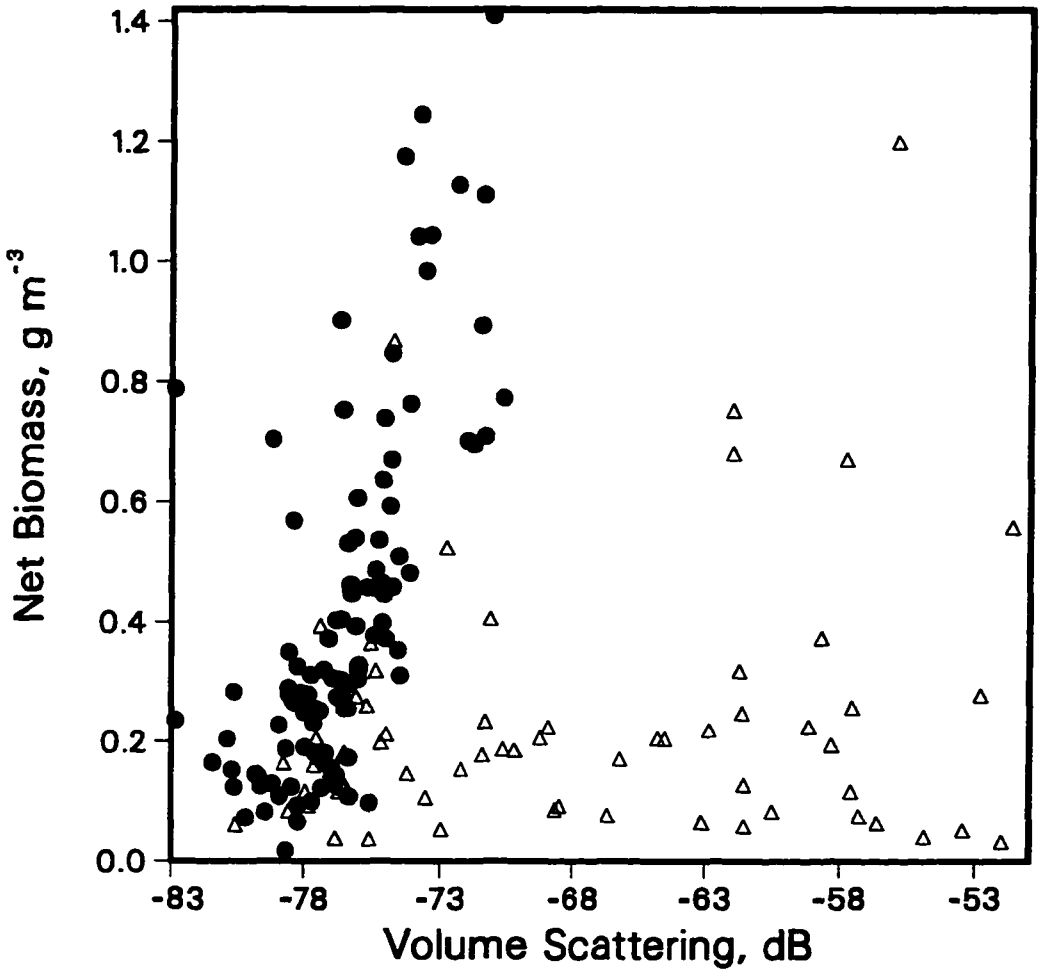

Figure APII-1. Scatter plot of volume scattering (dB) against net-caught zooplankton wet weight biomass from quiet regions (solid circles) and regions of turbulence and fish schools (open triangles). Data collected in the western Aleutian Islands, July 1993.

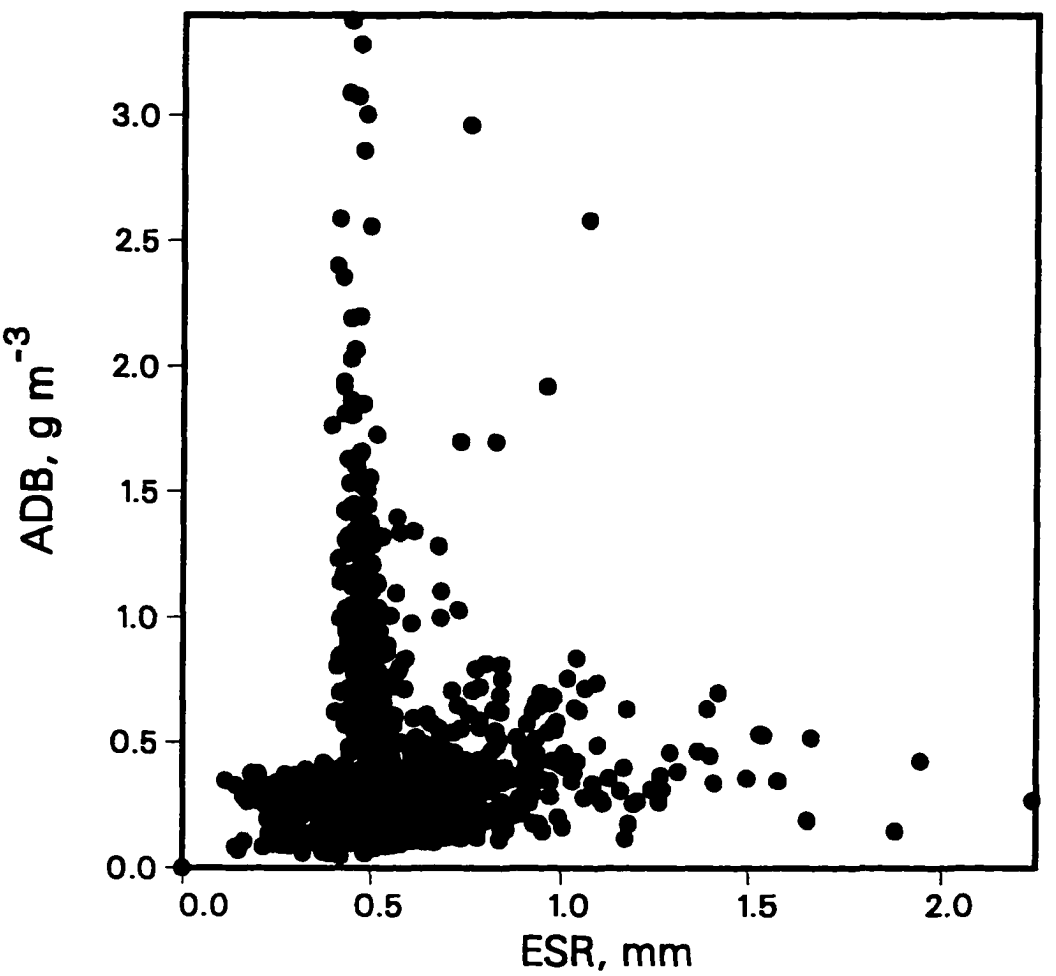

Figure APII-2. Equivalent spherical radius (ESR) of targets in each integration interval vs. acoustically determined biomass (ADB) in the corresponding interval for a transects run through scattering layers north of Kiska Island, 7 June 1992.

Literature cited

Anderson, V. C. 1950. Sound scattering from a fluid sphere. J. Acoust. Soc. Am. 22, 426-431.

Arsenev, V. S. 1967. Currents and water masses of the Bering Sea (in Russian), Nauka Press, Moscow, 135 p.

Brodskiy, K. A. 1948. The zoogeography of the northwestern Pacific Ocean. Dokl. Akad. Nauk SSSR, 60: 1053-1056.

Brodskiy, K. A. 1955. The zoogeographical regions of the pelagic zone in the far-eastern seas and the North Pacific Ocean (in reference to Calanoids). Dokl. Akad. Nauk SSSR 102(3): 649-652.

Brodskiy, K. A. 1957. The copepod fauna (Calanoida) and zoogeographic zonation in the North Pacific and adjacent waters. Izd. Akad. Nauk SSSR, Leningrad, 222 p.

Brodeur, R. D. and D. M. Ware. 1992. Long-term variability in zooplankton biomass in the subarctic Pacific Ocean. Fish. Oceanogr. 1(1): 32-38.

Coachman, L. K. 1986. Circulation, water masses and fluxes on the southeastern Bering Sea shelf. Cont. shelf. Res., 5:23-108.

Cochrane, N. A., D. Sameota, A. W. Herman and J. Neilson. 1991. Multiple-frequency acoustic backscattering and zooplankton aggregations in the inner Scotian Shelf basins. Can. J. Fish. Aquat. Sci., 48: 340-355.

Colebrook, J. M. 1985. Continuous plankton records: overwintering and annual fluctuations in the abundance of zooplankton. Mar. Biol., 84: 261-265.

Colebrook, J. M. 1986. Environmental influences on long-term variability in marine plankton. Hydrobiologia, 142: 309-325.

Cooney, R. T. 1989. Acoustic evidence for the vertical partitioning of biomass in the epipelagic zone of the Gulf of Alaska. Deep-Sea Res. 36(8): 1177-1189.

Cooney, R. T., Coyle, K. O. 1982. Trophic implications of cross-shelf copepod distributions in the southeastern Bering Sea. mar. Biol. 70: 187-196.

Costello, J. H., R. E. Pieper and D. V. Holliday. 1989. Comparison of acoustic and pump sampling techniques for the analysis of zooplankton distribution. J. Plank. Res., 11(4): 703-709.

Coyle, K. O., Chavtur, V. G., Pinchuk, A. I. 1996. Zooplankton of the Bering Sea. In: O. A. Mathisen and K. O. Coyle (Editors) Ecology of the Bering Sea: a review of the Russian literature. Alaska Sea Grant College Program Report No. 96-01. University of Alaska Fairbanks.

Coyle, K. O., Highsmith, R. C. 1994. Benthic amphipod community in the northern Bering Sea: analysis of potential structuring mechanisms. Mar. Ecol. Prog. Ser. 107: 233-244.

Coyle, K. O. and R. T. Cooney. 1993. Water column sound scattering and hydrography around the Pribilof Islands, Bering Sea. Cont. Shelf Res. 13(7): 803-827.

Coyle, K. O., G. L. Hunt, Jr., M. B. Decker and T. J. Weingartner. 1992. Murre foraging, epibenthic sound scattering and tidal advection over a shoal near St. George Island, Bering Sea. Mar. Ecol. Prog. Ser, 83: 1-14.

Dagg, M. J. 1993a. Sinking particles as a possible source of nutrition for the large calanoid copepod *Neocalanus cristatus* in the subarctic Pacific Ocean. Deep Sea Res. 1. 40(7): 1431-1445.

Dagg, M. J. 1993b. Grazing by the copepod community does not control phytoplankton production in the subarctic Pacific Ocean. Prog. Oceanog., 32: 163-183.

Damkaer, D. M. 1977. Initial zooplankton investigations in Prince William Sound, Gulf of Alaska, and Lower Cook Inlet. In: Environmental assessment of the Alaska continental shelf. Annual reports of the principal investigators for the year ending 1977, Vol. 10, pp. 137-274.

Dobrovol'skiy, A. D. and V. S. Arsen'yev. (1961). Hydrological features of the Bering Sea. Tr. IOAN, 38:

Farmer, D. M., E. A. D'Asaro, M. V. Trevorrow and G. T. Dairiki. 1995. Three-dimensional structure in a tidal convergence front. Cont. Shelf. Res. 15(13): 1649-1673.

Flagg, C. N. and S. L. Smith. 1989. On the use of the acoustic doppler current profiler to measure zooplankton abundance. Deep-Sea Res, 36(3): 455-474.

Foote, K. G. and J. J. Traynor. 1988. A comparison of walleye pollock target strength estimates derived from in situ measurements and calculations based on swim bladder form. J. acoust. Soc. Am., 83(1): 9-17.

Frost, W. B. 1983. Interannual variations of zooplankton standing stock in the open Gulf of Alaska. In: From year to year: interannual variability of the environment and fisheries of the Gulf of Alaska and the eastern Bering Sea. Wooster, W. S. (ed.), Washington Sea Grant Publication, Seattle, pp. 146-157.

Fulton, J. 1983. Seasonal and annual variations of net zooplankton at Ocean Station P, 1966-1980. Canadian Data Report of fisheries and Aquatic Sciences, No. 374.

Gifford, D. J., Dagg, M. J. 1991. The microzooplankton-mesozooplankton link: consumption of planktonic protozoa by the calanoid copepods *Acartia tonsa* Dana and *Neocalanus plumchrus* Marukawa. Marine microbial food webs, 5: 161-171.

Green, C. H. and P. H. Wiebe. 1990. Bioacoustic oceanography: New tools for zooplankton and micronekton research in the 1990. Oceanography, 3: 12-17.

Green, C. H., P. H. Wiebe and J. Burczynski. 1989. Analyzing zooplankton size distribution using high-

frequency sound. Limnol. Oceanogr., 34(1): 129-129.

Green, C. H., P. H. Wiebe, J. Burczynski and M. J. Youngbluth. 1988. Acoustic detection of high-density demersal krill layers in the submarine canyons off Georges Bank. Science, 241: 359-361.

Green, C. H., Wiebe, P. H., Myamoto, R. T., Burczynski, J. 1991. Probing the fine structure of ocean sound-scattering layers with ROVERSE technology. Limnol. Oceanogr., 36: 193-204.

Green, C. H., Landry, M. R. 1988. Carnivorous suspension feeding by the subarctic calanoid copepod *Neocalanus cristatus*. Can. J. Fish. Aquat. Sci., 45: 1069-1074.

Greenlaw, C. F. and R. K. Johnson. 1983. Multiple frequency acoustical estimation. Biological Oceanography, 2(2-3-4): 227-252.

Greenlaw, C. F. and W. G. Pearcy. 1985. Acoustic patchiness of mesopelagic micronekton. J. Mar. Res., 43: 163-178.

Greenlaw, C. F. 1979. Acoustic estimation of zooplankton populations. Limnol. Oceanogr. 24(2): 226-242.

Haury, L. R., H. Yamasaki and E. C. Itsweire. 1990. Effects of turbulent shear flow on zooplankton distribution. Deep-Sea Res. 37(3): 447-461.

Haury, L. R. and R. E. Pieper. 1987. Zooplankton: scales

of biological and physical events. In: Marine organisms as indicators, D. F. Soule & G. S. Kleppel (eds.), Springer-Verlag, New York, pp. 35-72.

Haury, L. R. and P. H. Weibe. 1982. Fine-scale multi-species aggregations of oceanic zooplankton. Deep-Sea. Res. 29: 915-921.

Haury, L. R., J. A. McGown and P. H. Wiebe. 1978. Patterns and processes in the time-space scales of plankton distributions. In: Spatial patterns in plankton communities. J. H. Steele (ed.), Plenum Press, New York, pp. 277-327.

Heinrich, A. K. 1959. The biological season in the plankton of the Bering Sea and the horizontal distribution of zooplankton biomass. Tr. Inst. Okeanol. Akad. Nauk SSSR 30:107-114.

Highsmith, R. C., Coyle, K. O. 1992. Productivity of Arctic amphipods relative to gary whale energy requirements. Mar. Ecol. Prog. Ser. 83: 141.

Holliday, D. V., Pieper, R. E. 1980. Volume scattering strength and zooplankton distributions at acoustic frequencies between 0.5 and 3 MHz. J. Acoust. Soc. Am. 67(1): 135-146.

Holliday, D. V. 1980. Use of frequency diversity for marine biological measurements. In: Diemer, F. P. et al. (Eds.): Advanced concepts in ocean measurements for marine biology. pp. 423-460, Univ. South Carolina Press,

Columbia.

Holliday, D. V. and R. E. Pieper. 1980. Volume scattering strength and zooplankton distributions at acoustic frequencies between 0.5 and 3 MHz. J. Acoust. Soc. Am. 67(1): 135-146.

Hunt, G. L. Jr., Harrison, N. M., Piatt, J. F. 1993. Foraging ecology as related to the distribution of planktivorous auklets in the Bering Sea. In: Vermeer, K., Briggs, K. T., Morgan, K. H. and Siegel-Causey, D. (eds.), The status, ecology and conservation of marine birds in the North Pacific. Can. Wildl. Serv. Spec. Pub., Ottawa, pp. 18-26.

Hunt, G. L. Jr., Harrison, N. M. 1990. Foraging habitat and prey taken by least auklets at King Island, Alaska. Mar. Ecol. Prog. Ser., 65: 141-150.

Hunt, G. L. Jr., Harrison, N. M., Cooney, R. T. (1990). The influence of hydrographic structure and prey abundance on foraging of least auklets. Studies in Avian Biology, no. 14: 7-22.

Hunt, G. L. Jr., Schneider, D. C. 1987. Scale dependent processes in the physical and biological environment of marine birds. In: Seabirds: feeding biology and role in marine ecosystems, Croxall, J. P. (eds.), Cambridge Univ. Press, pp. 7-41.

Huntley, M. E., M. Zhou and W. Nordhausen. 1995. Mesoscale distribution of zooplankton in the California Current in

late spring, observed by optical plankton counter. J. Mar. Res., 53: 647-674.

Incze, L. S., D. W. Siefert and J. M. Napp. 1997. Mesozooplankton of the Shelikof Strait, Alaska: abundance and community composition. Cont. Shelf. Res., 17(3): 287-305.

Kogeler, J. W., S. Falk-Petersen, A. Kristensen, R. Pettersen and J. Dalen. 1987. Density and sound speed contrast in sub-Arctic zooplankton. Polar Biol., 7: 231-235.

Landry, M. R., Fagerness, V. L. 1988. Behavioral and morphological influences on predatory interactions among marine copepods. Bull. Mar. Sci. 43(3): 509-529.

Love, R. H. 1977. Target strength of an individual fish at any aspect. J. acoust. Soc. Am., 62: 1397-1403.

Mackas, D. L., Sefton, H., Miller, C. B., Raich, A. 1993. Vertical habitat partitioning by large calanoid copepods in the oceanic subarctic Pacific during spring. Prog. Oceanog. 32: 259-294.

Macaulay, M. C., Wishner, K. F., Daly, K. L. 1995. Acoustic scattering from zooplankton and micronekton in relation to a whale feeding site near Georges Bank and Cape Cod. Cont. Shelf Res., 15 (4/5): 509-537.

Mann, K. H. and J. R. N. Lazier. 1991. Dynamics of marine ecosystems. Biological-physical interactions in the

ocean. Blackwell Scientific Publications, Boston, 466 p.

Miller, C. B. 1988. *Neocalanus flemingeri*, a new species of Calanidae (Copepoda:Calanoida) from the subarctic Pacific Ocean, with a comparative rediscription of *Neocalanus plumchrus* (Marukawa) 1921. Prog. Oceanog. 20: 223-273.

Miller, C. B. and M. J. Clemons. 1988. Revised life history analysis for large grazing copepods in the subarctic Pacific Ocean. Prog. Oceanog., 20: 291-313.

Miller, C. B. 1993. Development of large copepods during spring in the Gulf of Alaska. Prog. Oceanogr., 32: 295-317.

Motoda, S. and T. Minoda. 1974. Plankton of the Bering Sea. In: D. W. Hood and E. J. Kelley (eds.), Oceanography of the Bering Sea with emphasis on renewable resources: Proceedings of an international symposium, Hokkaido, Japan, 1972. Univ. Alaska Inst. Mar. Sci. Occas. Publ. 2, Fairbanks, pp. 207-241.

Napp, J. M., Ortner, P. B., Pieper, R. E., Holliday D. V. 1993. Biovolume-size spectra of epipelagic zooplankton using a multi-frequency acoustic profiling system (MAPS). Deep-Sea Res., 40(3): 445-459.

Obst, B. S., Russell, R. W., Hunt, G. L. Jr., Eppley, Z. A., Harrison, N. M. 1995. Foraging radius and energetics of least auklets (*Aethia pusilla*) breeding on three Bering Sea Islands. Physiol. Zool., 68: 647-672.

Overland, J. E., Spillane, M. C., Hurlburt, H. E., Wallcraft, A. J. 1994. A numerical study of the circulation of the Bering Sea basin and exchange with the North Pacific Ocean. J. Phys. Oceanog., 24: 736-758.

Parsons, T. R., Maita, Y., Lalli, C. M. 1984. A manual of chemical and biological methods for seawater analysis. Pergamon Press, Oxford.

Pieper, R. E. 1983. Quantitative estimates of euphausiid biomass determined by high-frequency acoustics. Biol. Oceanog., 2(2-3-4): 133-149.

Pieper, R. E. 1979. Euphausiid distribution and biomass determined acoustically at 102 kHz. Deep-Sea Res. 26/6A: 687-702.

Pieper, R. E. and D. V. Holliday. 1984. Acoustic measurements of zooplankton distributions in the sea. J. Cons. Int. Expl. Mer., 41: 226-238.

Pieper, R. E., D. V. Holliday and G. S. Kleppel. 1990. Quantitative zooplankton distributions from multifrequency acoustics. J. Plank. Res., 12(2): 433-441.

Reed, R. K. 1984. Flow of the Alaska Stream and its variations. Deep-Sea Res. 31(4): 369-389.

Reed, R. K., Stabeno, P. J. 1993. The recent return of the Alaskan Stream to Near Strait. J. Mar. Res., 51: 515-527.

Reed, R. K. and P. J. Stabeno, 1994. Flow along and across

the Aleutian Ridge. J. Mar. Res., 52: 639-648.

Sameoto, D. D. 1982. Euphausiid distribution in acoustic scattering layers and its significance to surface swarms. J. Plank. Res., 5(2): 129-143.

Simmard, Y. and D. L. Mackas. 1989. Mesoscale aggregation of euphausiid sound scattering layers on the continental shelf of Vancouver Island. Can. J. Fish. Aquat. Sci., 46: 1238-1249.

Simmard, Y., G. Lacroix and L. Legendre. 1986. Diel vertical migrations and nocturnal feeding of a dense coastal krill scattering layer (*Thysanoessa rachi* and *Meganyctiphanes norvegica*) in stratified surface waters. Mar. Biol., 91: 93-105.

Smith, S. L., R. E. Pieper, M. V. Moore, L. G. Rudstam, C. H. Green, J. E. Zamon, C. N. Flagg and C. E. Williamson. 1992. Acoustic techniques for the in situ observation of zooplankton. Arch. Hydrobiol. Beih. Ergebn. Limnol. 36: 23-43.

Smith, S. L., Vidal, J. 1986. Variations in the distribution, abundance and development of copepods in the southeastern Bering Sea in 1980 and 1981. Cont. Shelf. Res. 5: 215-239.

Sowls, A. L., S. A. Hatch and C. J. Lensink. 1978. Catalog of Alaska seabird colonies. U.S. Fish. Wildl. Ser. FWS/OBS 78/78.

Springer, A. M., McRoy, C. P., Turko, K. R. 1989. The paradox of the pelagic food webs in the northern Bering Sea. II. Zooplankton communities. Cont. Shelf Res., 9(4): 359-386.

Stabeno, P. J., Reed, R. K. 1992. A major circulation anomaly in the western Bering Sea. Geophysical Research Letters, 19(16): 1671-1674.

Stanton, T. K., P. H. Wiebe, D. Chu and L. Goodman. 1994. Acoustic characterization and discrimination of marine zooplankton and turbulence., ICES J. mar. Sci., 51: 469-479.

Stanton, T. K. 1989a. Sound scattering by cylinders of finite length. III. Deformed cylinders. J. Acoust. Soc. Am. 86(2): 691-705.

Stanton, T. K. 1989b. Simple approximate formulas for backscattering of sound by spherical and elongate objects. J. Acoust. Soc. Amer., 86(4): 1499-1510.

Tsuda, A. H. 1995. Fractal distribution of an oceanic copepod *Neocalanus cristatus* in the subarctic Pacific. J. Oceanogr. 51: 261-266.

Tsuda, A., Sygisaki, H., Ishimaru, T., Saino, T., Sato, T. 1993. White-noise-like distribution of the oceanic copepod *Neocalanus cristatus* in the subarctic North Pacific. Mar. Ecol. Prog. Ser. 97: 39-46.

Urick, R. J. 1975. Principles of underwater wound. McGraw-

Hill, New York.

Weibe, P. H., S. Boyd and J. L. Cox. 1975. Relationships between zooplankton displacement volume, wet weight, dry weight and carbon. Fish. Bull. 73: 777-786.

Wiebe, P. H., C. H. Green, T. K. Stanton and J. Burczynski. 1990. Sound scattering by live zooplankton and micronekton: Empirical studies with a dual-beam acoustical system. J. Acoust. Soc. Am., 88(5): 2346-2360.

Wishner, K., Durbin, E., Durbin, A., Macaulay, M., Winn, H. Kenney, R. (1988). Copepod patches and right whales in the Great South Channel off New England. Bull. Mar. Sci., 43(3): 825-844.